The dynamics of emotional and cognitive networks: Graph-based analysis of brain networks using *fMRI* and theoretical model for cingulo-frontal network dynamics in major depression

Juan Pablo Ramírez Mahaluf

Universitat de Barcelona

Programa de Doctorado en Biomedicina

Area: Neuroscience **Line:** Neurophysiology and computations in cortical systems

The dynamics of emotional and cognitive networks:

Graph-based analysis of brain networks using *fMRI* and theoretical model for cingulo-frontal network dynamics in major depression

Juan Pablo Ramírez Mahaluf

Doctoral thesis supervised by

Albert Compte Braquets

Barcelona, 2015

Theoretical Neurobiology of Cortical Networks

Systems Neuroscience Group

Institut d' Investigacions Biomèdiques August Pi i Sunyer

Lo que hoy somos descansa en lo que ayer pensamos,
y nuestros actuales pensamientos forjan nuestra vida futura.

A mi familia,

A Sessa y la terra.

Agradecimientos

Estas son las ultimas palabras que escribo en esta tesis, y sin duda, están cargadas de recuerdos, emociones, aprendizajes, nostalgia, sueños, penas y alegrías…

Esta tesis, resultado concreto de mi doctorado, simboliza una época maravillosa en mi vida, en la cual viví de todo. Seria absurdo aburrirlos con tal cantidad de historias, las cuales han marcado mi vida. Sin embargo, hoy sueño con poder recordarlas (y recordarlos) por siempre.

A continuación, un pequeño homenaje a quienes me acompañaron estos años, los héroes de esta travesía, los amigos del camino, a los que me escucharon, a quienes abrace en triunfos y derrotas, a quienes me regalaron caricias y miradas de compresión. Porque ustedes son todo, la esencia de estos años, la sal de este viaje.

Quisiera partir por mi mentor Albert, un genio de la vida. Agradezco la oportunidad de haberte conocido y de compartir estos años contigo. Eres un ejemplo de vida, una persona con una humanidad y sabiduría que encandila. Hacer el doctorado contigo, guiado por toda tu sabiduría y conocimiento, me ha dado herramientas exquisitas, que me permiten seguir soñando en aplicar técnicas de la neurociencia para mejorar la psiquiatría. Gracias por todos estos años de aprendizaje.

A mi padrino de doctorado Jaime, amigo y guía. Ha sido increíble compartir el laboratorio y las canchas de futbol contigo. Las risas y los análisis técnicos. Gracias por tu amistad y cercanía, por tus sabios concejos y por tus pases gol. Compañero y profesor, podemos decir que fuimos campeones! Gracias por todo Jaime.

A la profesora Helen Mayberg, por inspirar esta tesis con todo su conocimiento y experiencia, por recibirme en su Laboratorio y mostrarme su rica visión de la depresión, la psiquiatría y neurociencias. Una inspiración a seguir.

Al profesor Alex Roxin por su aporte a esta tesis, su colaboración fue fundamental para entender las matemáticas que subyacen el modelo teórico.

Nada hubiese sido tan entretenido sin mis compañeros del camino, mis amigos. He tenido la suerte de haberme encontrado con personas increíble sentadas justo a mi lado, intentando entender como funciona el cerebro o al menos poder encontrar un $p < 0.05$ perdido entre los datos. Queridas y queridos amigos, Dani, Maira, Klaus, Joao, Ainhoa, Gabriela, Genís, Joan, Marc, Diego, Marie y Marcos. Gracias por esos hermosos asaditos musicales, innumerables cafecitos, por los trasnoches trabajando, por los viajes, por todos los concejos y ayudas y por los infinitos divagues mentales… Son y fueron el sol del subterráneo, la luz que atraviesa la ventana.

A mis compañeros del futbol de la Violeta F.C., por todos estos años de juegos y risas, goles y patadas, de amistad y buena onda. Los 3 campeonatos ganados son parte del tesoro que me llevo conmigo.

A Sessa, quien me ha regalado todo su amor y ternura. Gracias por tu generosidad, por tus cariños y besos, y por abrirme tu casa y tu familia, allá en Solsona. Gracias a tus padres Manel y Teresa, por hacerme sentir como en casa.

Finalmente, a mis padres, Rodrigo y Susana, y a mis hermanos Andrés y Alejandra, quienes me han apoyado en todo momento. Sus visitas, sus llamadas y su amor incondicional me dieron fuerzas y energías para vivir tantos años lejos.

Table of Contents

Table of contents 1

Abstract 3

1. Introduction 11

1.1. Cognitive and emotional regulation 13
1.2. Graph theory 15
1.3. Major Depressive Disorder 17
1.4. Ventral anterior cingulate cortex is a critical hub in MDD 18
1.5. Dorsolateral prefrontal cortex presents activations opposed to vACC 20
1.6. Oscillations in the cingulo-frontal network 21
1.7. Mechanism behind vACC dysfunction 22
1.8. Mechanisms of serotonin treatment on vACC 23
1.9. Deep brain stimulation for treatment-resistant patients 23
1.10. Anatomy of cingulo-frontal network 24
1.11. Cingulo-frontal computational model for MDD 25

2. Objectives 27

3. Materials and methods 31

3.1. Methods for brain image analysis 33
3.1.1. Participants 33
3.1.2. Experimental Design 33
3.1.3. Behavioral analysis 35
3.1.4. *fMRI* acquisition 35
3.1.5. *fMRI* data analysis 35
3.1.6. Functional connectivity 37
3.1.7. Inter-individual *fMRI* activation 39
3.1.8 Graph analysis 39
3.2. Methods for cingulo-frontal modeling 44
3.2.1. Spiking network model 45
3.2.2. Firing-rate network model 48

4. Results 53

4.1. Results for brain image analysis 55
4.1.1. Behavioral analysis 55
4.1.2. *fMRI* BOLD response during working memory 57
4.1.3. sACC activation characterizes the high-sadness group 58
4.1.4. dlPFCl - sACCl interaction was modulated by sadness intensity 59
4.1.5. Community structure distinguishes emotional and cognitive networks 60
4.1.6. Hub identification and their modulation by strong emotional demands 67
4.1.7. Changes in functional connectivity underlie behavioral differences and hub modulations 70

4.2. Results for cingulo-frontal modeling 74
4.2.1. Healthy operation based on reciprocal suppression between the cognitive and emotional networks 74
4.2.2. Progressive nature of MDD 76
4.2.3. Serotonin treatment response decreases with the progression of the disease 78
4.2.4. Deep brain stimulation restores bistability in the treatment-resistant model 82
4.2.5. *fMRI* prediction from the spiking model 84
4.2.6. Dynamics of a rate-model network 88
4.2.7. MDD progression in the firing-rate model 90
4.2.8. Serotonin treatment in the firing-rate model 90
4.2.9. Deep brain stimulation in the firing-rate model 92
4.2.10. Oscillations as markers of bistable network dynamics 93
4.2.11. Why the region of bistability became narrower? 97
4.2.12. Other treatment mechanisms in the firing-rate model 100

5. Discussion 103

6. Conclusions 119

7. References 123

Abstract

This thesis is composed of two complementary projects. One focuses on the study of the dynamics between emotional and cognitive networks in healthy subjects using functional magnetic resonance imaging (fMRI). The second project builds on the results obtained in healthy subjects to formulate a computational model of the physiopathology and treatment mechanisms in major depression disorder (MDD). For each one of the projects, I did specific courses in order to gain experience in the methods applied, I presented my work in several conferences, and they are included in corresponding scientific publications, currently under editorial consideration. Both projects were performed in collaboration with other researchers. In the following, I summarize these projects, the collaborations and the additional activities associated.

1.

The regulation of cognitive and emotional processes is critical for diverse functions such as attention, problem solving, error detection, motivation, decision making and social behavior. Dysregulation of these processes is at the core of Major Depressive Disorder (MDD).

Currently neuroimaging and anatomical methods applied to emotional and cognitive processes present two views of brain organization: one view presents a considerable degree of functional specialization and the other view proposes that cognition and emotion are integrated in the brain. Here, we address this issue by studying the network topology underlying the competitive interactions between emotional and cognitive networks in healthy subjects. To this end, we designed a task that contrasted periods with very high emotional and cognitive demands. We concatenated two tasks: A Sadness Provocation (SP) followed by a Spatial Working Memory (WM) task.

We hypothesized that this behavioral paradigm would enhance the modularity of emotional and cognitive brain networks and would reveal the cortical areas that act as network hubs, which are critical for regulating the flow and integration of information between regions.

We collected fMRI data from 22 healthy subjects performing this task. We analyzed their

brain activity with a general linear model, looking for activation patterns linked to the various phases of the tasks, which we then used to extract 20 regions of interest (ROI) on a subject-by-subject basis. We computed the correlations between fMRI time series in pairs of ROIs, obtaining a matrix of correlations for each subject, and we then applied network measures from graph theory.

Subjects that scored highest their sadness intensity showed a more marked decrease in their cognitive performance after SP, and presented stronger activity in subgenual anterior cingulate cortex (sACC) and weaker activity in dorsolateral prefrontal cortex (dlPFC). The network analysis identified two main modules, one cognitive and one emotional. Analysis of connectivity degree and participation coefficient identified the areas that acted as hubs and their modulation: the left dlPFC degree decreased after sadness provocation and the left medial frontal pole (mFP) degree was modulated by sadness intensity. Functional connectivity analyses revealed that these hub areas modulated their connectivity following sadness experience: dlPFC and sACC showed stronger anticorrelation, and mFP and sACC strengthened their correlation.

Our results identify the hubs that mediate the interaction between emotional and cognitive networks in a context of high emotional and cognitive demands, and they suggest possible targets to develop new therapeutic strategies for mood disorders.

I. For the development of this project, I made the following courses:

1. II National course of Statistical Parametric Maps (SPM)

   IDIBAPS, CRC, Universitat de Barcelona

   Barcelona, Spain, 2010

2. FENS-IBRO Neuroimaging training program

   École Polytechique Fédérale de Lausanne, Université de Genéve, Université de Lausanne

   Lausanne-Geneve, Switzerland, 2011

II. This work was presented in the following conferences and meetings:

1. Talk: A graph model network during emotional and cognitive processing

Author: Juan P. Ramírez-Mahaluf

Invited to give a talk to Foundation Sant Joan de Déu (2015), Barcelona, Spain.

2. Poster: A graph model network during emotional and cognitive processing: searching for hubs

Authors: Joan Perramon, Juan P. Ramírez-Mahaluf, Pablo Villoslada, Albert Compte

Conference: Barcsyn 2014, Barcelona, Spain.

3. Poster: Mechanistic model of anterior cingulate cortex network during emotional and cognitive process

Authors: Juan P. Ramírez-Mahaluf, Begoña Otal, Pablo Villoslada, Albert Compte.

Conference: FENS-IBRO Neuroimaging training program 2011, Lausanne-Geneve, Switzerland.

III. This work was part of a project entitled: "Estudi de la dinàmica remissió-recaiguda de la depression a través de l'anàlisi de xarxa dels mapes de connectivitat de fMRI: implicacions per a la terapia". This project was supported by the Fundacio La Marató TV3 (Ref. 091430). Pablo Villoslada was the principal researcher of this project and Begonya Otal managed the organizational aspects of the project.

In addition, Joan Perramon helped me to develop and implement the graph analysis methods.

IV. Publication

The dynamics of emotional and cognitive networks: Graph-based analysis on the emotional-cognitive demands.

Authors: Juan P. Ramírez-Mahaluf, Joan Perramon, Pablo Villoslada, Albert Compte

In preparation.

2.

Several lines of evidence associate major depressive disorder (MDD) with a dysfunction of cingulo-frontal network dynamics following glutamate metabolism dysfunction in the ventral anterior cingulate cortex (vACC). However, we still lack a mechanistic framework to understand how these alterations underlie MDD and how treatments improve depression symptoms.

We built a biophysical computational model of two cortical areas (vACC, and dorso-lateral prefrontal cortex, dlPFC) that acts as a switch between emotional and cognitive processing: the two areas cannot be co-active due to effective mutual inhibition. We simulated MDD by slowing down glutamate decay in vACC, serotonergic treatments (SSRI) by activating serotonin 1A receptors in vACC, and deep brain stimulation by periodic stimulation of vACC interneurons at 130 Hz. We analyzed network dynamics mathematically in a simpler firing rate network model, and we derived the conditions for the emergence of cortical oscillations.

MDD networks differed from healthy networks in that vACC presented constant activation in the absence of emotional inputs, which was not suppressed by dlPFC activation. In turn, vACC hyper-activation prevented dlPFC from responding to cognitive signals, mimicking cognitive dysfunction in MDD. SSRI counteracted aberrant vACC activity but it also abolished its normal response to emotional stimuli. In treatment-resistant models, DBS treatment restored the switch function. Activity oscillations in the theta and beta/gamma bands correlated with network function, representing a marker of switch-like operation in the network.

The model articulates mechanistically how glutamate deficits generate aberrant vACC dynamics, and how this underlies emotional and cognitive symptoms in MDD. The model accounts for the progression of depression, dose-dependent SSRI treatment, DBS treatment of treatment-resistant models and EEG rhythmic biomarkers in a biophysical model of the pathophysiology of MDD.

I. For the development of this project, I made the following courses:

1. Dynamic models in systems neuroscience

   Organization for human brain mapping

   Barcelona, Spain, 2010

2. Latin-american summer school in computational neuroscience, LACONEU.

   Max Planck Institute (Germany), INRIA (France), Instituto de sistemas complejos,

   Centro Interdiciplinario de Neurociencias, Universidad Tecnica Federico Santamaria,

   Universidad de Valparaiso (Chile).

   Valparaiso, Chile, 2014

II. This work was presented in the following conferences and meetings:

1. Talk: Cingulate network dynamics and depression: A computational model

Author: Juan P. Ramírez-Mahaluf

Conference: Barcsyn 2014, Barcelona, Spain.

2. Poster: A computational model of Major Depression: The role of glutamate dysfunction on cingulo-frontal network dynamics.

Authors: Juan P. Ramírez-Mahaluf, Alex Roxin, Helen Mayberg, Albert Compte

Conference: Cognitive Rhythms Collaborative (Annual Retreat) 2015, Boston, US.

3. Poster: A computational model of Major Depression: The role of glutamate dysfunction on cingulo-frontal network dynamics.

Authors: Juan P. Ramírez-Mahaluf, Alex Roxin, Helen Mayberg, Albert Compte

Conference: Society for Neuroscience 2014, Washington DC, US.

4. Poster: Cingulate network dynamics and depression: from glutamate dysfunction to deep brain stimulation

Authors: Juan P. Ramírez-Mahaluf, Helen Mayberg, Albert Compte

Conference: Society for Neuroscience 2012, New Orleans, US.

5. Poster: Dynamics of cingulate cortex network during emotional and cognitive processes in Major Depression Disease: a computational model

Authors: Juan P. Ramírez-Mahaluf, Helen Mayberg, Albert Compte

Conference: The Federation of European Neuroscience Societies (FENS) 2012, Barcelona, Spain.

6. Poster: Computational network model of anterior cingulate cortex during emotional and cognitive process in major depression disease

Authors: Juan P. Ramírez-Mahaluf, Albert Compte

Conference: Barcsyn 2011, Barcelona, Spain.

7. Poster: Computational network model of anterior cingulate cortex during emotional and cognitive process in major depression disease.

Authors: Juan P. Ramírez-Mahaluf, Albert Compte

Conference: Society for Neuroscience 2011, Washington DC, US.

8. Poster: Dynamics of cingulate cortex network during emotional and cognitive process in major depression disease: A computational model.

Authors: Juan P. Ramírez-Mahaluf, Albert Compte

Conference: Dynamical Neuroscience XIX, Deep brain stimulation in mental illness, neurological disorders and cognitive impairment, 2011, Washington DC, US.

III. This work was made in collaboration with professor Helen Mayberg (Emory University, Atlanta GA, USA) and professor Alex Roxin (Centre de Recerca Matemàtica, CRM, Bellaterra).

For the collaboration with the Prof. Mayberg I did a short stay (October - December 2012) at Helen Mayberg Lab, in Emory University, Atlanta, US. The object of this stay was the clinical observation of the study: Deep brain stimulation for treatment resistant depression and learn about the biological basis and the brain areas involved in MDD. The stay was financed by "FPI (Formación de Personal Investigador) Estancia Corta" (Ref. EEBB-I-2012-04615). The collaboration with the Prof. Mayberg was crucial to build bridges between theoretical models and the clinical experience.

The Prof. Roxin derived the conditions for the emergence of cortical oscillations in the firing rate network model (page 87). The collaboration with Prof. Roxin was crucial to understand the mathematical basis of the Bogdanov-Takens bifurcation and the associated oscillations in our models.

IV. Publication

A computational model of Major Depression: The role of glutamate dysfunction on cingulo-frontal network dynamics.

Authors: Juan P. Ramírez-Mahaluf, Alex Roxin, Helen Mayberg, Albert Compte

Submitted to Cerebral Cortex, under review.

Introduction

Cognitive and emotional regulation

The relationship between cognition and emotion has fascinated philosophers for centuries. It is not surprising that much of that attraction has permeated brain science in general. Early reports, such as the now classic case of Phineas Gage (Harlow 1848), described how damage to specific parts of the brain caused changes (or lack thereof) in cognitive and emotional behaviors (Harlow 1848, 1868; Damasio 1994; Macmillan 2000; Kean 2014). The case of Gage was one of the first evidence that suggested that a lesion on the frontal lobe could alter aspects of personality, emotions or social interaction behaviors (Harlow 1848, 1868; Damasio et al. 1994; Macmillan 2000; Kean 2014). The case was used as evidence against phrenology, a crude precursor of modern cerebral localization theories (Barker 1995).

Emotion and cognition are central to the quality and range of everyday human experience (Dolan 2002). Today the understanding of neurobiological substrates of human emotion is still evolving, and the question of how emotion interacts with and influences cognition, and vice versa is re-emerging motivated by advances in functional neuroimaging techniques and computational tools (Pessoa 2008; Bullmore and Sporns 2009; Sporns 2014; Stephan and Mathys 2014; Wang and Krystal 2014).

Cognition refers to processes such as memory, attention, language, problem solving and planning (Fuster 2003). Many cognitive processes are thought to involve sophisticated functions that might be uniquely human (Fuster 2003). An archetypal example of neural correlate of a cognitive process is the persistent firing of cells in dorsolateral prefrontal cortex (dlPFC) as a monkey maintains information in mind for brief periods of time (Fuster and Alexander 1971; Kubota and Niki 1971). With the advance of functional magnetic resonance imaging (fMRI), a mounting literature now documents how a variety of cognitive processes are linked to specific parts of the brain (Cohen et al. 1993; Jonides et al. 1993; McCarthy et al. 1994; Bush et al. 2000; Corbetta and Shulman 2002; Cole and Schneider 2007; McNab and Klingberg 2008; Ginestet and Simmons 2011; Cole et al. 2012). According to this literature, in the vast majority of cases, cognitive processes appear to engage cortical regions, often in dorsal portions of the brain (Fig. 1.1).

The definition of emotion includes the concepts such as drive and motivation (states elicited by rewards and punishements) (Rolls 2007), conscious (or unconscious) evaluation of events (that is, appraisals) (Arnold 1960), basic emotions (for example, fear or sadness) (Ekman 1992) and moral (for example, pride and envy) (Moll et al. 2005).

Brain structures linked to emotion are both subcortical, such as the amygdala, ventral striatum and hypothalamus and cortical, such as orbitofrontal cortex, ventral anterior cingulate cortex, medial prefrontal cortex, and anterior insular cortex (Bush et al. 2000; Liotti et al. 2000; Shin LM et al. 2005; Viard et al. 2007; Drevets et al. 2008; Lang and Bradley 2010).

Previous work has studied the effect of emotions on cognitive functions (Dolan 2002; Bechara 2004; Smith et al., 2004; 2005; Erk et al., 2003; 2005). Behavioral studies have found attenuated spatial working memory (WM) performance during negative task-irrelevant affect (Dolcos et al., 2006, Dolcos and McCarthy 2006, Lavric et al., 2003, Schaefer et al., 2006 and Shackman et al 2006), although this effect was absent in verbal WM (Lavric et al., 2003, Shackman et al., 2006, Simon-Thomas and Knight, 2005 and Simon-Thomas et al., 2005). The authors suggest that this effect is due to competition for limited visuospatial attention resources (Lavric et al., 2003, Shackman et al., 2006). Nevertheless, there is some evidence showing more marked disruption of verbal WM, as compared to spatial WM, in conditions of anxiety (Ikeda,et al. 1996; Markham and Darke, 1991). Some of these studies also present functional neuroimaging results suggesting that emotional distractors affected the activity in dlPFC (Perlstein et al., 2002, Dolcos et al., 2006, Dolcos and McCarthy 2006, Dolcos et al., 2008). Using task-relevant stimuli, Perlstein and colleagues show that the dlPFC activity was influenced by the emotional valence of the stimuli: it was enhanced by pleasant and reduced by unpleasant stimuli (Perlstein et al., 2002). In more recent studies, Dolcos and collaborators have studied the effect of distractors, showing that the presence of negative emotional distractors was associated with impairments in cognitive performance and a marked decrease in dlPFC activity (Dolcos et al., 2006, Dolcos and McCarthy, 2006, Dolcos et al., 2008). However, most of these studies were performed using task-irrelevant aversive stimuli, task-relevant emotional stimuli or inducing anxiety during the WM task, therefore, are subject to possible confounds due to attention capture by the noxious stimulus.

As described above, the early view of the brain organization supported the notion that there is a considerable degree of functional specialization and that many regions can be conceptualized as either “affective” or “cognitive” (Fig. 1.1A) (Damasio 1994; Drevets and Raichle 1998; Bush et al. 2000). However, subdivision of the brain in "emotional brain" and "cognitive brain" has been questioned, based on the fact that brain regions viewed as "affective" are also involved in cognition and vice versa, and in most of the daily activities, cognition and emotion are integrated in the brain (Fig. 1.1B) (Young et al. 1994; Phelps 2006; Pessoa 2008). To study the functional organization of emotional and cognitive networks, the graph theory approach could be an appropriate method.

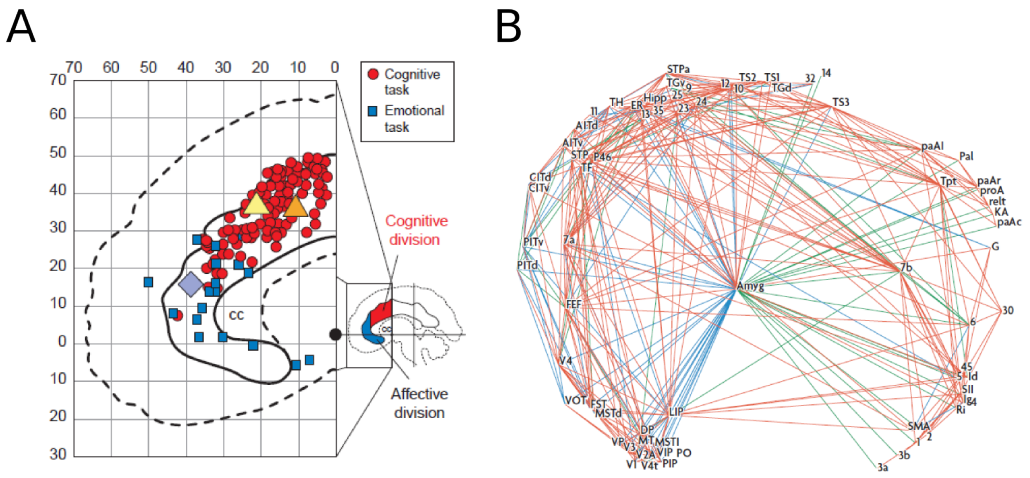

Figure 1.1: Specialization and integration, two brain organization views.
A. Activations during cognitive tasks (red circles) and during emotional tasks (blue squares) in anterior cingulate cortex. Note a clear distinction between the “affective division” and “cognitive division”. **B.** Brian connectivity graph, quantitative analysis of brain connectivity reveals several clusters of highly interconnected regions (represented by different colors). The amygdala (Amyg. Centre of figure) was connected to all but 8 cortical areas, involving multiples region clusters. Figure adapted from Bush et al., 2000 and Young, 1994, respectively.

Graph theory

We have known since the nineteenth century that the neuronal elements of the brain constitute a formidably complicated structural network (Cajal 1902, 1909, 1928). Since the twentieth century it has also been widely appreciated that this anatomical substrate supports the dynamic emergence of coherent physiological activity, such as phase-locked high-

frequency electromagnetic oscillations, that can span the multiple spatially distinct brain regions that make up a functional network (Singer 1999; Varela et al. 2001; Fries 2005). Such networks are thought to provide the physiological basis for information processing and mental representations (Bressler 1995; Rodriguez et al. 1999).

Recent developments in the quantitative analysis of complex networks, based largely on graph theory, have been rapidly translated to studies of brain network organization. Graph theoretical approaches to the analysis of complex networks provide a powerful new way of quantifying the brain's structural and functional systems (Bassett and Bullmore 2009; Bullmore and Sporns 2009; Sporns 2014).

In the graph theory a network is defined by a collection of nodes (vertices) and edges (connections). Depending on the technical approach, structural and functional brain networks can be explored using graph theory (Bullmore and Sporns 2009; Rubinov and Sporns 2010). Structural networks are commonly extracted from histological (tract tracing) or neuroimaging (diffusion tensor (or spectrum) imaging) data. Functional networks are commonly extracted from neuroimaging (fMRI) or neurophysiological (electroencephalography (EEG), magnetoencephalography (MEG)) data (Bassett and Bullmore 2009; Rubinov and Sporns 2010). In addition to the type of connectivity, edges are also differentiated on the basis of their weight and directionality. Binary edges denote the presence or absence of connections, while weighted edges contain information about connection strengths (Rubinov and Sporns 2010). The directionality of the edges differentiates between directed and undirected graphs. For directed graphs the adjacency matrix (which indicates the number of edges between each pairs of nodes in a graph) is asymmetrical and for undirected graph the adjacency matrix is symmetrical (Rubinov and Sporns 2010).

The brain's structural and functional systems have features of complex networks — such as small-world topology, highly connected hubs and modularity — both at the whole-brain scale of human neuroimaging and at a cellular scale in non-human animals (Sporns et al. 2004, 2007; Rubinov and Sporns 2010).

Network analysis of blood-oxygen level dependent (BOLD) time series has focused on characterizing the large-scale properties of the neutral state datasets, in which participants lie passively in the scanner without performing an explicit task (Wang, Zuo, et al. 2010).

Recently, graph theory work suggests that the functional architecture of the human brain is modulated by age (Achard and Bullmore 2007; Meunier et al. 2009), sex (Tian et al. 2011), intelligence (Heuvel et al. 2009), genetic predisposition (Fornito et al. 2011), development (Hwang et al. 2013) and brain disorders (Liu et al. 2008; Lynall et al. 2010; Sanz-Arigita et al. 2010).

Moreover, recent studies are also reporting the modulation of brain topologies constructed from fMRI data during active task performance: for instance, during working memory (Wang, Li, et al. 2010), visual stimulation (Moussa et al. 2011), motor learning (Bassett et al. 2011; Heitger et al. 2012), auditory stimulation (Ma et al. 2012) and emotion processing (Kinnison et al. 2012).

In the first section of this thesis we combine a paradigm design and graph theory method to explore the network topology underlying the competitive interactions between emotional and cognitive networks with functional magnetic resonance imaging (fMRI). It was designed as a paradigm with a strong conflicting emotional and cognitive demand, with a purely emotional task, Sadness Provocation (Liotti et al. 2000) followed by a purely cognitive task, spatial working memory (McNab and Klingberg 2008).

The hypothesis is that a paradigm with a strong conflicting emotional and cognitive demand would enhance the modularity of emotional and cognitive brain networks in healthy participants and thus reveal the cortical areas that act as network hubs, which are critical for regulating the flow and integration of information between communities (Sporns et al. 2007). In addition, our approach would reveal if the hubs are being modulated according to emotional or cognitive demands (Cole et al. 2013). Our underlying assumption was that in strong emotional states the system is pushed towards a depression-like physiopathology, so that this study's results can be relevant to generate hypotheses for MDD.

Major depressive disorder

Major depressive disorder (MDD) is a disabling psychiatric condition with high prevalence and representing a clinical and economic burden. MDD is the most common of all psychiatric disorders (Kessler et al. 2003), characterized by persistent negative mood and selective deficits in cognitive, circadian, and motor functions. MDD is characterized by its

relapsing dynamics, psychiatric studies revealing high rates of relapse, up to 75%, and extensive disability or suicide in over 20% of cases (Kennedy et al. 2003; Furukawa et al. 2009). As the duration of depressive episodes increases, the probability of recovery substantially decreases over time (Fig. 1.2) (Kendler 2000; Kendler et al. 2001).

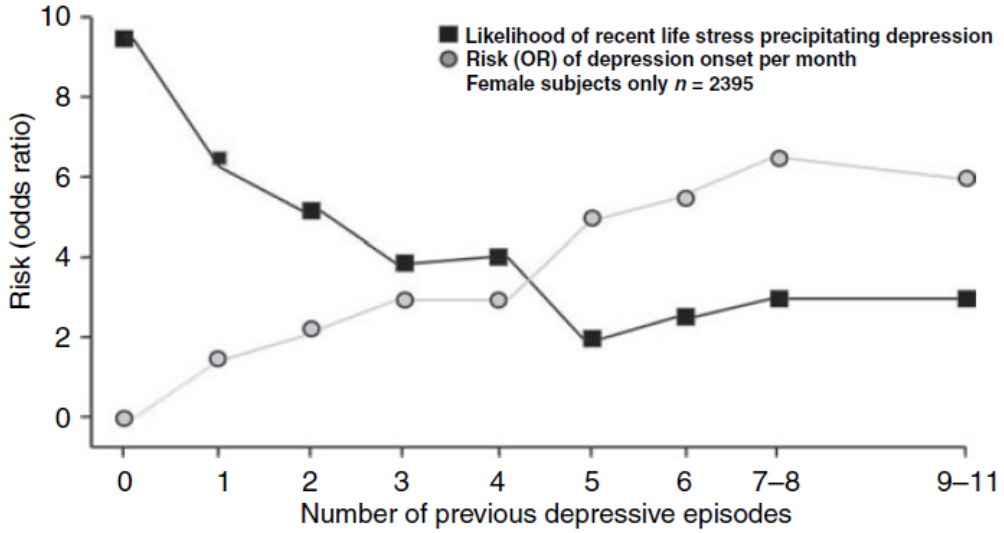

Figure 1.2: Major depression as a progressive illness.
As the number of major depressive episodes increase, the risk for subsequent episodes is predicted more from the number of prior episodes and less from the occurrence of a recent life stress. Figure adapted from Maletic et al., 2007 and Kendler et al., 2001.

While much evidence related to MDD has been acquired using a broad range of methods, there is no single mechanistic model able to integrate and explain the variety of observations. In the second section of this thesis, I built a computational model of MDD, based on the results from the neuroimaging analysis section and from the following evidences from MDD patients.

Ventral anterior cingulate cortex is a critical hub in MDD

Converging clinical, biochemical, neuroimaging, and postmortem evidence demonstrate cortical, subcortical and limbic involvement in the physiopathology of MDD (Mayberg 1997; Manji et al. 2001; Vaidya and Duman 2001; Nemeroff 2002; Nestler et al. 2002).

Furthermore, multiple studies point at the ventral anterior cingulate cortex (vACC) as the critical hub within this distributed network of regions that drives alterations in system dynamics in MDD. For one, the vACC is consistently involved in acute sadness (Mayberg et al. 1999; Liotti et al. 2000). Secondly, neuroimaging studies reveal hyperactivity of vACC in MDD patients (Fig.1.3A) (Mayberg et al. 1999, 2005; Seminowicz et al. 2004). Thirdly, vACC hyperactivity is reduced after clinical response to MDD treatments: selective serotonin reuptake inhibitors (SSRIs) medication (Fig.1.3B) (Mayberg et al. 2000; Drevets et al. 2002; Goldapple et al. 2004), electroconvulsive therapy (ECT) (Nobler et al. 2001), repetitive transcranial magnetic stimulation (rTMS) (Mottaghy et al. 2002; Fox et al. 2012), ablative surgery (Malizia 1997; Dougherty et al. 2003), vagus nerve stimulation (Pardo et al. 2008), and deep brain stimulation (DBS) (Fig.1.3C) (Mayberg et al. 2005). In addition, patients responding to treatment differed from non-responders in network subsystems involving both limbic afferents and cortical efferents of vACC (Seminowicz et al. 2004). Finally, the vACC drives the dynamics of default mode network (DMN) in resting depressed patients in correlation with the length of their depressive episodes (Greicius et al. 2007).

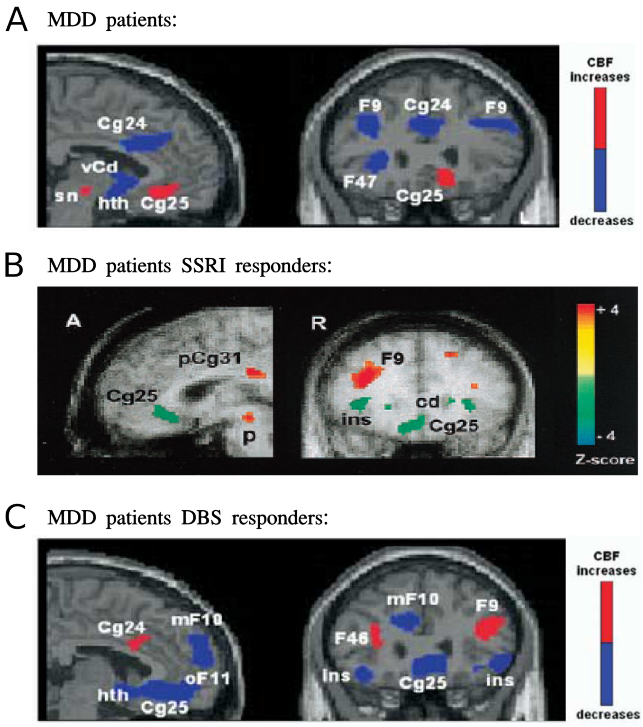

Figure 1.3: The vACC and dlPFC activities characterize the brain images patterns in MDD.

A. Cerebral blood flow (CBF) changes in MDD patients show vACC hyperactivity and dlPFC and dACC hypoactivity.

B. Positron emission tomography (PET) changes in treatment responders following 6 weeks of fluoxetine show decrease in the vACC activity and increase in dlPFC activity relative to the baseline.

C. CBF responders following 3 months of DBS, show decrease in the vACC activity and increase in dlPFC activity relative to the baseline.

Figure adapted from Mayberg et al., 2005 and Mayberg et al., 2000.

Also, in rodent models of depression optogenetic stimulation in the medial prefrontal cortex (homologous to vACC in humans) modulates depression-related behavior (Covington et al. 2010; Warden et al. 2012; Kumar et al. 2013).

Dorsolateral prefrontal cortex presents activations opposed to vACC

On the other hand, MDD is also characterized by hypoactivity in both dorsal anterior cingulate cortex (dACC) and dorsolateral prefrontal cortex (dlPFC) (Fig.1.3A)(Bench et al. 1992; Mayberg 1997; Kennedy 2001; Videbech et al. 2002; Oda et al. 2003; Mayberg et al. 2005; Brooks et al. 2015) which is reverted after successful treatment with serotonergic medications (Fig.1.3B) (Mayberg et al. 2000; Kennedy 2001; Botteron et al. 2002; Vlassenko et al. 2004), and DBS (Fig.1.3C) (Mayberg et al. 2005).

This opposite alteration of dlPFC and vACC in MDD seems to reflect an operating principle of these networks, rather than disease-dependent impairments specific to each area. Indeed, in healthy humans the vACC routinely increases its activity in response to emotional tasks (Fig. 1.1A) (Drevets and Raichle 1998; Bush et al. 2000; Liotti et al. 2000; Smith et al. 2011) and it reduces its activity upon cognitive demands (Drevets and Raichle 1998; Bush et al. 2000; Simpson et al. 2001). Conversely, dlPFC activates typically in cognitive tasks (Cohen et al. 1993; Jonides et al. 1993; McCarthy et al. 1994), and it decreases its activation in emotional tasks (Perlstein et al. 2002; Dolcos and McCarthy 2006; Dolcos et al. 2008).

In addition to their opposite functionality, the vACC and dlPFC are intrinsically anticorrelated during spontaneous activity in depressed patients (Fox et al. 2012), often embedded in larger networks of consistently correlated areas (for instance DMN (Raichle et al. 2001; Greicius et al. 2003; Fox and Raichle 2007) and cognitive control network (Cole and Schneider 2007; Cole et al. 2012), respectively). We hypothesize that this anticorrelation is a result of mutual disynaptic inhibition between vACC and dlPFC. Two lines of evidence give support to this mechanistic hypothesis. For one, there is an anatomic substrate for such mutual interaction in that vACC has prevalent, large synapses onto inhibitory neurons in dlPFC (Medalla and Barbas 2010). For a second, the sites of strongest

anticorrelation in dlPFC and vACC are the locations where TMS has the best clinical efficacy in depressed patients (Fig.1.4) (Fox et al. 2012).

Figure 1.4: Anticorrelated activity between vACC and dlPFC in MDD patients.
Regional time courses were extracted from a seed region in the subgenual cingulate and used to identified the peak anticorrelation in the left dorsolateral prefrontal cortex (arrow) that serve as optimized targets for focal brain stimulation.
Figure adapted from Fox et al., 2012.

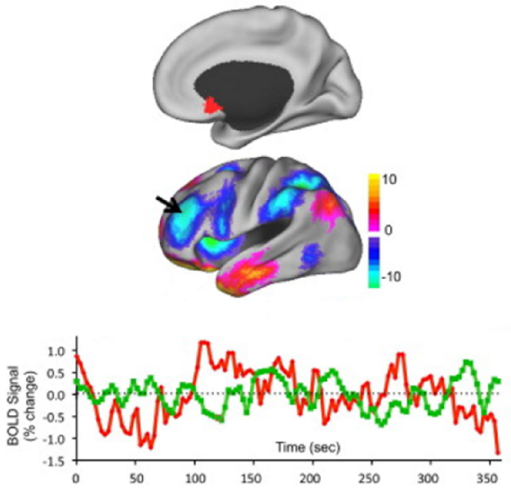

Oscillations in the cingulo-frontal network

In line with this hypothesis, EEG and MEG studies demonstrate the coordination of oscillatory activity in prefrontal and anterior cingulate cortex in the time scales of synaptic interactions during focused attention: Rhythmic cortical activation at 4-8 Hz is generated between these two regions in what is usually termed frontal midline theta (Asada et al. 1999; Tsujimoto et al. 2006; Hsieh and Ranganath 2014); and alpha (8-12 Hz) and beta/low-gamma (12-40 Hz) synchronization, characteristic of cognitive operation in the fronto-parietal network (Ray and Cole 1985; Siegel et al. 2012), is recruited by negative valence information in vACC (Lipsman, Kaping, et al. 2014). Importantly, alterations of these fast circuit dynamics are associated with MDD: the amplitude of the theta vACC rhythm in MDD patients has been shown to correlate with treatment outcome (Fig.1.5A) (Pizzagalli et al. 2001; Mulert et al. 2007; Iosifescu et al. 2009; Korb et al. 2009; Pizzagalli 2011; Broadway et al. 2012), and beta band activity in frontal scalp electrodes correlates positively with the severity of depression (Fig.1.5B) (Pizzagalli et al. 2002).

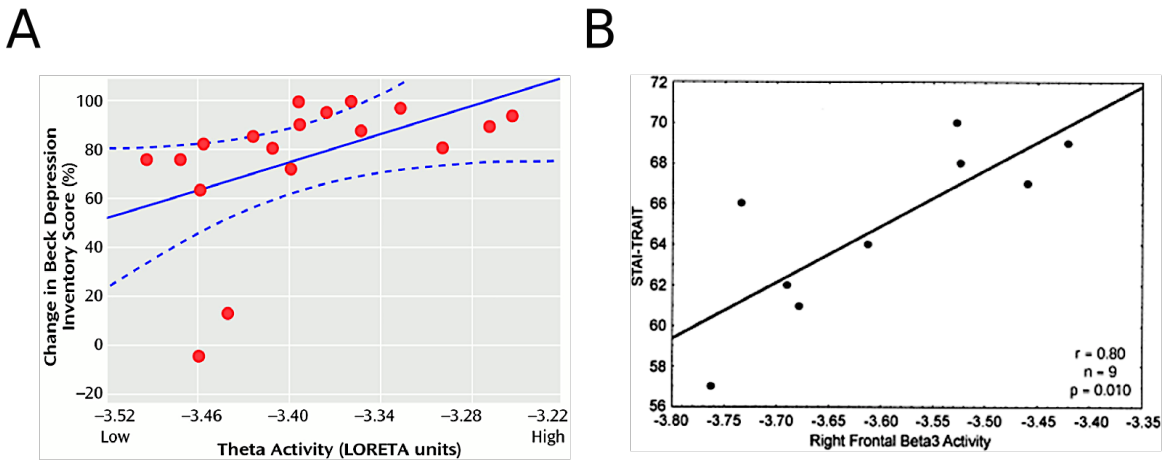

Figure 1.5: Oscillations in MDD patients.
A. Theta in vACC predicted degree of treatment response. **B.** Beta band correlates with depression severity. Figure adapted from Pizzagalli et al., 2001 and 2002, respectively.

Mechanism behind vACC dysfunction

In addition to systems-level anomalies, a picture of cellular and synaptic vACC dysfunction in MDD is now emerging. Smaller vACC volume characterizes MDD in neuroanatomical studies (Drevets et al. 1997; Botteron et al. 2002; Hastings et al. 2004; Yucel et al. 2008), partly reflecting a reduction in glial cell density and neuronal soma size (Ongür, Drevets, et al. 1998; Rajkowska et al. 1999; Cotter et al. 2001; Manji et al. 2001). Functionally, the down-regulation of the glutamine synthetase and glial high-affinity glutamate transporters (Choudary et al. 2005) suggests increased glutamatergic activity in the synaptic cleft in MDD patients (Fig.1.6). Additional converging evidence points at altered glutamatergic metabolism as a mediator of MDD pathology (Sanacora et al. 2012). Indeed, the

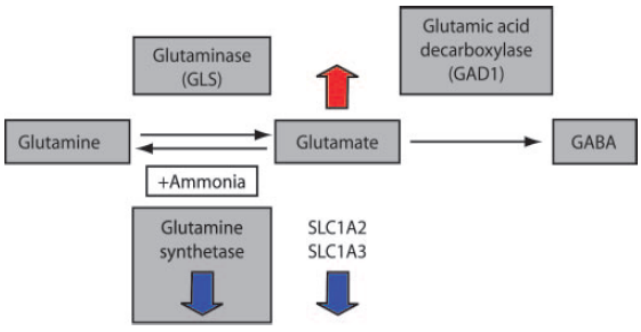

Figure 1.6: Schematic drawing showing the metabolic steps, substrates and enzymes involved in glutamate recycling.
The down-regulation of the glial high-affinity glutamate transporters and glutamine synthetase are shown blue arrow pointing down and potentially accumulating glutamate levels are shown by orange arrow pointing up. Figure adapted from Choudary et al., 2005.

progressive nature of MDD (Keller et al. 1992; Kendler 2000; Kendler et al. 2001) has been correlated with progressive change of glutamate metabolism in vACC (Portella et al. 2011), and in resting-state studies glutamate metabolism alterations correlate with vACC hyperactivation and MDD symptoms (Walter et al. 2009; Horn et al. 2010).

Mechanism of serotonin treatment on vACC

Selective serotonin reuptake inhibitors (SSRIs) is the first-line treatment for depression, although antidepressant efficacy is comparable among the different classes of drugs (Steffens et al. 1997), the SSRIs appear to be more effective that tricyclic antidepressants in clinical practice due to their relatively greater safety and tolerability (Simon et al. 1996). Nonetheless, 29% to 46% of the depressed patients fail to respond fully to antidepressant medication. Specifically, it has been suggested that 12% to 15% are partial responders and 19% to 34% are non-responders (Fava and Davidson 1996; Fava 2003).

Our understanding of the mechanisms of serotonin treatments in MDD is still evolving. The uneven distribution of serotonin receptors in the cingulate gyrus, with the highest density of 5-HT_{1A} receptors in the vACC (Santana et al. 2004; Palomero-Gallagher et al. 2009), suggests that the selective action of SSRI treatments might be mediated by hyperpolarization of vACC neurons through the 5-HT_{1A} receptor (Fig 1.3B) (Andrade et al. 1986; Béïque et al. 2004; Castañé et al. 2015).

Deep brain stimulation for treatment-resistant patients

High-frequency DBS in the subgenual white matter has been reported as an effective strategy for treatment-resistant patients (Mayberg et al. 2005; Lozano et al. 2008; Kennedy et al. 2011). Chronic stimulation of the subgenual cingulate white matter was associated with remission of symptoms, marked reduction in vACC activity and increase in dlPFC activity relative to the baseline (Fig 1.3C) (Mayberg et al., 2005). The effective action of DBS mainly targets the subgenual portion of ACC (vACC) (Johansen-Berg et al. 2008). Current evidence suggests mainly two possible mechanism for the DBS therapeutic action; one plausible scenario is that DBS may result in the activation of interneurons in vACC

(Mayberg et al. 2005), another possible scenario is that the response to DBS is mediated by the serotonergic system (Hamani et al. 2010, 2012). In rodent model, activation of specific mPFC subregions or projections is likely to have differential effects on depression-related behavior (Vidal-Gonzalez et al. 2006; Sierra-Mercado et al. 2011). Optogenetic stimulation of specific glutamatergic mPFC projections to either the dorsal raphe nucleus or the lateral habenula has been shown to lead to increased or decreased escape-related activity in the forced-swim test, respectively (Warden et al. 2012). Other studies (Covington et al. 2010; Kumar et al. 2013) have shown that optogenetic stimulation of mPFC neuronal cell bodies reduces depression-related behavior.

Anatomy of cingulo-frontal network

Anatomically, the vACC includes the BA25 and the ventral portions of BA32 and BA24 and has been described as both a visceral-motor (Freedman et al. 2000; Öngür and Price 2000) and emotional-centric region (Bush et al. 2000) and the dlPFC includes the BA46 and BA9 and has been described as a cognitive region (MacDonald et al. 2000; Cole and Schneider 2007). There is experimental evidence for anatomical connections between these two regions. While only weak evidence of direct projections between BA25 and BA9 has been reported (Vogt and Pandya 1987; Barbas et al. 1999), BA25 is instead densely connected with BA32 (Barbas and Pandya 1989), which in turn is well connected with BA9 and targets preferentially BA9 inhibitory neurons (Barbas and Pandya 1989; Barbas et al. 1999; Medalla and Barbas 2010). These connections provide an effective inhibitory interaction between vACC and dlPFC.

Note that for the brain images analysis we use the term subgenual anterior cingulate cortex (sACC), which refers specifically to BA25. Due to good spatial resolution of the fMRI, we use a precise anatomy definition. For the computational modeling, as we mention above, we use ventral anterior cingulate cortex (vACC), which is an area defined functionally and that includes 3 brodmann areas.

Cingulo-frontal computational model for MDD

Taken together, these data indicate that the vACC and its interactions with the dlPFC play a key role in the brain-network dynamics abnormalities that subserve MDD and the associated cognitive deficits, and in the outcome of treatments. We hypothesized that MDD would be caused by unbalanced mutual inhibition between emotional (vACC) and cognitive (dlPFC) networks due to deficient glutamate reuptake in vACC. In this view, vACC and dlPFC circuits, as critical hubs of larger computing networks, serve a "switch-like" function of driving the computations being carried out in larger distributed networks, and hyperactivation of the vACC would result in exacerbated emotional and deficient cognitive processing.

The wealth of converging evidence onto specific mechanisms suggests that a computational modeling approach may be able to integrate these data, test the hypotheses dynamically and provide a detailed mechanistic understanding of MDD on which to base model-derived hypotheses for further experiments. In the second part of this thesis, we provide here a biophysical computational model of MDD pathophysiology based on the neural dynamics within vACC and between vACC and dlPFC, and their modulation by glutamate metabolism deficits and serotonergic treatments. Our cingulate-frontal network model can integrate coherently the core clinical symptoms, disease progression, electrophysiology and the response to SSRI treatments in MDD.

Objectives

1. To identify the hubs of cognitive and emotional networks in the brain and their modulation by emotional and cognitive demand.
    a. To design a behavioral paradigm which enhances the competitive interaction between emotional and cognitive networks.

    b. To perform an *fMRI* experiment with healthy participants under highly competitive emotional and cognitive demands.

    c. To preprocess and analyze the *fMRI* data in order to determine the brain areas activated and their functional connectivity during the paradigm.

    d. To apply network measures from graph theory, to determine the community structure and the modularity of emotional and cognitive networks.

2. To apply a neurobiological modeling approach constrained with anatomical, electrophysiological and functional imaging data to build a computational model of Major Depression Disorder.
    a. To understand the role of the glutamate dysfunction in MDD using a biophysical computational model of the cingulo-frontal network

    b. To understand the network mechanism of vACC in the progressive nature of MDD.

    c. To understand the network mechanism by which serotonin treatment can alleviate the symptoms in MDD.

    d. To understand the network mechanism by which DBS treatment can alleviate the symptoms in MDD treatment-resistant patients.

    e. To identify network mechanism underlying the pattern of oscillatory brain activity in MDD.

Materials and Methods

Methods for brain images analysis

Participants

Twenty-two healthy subjects (average age and standard deviation 28.9 ± 3.9 years of age, 10 males) without any psychiatric, neurological or medical illness were recruited. All participants were screened with the Mini-International Neuropsychiatric Interview (M.I.N.I.) to specifically ensure the absence of any ICD-10 psychiatric disorders (Sheehan et al. 1998) as well as those using psychoactive medications. All subjects were screened with Charlson comorbidity index (Charlson et al. 1987). All volunteers had normal or corrected-to-normal vision and were right-handed, native Spanish speakers. The study was approved by the IRB of the Hospital Clinic of Barcelona and written informed consent was obtained from all participants. Participants were requested to avoid moving during the whole MRI scan.

Experimental Design

The study was composed of two different paradigms (Fig. 2.1). In the first paradigm, subjects were first instructed to rest in a "neutral emotional state" while keeping their eyes closed in a 2-min neutral-state scan. Following this resting condition, a spatial working memory task (WM1) with a filtering component was carried out during scanning. Twenty working memory trials with a pseudo-randomly stimulus were used following previous studies (McNab and Klingberg 2008). In brief, 5 dot stimuli were presented for 1-sec at random locations in a grid of 16 possible positions. Of these stimuli, three were red dots and two were yellow dots. Participants were instructed to remember only the position of the red dots. Stimuli were followed by a dark screen during a delay of 4 seconds and then a probe stimulus was displayed for 4 sec. at one grid location (Fig. 2.1). On presentation of the probe stimulus, participants were required to make a button press with the index or middle finger of their right hand, depending if one of the red dots had been presented at the location indicated by the probe (yes or no).

In 25% of the trails, a yellow dot would have been presented at the location indicated by the probe. In these trials, an error response of the participants (yes response) indicates a failure

to apply the filtering component of the task. We define this type of error as a cognitive inhibition error (McNab and Klingberg 2008; Gohier et al. 2009).

In the second paradigm, participants performed an emotional task, the sadness provocation task (SP) (Liotti et al. 2000). All subjects had prepared in advance a short autobiographical narrative of personal events in which they felt particularly sad, e.g. sad experiences most commonly centered on loss of relatives, friends, or significant relationships. Before all "sad scans", the narrative texts were presented on the screen. Subjects were asked to generate a state of sadness comparable to that originally experienced. After the maximum mood intensity was achieved, the subjects closed their eyes and were instructed to stop visualizing, thinking, or ruminating on the text and to focus on their feelings of sadness in a 2-min neutral-state scan. After the sadness scan the subjects performed a second spatial working memory task (WM2) with filtering component, identical to that described in the first paradigm. After the scan session, participants performed a rating of the sadness intensity reached (level of sadness on a 0–7-point scale, average sadness intensity and standard deviation 5.6 ± 0.8) (Brans and Verduyn 2014).

All participants trained for all tasks on the days before the scanner session. We did not reverse the order of the paradigms, to avoid the sadness affect on the Neutral-WM1 paradigm.

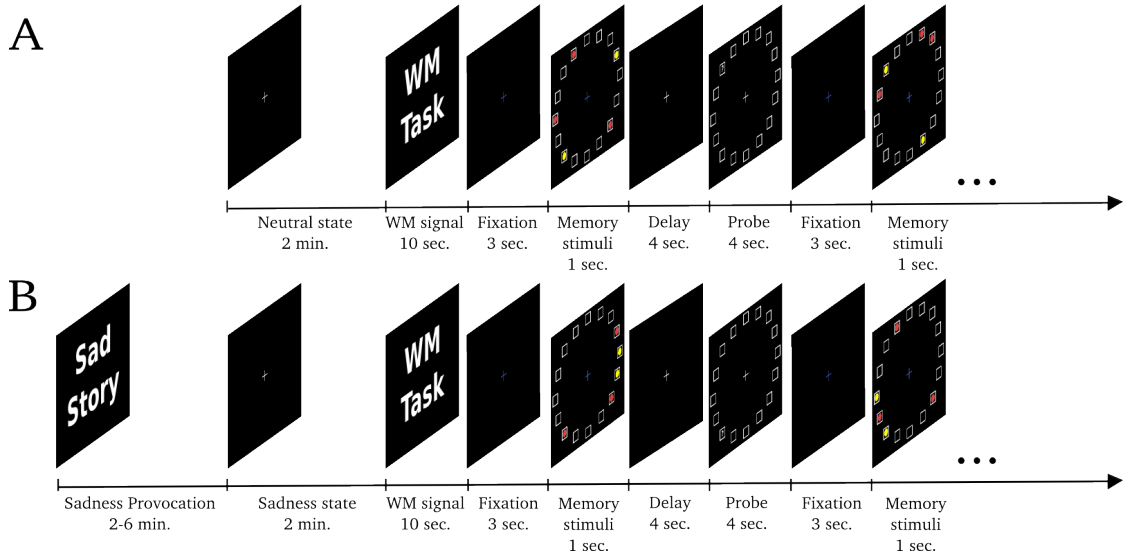

Figure 2.1: Sadness makes the difference between the two paradigms.
A. The first paradigm is composed of two tasks, a neutral state followed by twenty trials of spatial working memory with filtering component. **B.** In the second paradigm, the participants underwent a sadness provocation task. When maximal sadness was achieved, participants closed their eyes for a 2-min scan, which was then followed by another twenty trials of spatial working memory with filtering component. Note that in both paradigms the same stimuli were presented, the only difference being the sadness induced before the second paradigm.

Behavioral analysis

Two participants were excluded from the behavioral analysis because they reported difficulty in distinguishing the color of the dots during the working memory tasks. We measured working memory performance through the fraction of errors, the reaction times and the fraction of cognitive inhibition errors for each subject in WM1 and WM2.

Participants were divided into two groups depending on their sadness intensity: "*high-sadness* group" were those whose subjective sadness rating ranked above the overall mean (range 6-7) and "*low-sadness* group" were those participants whose rating ranked below the mean (range 4-5.5).

A 2-factor ANOVA was used to statistically assess the interaction between working memory performance (fraction of errors in WM1 and WM2) and sadness intensity (*high-sadness* group and *low-sadness* group).

fMRI acquisition

Brain images were acquired on a 3 Tesla TimTrio scanner (Siemens, Erlangen, Germany) using the 8-channel phased-array head coil supplied by the vendor. A custom-built head holder was used to prevent head movement, and earplugs were used to attenuate scanner noise. High-resolution three-dimensional T1-weighted magnetization prepared rapid acquisition gradient echo (MPRAGE) images were acquired for anatomic reference (TR=2200ms, TE=3ms, FA=7^{o}, 1.0mm isotropic voxels). T2-weighted scan was used in order to identify pathological findings (TR=3780ms, TE=96ms, FA=120^{o}, voxel size 0.8x0.6x3.0mm, 3.0mm thick, 0.3mm gap between slices, 40 axial slices). Functional data were acquired using a gradient-echo echo-planar pulse sequence sensitive to blood oxygenation level-dependent (BOLD) contrast (TR=2000ms, TE=30ms, FA=85^{o}, 3.0mm isotropic voxels, 3.0mm thick, no gap between slices). Presentation® fMRI task paradigm software and data acquisition was synchronized to stimulus pulse sent by the scanner. Head motion was restricted using a pillow and earplugs were used to attenuate scanner noise.

fMRI data analysis

Preprocessing and statistical analysis were carried out with SPM8 (Welcome Department of

cognitive Neurology, http://www.fil.ion.ucl.ac.uk/spm). Preprocessing included alignment along the anterior commissure-posterior commissure line and realignment of the scans for motor correction, normalization to the Montreal Neurological Institute (MNI) template (interpolating to 3-mm cubic voxels) and spatial smoothing with a Gaussian kernel of 10-mm. For the functional connectivity analysis the spatial smoothing was not applied.

A random-effect, epoch-related statistical analysis was performed in a two-level procedure. At the first level, a general linear model (GLM) was estimated by using regressors for each instruction condition, neutral and sadness epochs, and fixation period, memory stimulus, delay period and probe stimulus. Regressors were convolved with a canonical hemodynamic response function. The data were high-pass filtered (128 s cutoff) to remove low-frequency drifts.

Images from contrasts of interest for each participant were used in a second-level analysis, treating participants as a random effect. A paired sample t-test was used to investigate the resulting statistical maps for the contrast *delay-fixation* in WM1 and WM2. The voxel significance was evaluated in a whole-brain analysis testing the global null hypothesis that *delay-fixation* showed no significant activation. This analysis was corrected for multiple comparisons (false discovery rate (FDR), $P < 0.05$). This analysis led us to identify 10 different cortical areas implicated in cognitive processing in this task (see Table 2.1).

Subsequently, a paired sample t-test was used to statistically assess the difference between delays of WM1 and WM2. A mask was created including the activated areas in both WM1 and WM2 in order to compare the difference in the level of activation between WM1 and WM2. The voxel significance was evaluated in the mask testing the global null hypothesis that $delay_{WM1}$- $delay_{WM2}$ did not show significant activation. This analysis was corrected for multiple comparisons in the working memory mask (false discovery rate (FDR), $P < 0.05$).

We used a 2-factor ANOVA to statistically assess the interaction between delay activity in the two tasks ($delay_{WM1}$ and $delay_{WM2}$) and sadness intensity (*high-sadness* and *low-sadness* groups). The voxel significance was evaluated in a mask testing the global null hypothesis that $delay_{WM1}$ - $delay_{WM2}$ and *high-sadness* - *low-sadness* groups did not show significant interactions.

We further used a 2-factor ANOVA to statistically assess the interaction between brain activity in the passive conditions (*Neutral* and *Sadness*) and sadness intensity (*high-sadness*

and *low-sadness* groups). Voxel significance was evaluated in a whole-brain analysis testing the global null hypothesis that the interaction between *Sadness/Neutral* and *high-sadness/low-sadness* groups was not significant. This analysis led us to identify 9 different cortical and subcortical areas implicated in emotional processing in this task ($P_{unc} < 0.05$) (see Table 2.1).

For the sACC, which shows significant interaction (small volume correction, 5 mm square at -6 21 -9, FWE-corrected, $p = 0.038$), a paired sample t-test was used to statistically assess the difference between *Sadness* and *Neutral* epochs in the *high-sadness* group.

Functional connectivity

Cognitive and emotional regions of interest (ROIs) were determined from global analysis as indicated above (see list of ROIs in Table 2.1). Some areas known to be related to emotional processing did not survive to the correction by multiple comparisons; medial orbitofrontal gyrus left, subgenual anterior cingulate cortex right, medial frontal pole bilateral, hippocampus bilateral and amygdala bilateral. Medial orbitofrontal gyrus right did not show significant activation and was added as a cortical counterpart of the medial orbitofrontal gyrus left. We check the locations of the emotional ROIs by using coordinates extracted from the literature (Bush et al. 2000; Liotti et al. 2000; Mayberg et al. 2005; Shin LM et al. 2005; Viard et al. 2007; Drevets et al. 2008). Each ROI was defined as a 5 x 5 x 5 voxel cube centered around the detected peak activations (for coordinates see Table 2.1).

The ROI signals were obtained by linear detrending preprocessed data without spatial smoothing for each voxel, and then by averaging across all voxels within the ROI. We removed covariations common to all ROIs by applying a global signal regression (Fox et al. 2009; Keller et al. 2013). This procedure removes global fluctuations variability related to physiological artifacts such as heart rate, respiration, and scanner noise that are seen throughout the brain artificially but could also introduce spurious anticorrelations (Fox et al. 2009; Murphy et al. 2009; Anderson et al. 2011). It has been reported that this preprocessing step can improve the specificity of resting state correlations and the correspondence with anatomy (Fox et al., 2009) and electrophysiology (Keller et al., 2013). Due to possible spurious anticorrelations, in our analysis we focus on comparisons between correlations rather than the actual quantitative value of measured correlations and in

addition, we repeated the analysis without global signal regression, showing that the anticorrelations presented in this thesis are not due to the preprocessing step (Discussion).

To focus on temporal fluctuations of the BOLD signal not related to the imposed structure of the task (change of task in a time scale of 2 min) ROI signals were band-pass filtered in the range 0.018 – 0.26 Hz (i.e. maintaining temporal fluctuations in time scales from 4 seconds to 1 minute, approximately). As a proxy for functional connectivity between areas, we used the Pearson correlation coefficient between signals for each pair of ROIs in our

Table 2.1: Regions identified in the task-based analysis

Regions	**Hemisphere**	**Abbrev.**	**MNI coordinates**		
			x	***y***	***z***
Dorsolateral prefrontal cortex (Middle frontal gyrus)	Left	dlPFCl	-45	24	30
	Right	dlPFCr	42	15	39
Inferior frontal gyrus	Left	iFGl	-33	22	0
	Right	iFGr	48	19	0
Medial superior frontal gyrus	Left	mSFGl	-7	27	45
	Right	mSFGr	8	35	42
Intraparietal sulcus	Left	IPSl	-33	-50	41
	Right	IPSr	40	-50	42
Postcentral gyrus	Left	PCGl	-33	-24	57
	Right	PCGr	54	-21	48
Subgenual anterior cingulate cortex	Left	sACCl	-5	22	-7
	Right	sACCr	15	28	-9
Medial frontal pole	Left	mFPl	-8	66	6
	Right	mFPr	8	66	9
Amygdala	Left	Amyl	-27	-12	-15
	Right	Amyr	27	-9	-18
Hippocampus	Left	Hipl	-18	-21	-27
	Right	Hipr	21	-21	-15
Medial orbitofrontal gyrus	Left	mOFGl	-15	48	-9
	Right	mOFGr	15	48	-9

database (Table 2.1) and in each of the two behavioral paradigms of our task (Fig. 2.1).
We tested the functional significance within our task of correlations between ROIs identified as hubs of the network (see below) with ANOVA tests. For sACCl-dlPFCl and sACCl-mFPl correlations, we ran a 3-factor ANOVA tests with the factors: paradigm (*Neutral-WM1* vs. *Sadness-WM2)*, sadness intensity (*high-sadness* vs. *low-sadness* groups) and participant identity as a random factor. The interaction between sadness intensity and paradigm was significant for both connections (false discovery rate (FDR), $P < 0.05$; p=0.0006 for sACCl-dlPFCl; $p = 0.0434$ for sACCl-mFPl), so we separated the data for each groups and we performed a paired sample t-test comparing correlations for different sadness groups and paradigms.

Inter-individual fMRI activation

In order to analyze the relation between the sACCl and dlPFCl BOLD activity during sadness and working memory we performed an inter-individual analysis. Then, we calculated de mean activity for Neutral, Sadness, WM1 and WM2 epochs. We subtracted Sadness-Neutral and WM2-WM1 for each subject and we obtained the Pearson and Spearman correlation coefficients across the population of subjects, and also separately for the "*high-sadness"* and *"low-sadness*" groups. To test if the difference in the correlations between *high-sadness* and *low-sadness* groups was significant we performed a permutation test, permuting data from the two groups and calculating the difference on the correlations between the random samples. We reported a significant difference if the difference of measure between groups was larger that 95% of the differences generated in random samples.

Graph analysis

We can study the structure of networks by representing them as graphs, which are the sets of vertices (or nodes, here equivalent to brain regions) and corresponding sets of edges (or connections, here equivalent to functional connections between ROIs) (Bullmore and Sporns 2009). For each subject and behavioral paradigm (Fig. 2.1), the correlation matrix

between our ROIs represents the adjacency matrix that summarizes the properties of the weighted graph that represents the corresponding brain network. The symmetrical adjacency matrix resulting from our undirected graph was characterized for have positive and negative weights. The algorithms used in graph analysis were chosen taking account the positive and negative weights (Rubinov and Sporns 2011).

As described below, basic graph measures such as community structure, quality of partition, node degree, participation coefficient and global efficiency were calculated using standard graph theory methods on Matlab (Brain Connectivity Toolbox developed by O. Sporns, Indiana University, Bloomington, IN; http://www.brain-connectivity-toolbox.net/) (Rubinov and Sporns 2010, 2011).

We calculated the community structure in the mean correlation matrix across subjects. To identify the best partition in modules (communities), we quantified communities by a quality function that compares the number of intra-community edges to what one would expect by chance, and we optimized this quality function. The quality of the partitions resulting from this method is often measured by the so-called modularity of the partition. The modularity of a partition is a scalar value between -1 and 1 that measures the density of links inside communities as compared to links between communities.

The code gets matrix *B* (defined by Eq. 1) by its input and implements a Louvain-like greedy community detection method using the modularity/quality matrix B that encodes the quality function *Q*, defined by summing over all elements *B (i,j)* such that nodes *i* and *j* are placed in the same community and dividing it by the overall sum (see Eq. 2) (Blondel et al. 2008).

$$B_{ij} = A_{ij} - \left(\frac{g^{+} \cdot k_i^{+} \cdot k_j^{+\mathrm{T}}}{\sum_{n \in N} k_n^{+}} - \frac{g^{-} \cdot k_i^{-} \cdot k_j^{-\mathrm{T}}}{\sum_{n \in N} k_n^{-}} \right), \tag{1}$$

where A is our adjacency matrix, $k^{+}_{i} = \sum_{j \in N} A^{+}_{ij}$ is the sum of the weights of the positive edges attached to node *i*, $k_I = \sum_{j \in N} A^{-}_{ij}$ is the sum of the weights of the negative edges attached to node *i*, and g^{+} and g^{-} are the resolution parameters that are assigned to positive and negative weights respectively.

$$Q = \frac{1}{\sum_{n \in N} k_n^+ + \sum_{n \in N} k_n^-} \sum_{i,j \in N} \left[B_{ij} \right] \delta(c_i - c_j), \tag{2}$$

The algorithm proceeds in two phases that are repeated iteratively. Assume that we start with a weighted network of N nodes.

1. First, assign a different community to each node of the network. So, in this initial partition there are as many communities as there are nodes. Then, for each node *i* we consider the neighbors *j* of *i* and we evaluate the gain of modularity that would take place by removing *i* from its community and by placing it in the community of *j*.

The node *i* is placed in the community for which this gain is maximum. If no positive gain is possible, *i* stays in its original community. This process is applied repeatedly and sequentially for all nodes until no further improvement can achieved and the first phase is then complete. This first phase stops when a local maximum of the modularity is attained, i.e., when no individual move can improve the modularity.

2. The second phase of the algorithm consists in building a new network whose nodes are now the communities found during the first phase. To do so, the weights of the links between the new nodes are given by the sum of the weight of the links between nodes in the corresponding two communities. Links between nodes of the same community lead to self-loops for this community in the new network.

Once this second phase is completed, it is then possible to reapply the first phase of the algorithm to the resulting weighted network and to iterate. It is denoted by "pass" a combination of these two phases. By construction, the number of meta-communities decreases at each pass. The passes are iterated until there are no more changes and a maximum of modularity is attained.

This code returns two values. An output vector S that encodes the obtained community assignments, with $S(i)$ identifying the community to which node *i* has been assigned and the output Q that gives the quality of the resulting partition of the network (see Eq. 2 above).

Once we calculated the community structure, we measured the degree and the participation coefficient of each node. These measurements were done using only the strongest (and most relevant) connections, using a threshold set at 30% to 45% of the strongest correlations in absolute value (both positive and negative correlations) of the adjacency

matrix for each subject.

The degree of a node is the number of links connected to that node. The degree has a straightforward neurobiological interpretation: nodes with a high degree are interacting, structurally or functionally, with many other nodes in the network. Connection weights are ignored in the calculation of the degree. Mathematically, the degree of a node *i* is defined as:

$$k_i = \sum_{j \in N} a_{ij},$$

(3)

In the results, we consider high-degree areas when their degree is greater than the network mean degree plus one standard deviation. These areas are candidates to be defined as hubs of the networks, as previously argued in the literature (Sporns et al. 2007).

The Participation coefficient is a measure of diversity of intermodular connections of individual nodes. This measure requires a previously determined community structure (see above). The weighted participation coefficient of the network is defined mathematically as

$$y_i = 1 - \sum_{m \in M} \left(\frac{k_i(m)}{k_i} \right)^2,$$

(4)

where M is the set of modules, and $k_i(m)$ is the number of links between i and all nodes in module m. Nodes with a high degree but with a low participation coefficient are known as provincial hubs, and they are likely to play an important part in the facilitation of modular segregation and interact strongly with nodes in its own module. On the other hand, nodes with a high degree and a high participation coefficient are known as connector hubs, and they are likely to facilitate global intermodular integration, i.e. they constitute very central nodes in the network that mediate intermodular interaction (Sporns et al. 2007).

The Global efficiency measures the average strength of the shortest paths in the network and can be interpreted as the overall “efficiency of communication” minimizing the cost of communication over the most direct paths in the networks. Global efficiency requires as inputs a measure of node dissimilarity, or the “cost” of a connection; which was defined as the inverse of the functional connection weight (i.e., $1/A_{ij}$). We calculate the Global efficiency for each community, separately. Since within each community most of the

functional connectivity weights are positive, negative weights were set to zero for this analysis (Rubinov and Sporns 2010). Note that a value of zero does not pose problems in this respect because in such cases the algorithm is designed to handle the exception (Brain Connectivity Toolbox developed by O. Sporns, Indiana University, Bloomington, IN). More formally, global efficiency *GE* is defined as follows:

$$GE = \frac{1}{n(n-1)} \sum_{\substack{i,j \in N \\ i \neq j}} \frac{1}{d_{ij}}, \tag{5}$$

where n is the number of nodes in the network, N is the set of nodes, and d_{ij} is the cost of the shortest path between nodes i and j

Statistical significance to compare groups was performed by a permutation test, where we permuted randomly the data from two groups and we repeated the measure 1,000 times. We reported a significant difference if the difference of the measure between the actual groups was larger that 95% of the samples generated randomly ($p < 0.05$).

Methods for cingulo-frontal modeling

To address the second main objective of this thesis, we built a simplified computational network model composed of two subcircuits, one involved in emotional (vACC) and one in cognitive processing (dlPFC) (Fig. 2.2).

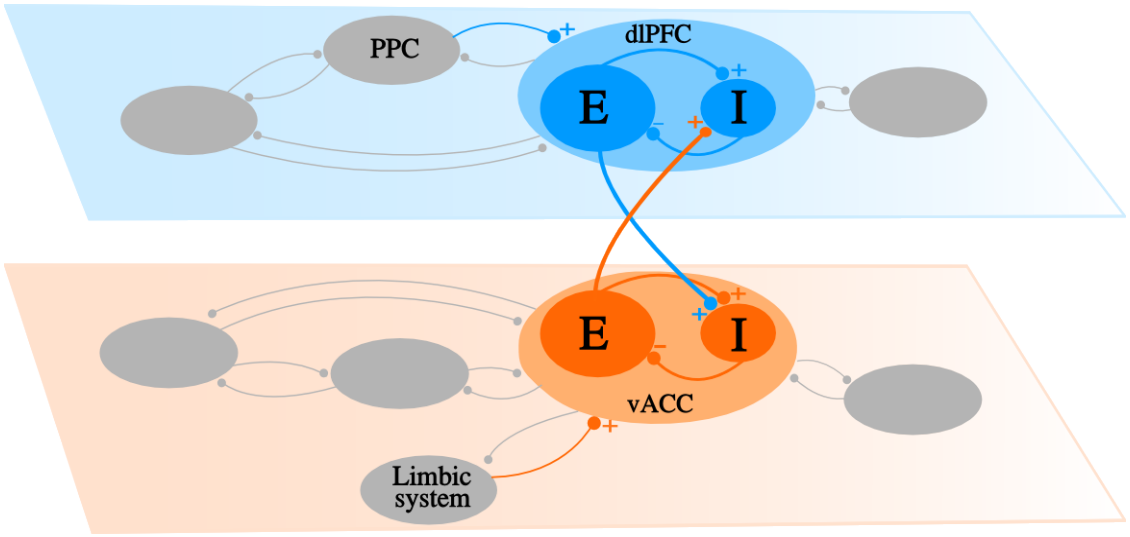

Figure 2.2: Architecture of the model.
The conceptual network model included two subsets of networks: i) the emotional network (light orange) including ventral anterior cingulate cortex (vACC, in orange) and ii) the cognitive network (light blue) including dorsolateral prefrontal cortex (dlPFC, in blue). In color, vACC (orange) and dlPFC (blue), the hubs of each network, reciprocally connected via disynaptic inhibition. Each subnetwork included recurrently coupled excitatory pyramidal cells (E cells) and inhibitory interneurons (I cells). Emotional inputs from the limbic system target vACC (orange), cognitive inputs from posterior parietal cortex (PPC) impinge on dlPFC (blue).

vACC was assumed to receive inputs from the limbic system (amygdala and hippocampus) (Ishikawa and Nakamura 2003), and respond to the emotional components of the task as part of a larger network of areas dealing with emotion (Devinsky et al. 1995; Ishikawa and Nakamura 2003; Vogt 2009). Inputs from posterior parietal cortex activated dlPFC in response to cognitive demands (MacDonald et al. 2000; Edin et al. 2009). vACC and dlPFC circuits mutually suppressed each other's activity through disynaptic inhibition (Fig. 2.2). vACC and dlPFC represent the network hubs that drive activity in larger computing networks (DMN and CCN, respectively), which we do not simulate for simplicity. We

associate hyperactivation (hypoactivaton) of the vACC or dlPFC circuits with exacerbated (deficient) emotional or cognitive processing, respectively.

Spiking network model

We built our cingulo-frontal network of vACC and dlPFC interconnected subnetworks with excitatory and inhibitory spiking neurons (integrate-and-fire model (Tuckwell 1988)) using the Brian simulator (www.briansimulator.org). Each subnetwork contained $N_E = 800$ pyramidal cells and $N_I = 200$ interneurons, where their membrane potential V_m followed:

$$C_m \frac{dV_m}{dt} = -g_m\left(V_m(t) - V_L\right) - I_{syn}(t) \tag{6}$$

with resting potential $V_L = -70$ mV, leak conductance g_m, and membrane capacitance C_m (McCormick et al. 1985). When V_m crosses a prescribed threshold $V_{th} = -50$ mV, an action potential is emitted and the membrane voltage is kept at a reset potential $V_{res} = -55$ mV for a refractory time period τ_{ref}. See parameter values in Table 2.2.

Table 2.2: Parameter values used in the simulations.

Single-cell parameters

Pyramidal cells	Interneurons
$g_m = 25$ nS	$g_m = 20$ nS
$C_m = 0.5$ nF	$C_m = 0.2$ nF
$\tau_{ref} = 2$ ms	$\tau_{ref} = 1$ ms

Synaptic parameters

onto pyramidal neurons	onto interneurons
$g^{syn}_{AMPA,ext} = 0.21$ nS	$g^{syn}_{AMPA,ext} = 0.16$ nS
$g^{syn}_{AMPA,rec} = 0.024$ nS	$g^{syn}_{AMPA,rec} = 0.008$ nS
$g^{syn}_{NMDA,rec} = 0.044$ nS	$g^{syn}_{NMDA,rec} = 0.024$ nS
$g^{syn}_{GABA} = 0.1$ nS	$g^{syn}_{GABA} = 0.097$ nS

The total synaptic current $I_{syn}(t)$ was given by recurrent excitatory inputs through AMPA ($I_{AMPA,rec}$) and NMDA ($I_{NMDA,rec}$) receptors, inhibitory inputs through $GABA_A$ receptors (I_{GABA}) , and excitatory inputs from external areas through AMPA receptors ($I_{AMPA,ext}$):

$$I_{syn}(t)=I_{AMPA,ext}(t)+I_{AMPA,rec}(t)+I_{NMDA,rec}(t)+I_{GABA,rec}(t) \quad (7)$$

Conductance-based postsynaptic currents were modeled according to $I_{syn} = g_{syn}\, s\, (V_m - V_{syn})$, where g_{syn} is a synaptic conductance (Table 2.2), s is a synaptic gating variable, and V_{syn} is the synaptic reversal potential (excitatory synapses V_{syn}= 0, inhibitory synapses V_{syn}= –70 mV). AMPAR and $GABA_AR$ synaptic gating variables were modeled as an instantaneous jump of magnitude 1 when a spike occurred in the presynaptic neuron followed by an exponential decay with time constant $\tau_{AMPA} = 2$ ms for AMPARs and $\tau_{GABA} = 10$ ms for $GABA_ARs$. The NMDA conductance was voltage-dependent, with g_{syn} multiplied by $1/(1 + [Mg^{2+}] \exp(-0.062\, V_m)/3.57)$, $[Mg^{2+}] = 1.0$ mM, and its gating variable s was modeled by:

$$\frac{ds}{dt} = \frac{-1}{\tau_{NMDA}} s + \alpha_s x(1-s) \quad , \qquad \frac{dx}{dt} = \frac{-1}{\tau_x} x + \sum_i \delta(t - t_i) \quad (8)$$

where x models neurotransmitter concentration in the synapse, t_i are presynaptic spike times, and $\tau_{NMDA} = 100$ ms is the decay time, $\tau_x = 2$ ms is the rise time, and $\alpha_s = 0.5$ kHz controls the saturation properties of NMDAR.

The unspecific external input $I_{AMPA,ext}$ was modeled as uncorrelated Poisson spike trains through AMPA synapses of conductance g_{ext} to each neuron at a rate ν_{ext} = 1,800 Hz. Neurons in and across each model circuit, vACC and dlPFC, were connected all to all. The two circuits were reciprocally connected through AMPA excitatory synapses onto inhibitory neurons with conductance $g^{syn}_{AMPA} = 0.1$ nS (Fig. 2.2).

In MDD networks, we simulated deficient glutamate re-uptake by increasing the time constant of synaptic glutamate decay τ_{AMPA} (Choudary et al. 2005): τ_{AMPA} = 2.05 ms (mild MDD), τ_{AMPA} = 2.1 ms (moderate MDD), τ_{AMPA} = 2.15 ms (severe MDD). Glutamate transporters can remove glutamate from the synaptic cleft with an effective time constant of 0.5 ms (Auger and Attwell 2000), a much faster time scale than the effective time constant

of NMDAR-mediated synaptic transmission ($\tau_{NMDA} \approx 100$ ms), so that the impact of glutamate re-uptake slow-down should be marginal on NMDAR-mediated transmission.

The action of SSRIs via 5-HT_{1A} receptors in vACC was simulated as a hyperpolarization of excitatory cells (Andrade et al. 1986; Béïque et al. 2004; Castañé et al. 2015), by reducing the resting potential from its value in the healthy condition ($V_L = -70$ mV) to a value that depends on the dose of SSRI (for the maximal SSRI dose used, $V_L = -70.6$ mV, see Fig. 3.14 and 3.15).

We simulated DBS by applying periodic trains of excitatory inputs at 130 Hz onto inhibitory neurons of vACC through AMPA synapses with conductance $g^{syn}_{AMPA} = 0.62$ nS.

We simulated the temporal evolution of fMRI signals by convolving the total synaptic activity $I_{syn}(t)$ in each circuit with the standard hemodynamic response function (Glover 1999; Horwitz and Tagamets 1999; Deco et al. 2004):

$$h(t) = \frac{t^{n_1} e^{\frac{-t}{t_1}}}{c_1} - \frac{a_2 t^{n_2} e^{\frac{-t}{t_2}}}{c_2} \qquad c_i = max\left(t^{n_i} e^{\frac{-t}{t_i}} \right) \tag{9}$$

where $n_1 = 6.0$, $t_1 = 0.9$ sec, $n_2 = 12.0$, $t_2 = 0.9$ sec, and $a_2 = 0.2$ (Glover 1999). We calculated numerically the convolution:

$$S_{fMRI}(t) = \int h(t - t') I_{syn}(t') dt' \tag{10}$$

by sampling $I_{syn}(t)$ every 0.1 sec, and we computed a percent signal change over 50 simulations (Fig. 3.17) by normalizing $S_{fMRI}(t)$ by the mean S_{fMRI} in the first 10 sec (rest epoch) of the healthy network. In Fig. 3.18 and 3.19 B-C we computed a percent signal change over 50 simulations by normalizing $S_{fMRI}(t)$ by the mean S_{fMRI} in the first 10 sec (rest epoch) of each network. In Fig. 3.19A we computed a percent signal change over 50 simulations by subtracting the mean S_{fMRI} in the first 10 sec (rest epoch) of the healthy network and normalizing by the mean S_{fMRI} in the first 10 sec (rest epoch) of the healthy network.

Spectral analysis was performed using the Chronux software package (Bokil et al. 2010) on Matlab. Chronux built-in multitaper spectral estimation (5 tapers, time-bandwidth = 3 Hz) was used to estimate frequency spectra (power spectra). In order to have long enough time series to perform the spectral analysis in the studied range of frequency, we used a window size of 1 second taken from activated states. To compare the spectral properties of LFP obtained from differents network models simulations, we normalized each power spectrum by the variance of the signal. Error bars for spectral estimation represent the jackknife 95% confidence interval (CI).

Firing-rate network model

The dynamics of the network can be analyzed conceptually in a simpler firing rate model:

$$\begin{aligned}
\tau_e \frac{dr_e^v}{dt} &= -r_e^v + \varphi_e\left(G_{ee} f_D r_e^v - G_{ei} r_i^v + I_e^v + I_e f_D + \Delta I_e\right) \\
\tau_i \frac{dr_i^v}{dt} &= -r_i^v + \varphi_i\left(G_{ie} f_D r_e^v - G_{ii} r_i^v + G_x r_e^d + I_i^v + I_i f_D + \Delta I_i\right) \\
\tau_e \frac{dr_e^d}{dt} &= -r_e^d + \varphi_e\left(G_{ee} r_e^d - G_{ei} r_i^d + I_e^d + I_e\right) \\
\tau_i \frac{dr_i^d}{dt} &= -r_i^d + \varphi_i\left(G_{ie} r_e^d - G_{ii} r_i^d + G_x r_e^v + I_i^d + I_i\right)
\end{aligned} \tag{11}$$

where r_e^v and r_i^v (r_e^d and r_i^d) are the firing rates of the excitatory and inhibitory populations in the ventral (dorsal) sub-network. Excitatory and inhibitory neurons were characterized by the time constants τ_e and τ_i, respectively, and φ_e and φ_i are the corresponding neuronal input-output function relating output firing rate to input currents. Within each sub-network, G_{ee} is the effective connection strength between excitatory neurons, G_{ie} is the effective connection strength from excitatory to inhibitory neurons, G_{ii} is the effective connection strength between inhibitory neurons, and G_{ei} is the effective connection strength from inhibitory to excitatory neurons. G_x is the effective excitatory connection strength across sub-networks, targeting only inhibitory neurons. I_e and I_i are inputs from neurons external to the network, which control the excitability of neurons and determine the neurons' spontaneous firing rates. I_e^v, I_e^d, I_i^v and I_i^d are excitatory inputs from neurons external to the

network (e.g. parietal cortex or amygdala), which represent either emotional or cognitive stimuli. Parameters f_D ($f_D > 1$), ΔI_e and ΔI_i were used to simulate glutamate dysfunction associated with MDD, modulation of excitability associated with SSRI treatments and modulation of interneurons associated with DBS treatment respectively, in the vACC sub-network.

To gain an understanding of the dynamics in Eqs. (11) which are relevant for this thesis, we actually need only analyze a single isolated area: dorsal or ventral. The reason is that when one area is activated, it strongly inhibits the other, effectively shutting it off. Therefore we can consider the system of two coupled equations.

$$\tau_e \frac{dr_e^v}{dt} = -r_e^v + \varphi_e\left(G_{ee} f_D r_e^v - G_{ei} r_i^v + I_e^v + I_e f_D + \Delta I_e\right)$$
$$\tau_i \frac{dr_i^v}{dt} = -r_i^v + \varphi_i\left(G_{ie} f_D r_e^v - G_{ii} r_i^v + I_i^v + I_i f_D + \Delta I_i\right)$$

(12)

The intrinsic dynamics of this network depends crucially on the effective strength of synaptic connections as well as on the relative time constants of integration of the excitatory and inhibitory populations of neurons. Specifically, the networks can exhibit bistable behavior only if the effective gain associated with changes in total inhibitory input received by the population of excitatory neurons is overcome by sufficiently strong gain in recurrent excitation. This condition is met when the parameters satisfy the following formula

$$f_D G_{ee} \varphi_e' > 1 + \frac{f_D G_{ei} G_{ie} \varphi_i' \varphi_e'}{1 + G_{ii} \varphi_i'}$$

(13)

where $\varphi_e'(\varphi_i')$ is the gain of the excitatory (inhibitory) population of neurons, evaluated for a given level of external input. Strictly speaking this condition indicates the presence of a so-called Saddle-Node bifurcation.

Furthermore, oscillations can also emerge in the networks if the gain in the recurrent excitation is both sufficiently strong and fast to transiently overcome fluctuations in the inhibitory feedback. This Hopf Bifurcation happens when

$$f_D G_{ee} \varphi_e' > 1 + \frac{\tau_e}{\tau_i}\left(1 + G_{ii}\varphi_i'\right)$$

(14)

And the resulting oscillatory instability has a frequency

$$\omega = \sqrt{\frac{1 + G_{ii}\varphi_i'}{\tau_i \tau_e}}\left[1 + \frac{f_D G_{ei} G_{ie} \varphi_i' \varphi_e'}{1 + G_{ii}\varphi_i'} - f_D G_{ee}\varphi_e'\right]^{1/2}$$

(15)

It is easy to see from this formula that when the networks are in the bistable regime, and hence Eq. (14) is nearly satisfied, the frequency of oscillations is low, i.e. oscillations are slow. The frequency of oscillation goes to zero exactly when Eq. (13) is satisfied, indicating the co-occurence of a Saddle-Node and a Hopf bifurcation. Experimentally, cortical oscillations are characterized by broad peaks in the power spectrum. Such structures can be obtained from simulations when oscillations are not stable limit cycles but rather reflect the presence of damped oscillatory modes which are driven by ongoing fluctuations in the network activity. In our networks there is a broad range of parameter values for which Eqs. (13) and (14) are nearly satisfied and hence for which such damped oscillations occur in the bistable regime.

We investigated how the parameter f_D affected these dynamics when the system was residing in such a bistable, damped oscillatory regime for $f_D = 1$. To this end we specified the input-output functions as

$$\varphi_e(x) = \begin{cases} 0, & if\ x < 0 \\ Ax^2, & if\ 0 \le x \le 1 \\ 2A\sqrt{x - 3/4}, & if\ x > 1 \end{cases}$$

(16)

and $\varphi_i(x) = \alpha\ \varphi_e(x)$. We found that the bistable range of the dynamics ΔI_e could increase or decrease as f_D grew. The condition that makes sense in our context is a reduction of ΔI_e with f_D, because that means that more advanced MDD has more difficult treatment (Fig. 2.17). We found that this dependency was achieved if inhibitory neurons operated in the

fluctuation-driven regime where their response to external inputs is supralinear, and not if they were linearly or sublinearly transforming input currents into output firing rates.

In the graphs of Figs. 3.20, 3.21, 3.22, 3.23, 3.24, 3.25, 3.26 3.27 and 3.28 we used the parameters G_{ee} = 0.09 s, G_{ie} = 0.04 s, G_{ei} = 0.0275 s, G_{ii} = 0.0075 s, G_x = 0.025 s, I_{ex} = 0.163, I_{ix} = 0.1, I_e^v = 0, I_e^d = 0, I_i^v = 0, I_i^d = 0, τ_e = 20 ms, τ_i = 20 ms, A = 20 Hz, α = 4, f_D = 1(healthy), f_D = 1.05(mild MDD), f_D = 1.15(moderate MDD), f_D = 1.25(severe MDD). In figure 3.23: ΔI_e^v=0.005, ΔI_e^v=0.02, ΔI_e^v=0.08, initial condition, r_e^v = 4 sp/s.

Results

Results for brain image analysis

We recorded fMRI activity in 22 participants while they engaged in two identical working memory tasks, separated by a period in which a sadness state was induced by remembering a previously identified biographical sketch (Fig. 2.1). We sought to identify the functional changes induced by the sadness state in brain networks engaged in regulating the interaction between cognition and emotion.

Behavioral analysis

We first tested if performance in the working memory task was affected by sadness provocation. Across participants, the mean number of error trials, of cognitive inhibition error trials (Materials and Methods), and the mean reaction times did not change significantly from the working memory session before sadness induction (WM1) to the working memory session after sadness induction (WM2) (Table 3.1, paired sample t-test: $p = 0.5$, $p = 0.6$, $p = 0.85$, respectively).

Table 3.1: Behavioral measure

Tasks	**Mean errors ± SEM**	**Cognitive inhibition errors ± SEM**	**Reaction time ± SEM**
Working memory 1	3.15 ± 0.48	1.35 ± 0.24	1.334 ± 0.059 sec.
Working memory 2	3.4 ± 0.5	1.3 ± 0.24	1.307± 0.061 sec.

After the scan session, participants reported their subjective rating of the sadness intensity reached on a 0-7 points scale (5.6 ± 0.17, mean ± SEM). In the following, we use this measure to identify effects associated specifically with the experience of sadness. To this end, we divide our participants in two groups: the *high–sadness* group, with sadness report above the mean of all participants (n=12, mean=6.14, median=6 range= 6-7) and the *low-sadness* group, including participants with sadness report below the mean (n=10, mean=4.85, median=5, range= 4-5.5).

Only in the *high-sadness* group*,* working memory performance was diminished by sadness

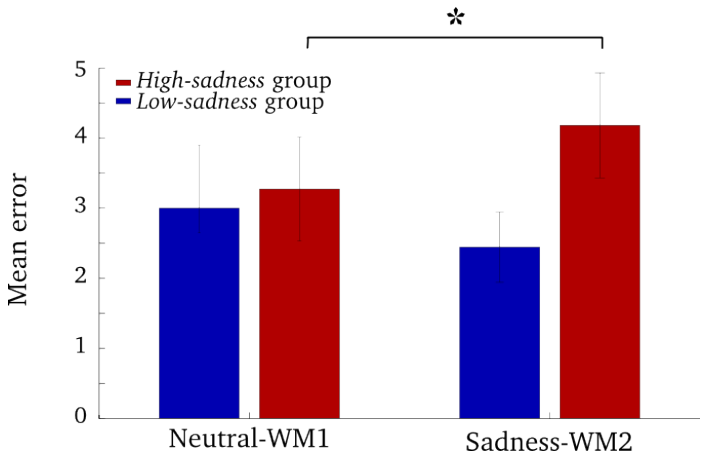

Figure 3.1: Sadness intensity disrupts WM performance.

Mean errors trials during working memory tasks: The *high-sadness* group presents more errors in WM2 relative to WM1.

provocation, as reflected in a significant increase in the errors in WM2 relative to WM1 (Fig. 3.1, Table 3.2), (3-way ANOVA, p = 0.04 for the interaction between *high-sadness/low-sadness* groups and WM1/WM2, paired sample t-test p = 0.033 for WM1-WM2 errors in the *high-sadness* group, p = 0.37 for WM1-WM2 errors in the *low-sadness* group).

There was no significant interaction between *sadness intensity* and WM1/WM2 when analyzing cognitive inhibition errors or reaction times (3-way ANOVA, p = 0.17 and p = 0.35, respectively). We note, however, that participants had very low numbers of cognitive inhibition errors in our task and this diminished the statistical power of our test. A careful investigation of the effects of sadness induction on cognitive inhibition would require of a specific task design in another experiment.

Table 3.2: Mean number of errors in *high-sadness* and *low-sadness* groups

	***High-sadness*:** **Mean errors ± SEM**	***Low-sadness:*** **Mean errors ± SEM**
Working memory 1	3.27 ± 0.74	3 ± 0.62
Working memory 2	4.18 ± 0.75	2.44 ± 0.5

fMRI BOLD response during working memory

We first identified the cortical areas that are supporting the memory component of the working memory task in the cognitive network during WM1 and WM2. We conducted a whole brain analysis (see Materials and Methods) to find regions activated in a *delay-fixation* contrast. We found significant activation (FDR, $p < 0.05$, Fig. 3.2) in the cognitive areas: dorsolateral prefrontal cortex (dlPFC), intraparietal sulcus (IPS), medial superior frontal gyrus (mSFG), postcentral gyrus (PCG) and inferior frontal gyrus (iFG) (Figs. 3.2A for WM1 and 3.2B for WM2, for coordinate see Table 2.1,).

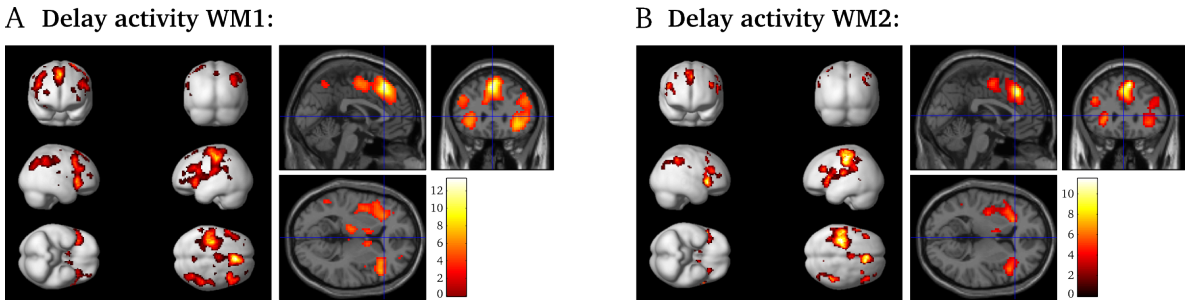

Figure 3.2: Pattern of activation during working memory.

A, B. Significant activations in cognitive areas (dlPFC, mSFG, iFG, IPS and PCG) during delay relative to fixation in WM1 (**A**) and WM2 (**B**).

When we tested the difference in delay activity between WM1 and WM2 epochs in a $delay_{WM1}$- $delay_{WM2}$ contrast (Fig. 3.3), we found a significant reduction in activity during $delay_{WM2}$ in dlPFC, IPS, mSFG, iFG and PCG (FDR, $p < 0.05$). However, we could not attribute this decrease unambiguously to sadness experience, as we could not find an interaction between the factors *high-sadness/low-sadness* and WM1/WM2 in none of these areas (2-way ANOVA, FDR $p < 0.05$, mask with areas in Fig. 3.2).

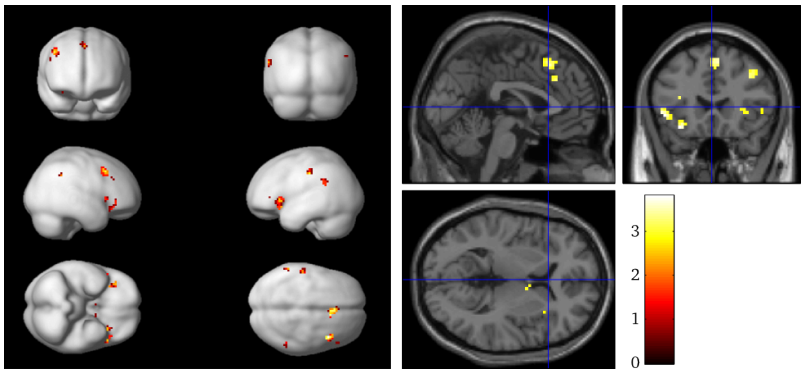

Figure 3.3: Decrease in activations during working memory after sadness.

Significantly greater cognitive areas activation during delay WM1 comparing with delay WM2 (after sadness).

sACC activation characterizes the high-sadness group

We then looked for the anatomical regions activated during the sadness provocation epoch (*Sadness* epoch). Previous studies have pointed to subgenual anterior cingulate cortex (sACC) as an area involved in sadness processing. Across all participants, we did not find a significant activation in the sACC, or in any other area, in the *Sadness* epoch relative to the Neutral epoch (2-way ANOVA whole brain analysis with factors epoch and sadness intensity, T-contrast, FDR $p<0.05$). Nevertheless, it is known that factors associated with individual differences at both neuroanatomical and behavioral levels may account for the difficulty in detecting sACC activation (Smith et al. 2011). We thus resorted to a region of interest (ROI) analysis, where we defined the sACC ROI (5-voxel cube, center in Table 2.1) based on available evidence from previous neuroimaging studies (Liotti et al. 2000; Mayberg et al. 2005; Drevets et al. 2008). Using this ROI as a mask in the above analysis, we found a significant interaction between *Sadness/Neutral* epoch and *high-sadness/low-sadness* groups in the left hemisphere (sACCl, Fig. 3.4, cluster of 6 voxels (left panel), peak activation at –6 21 –9, small volume correction (SVC) and FWE $p = 0.038$).

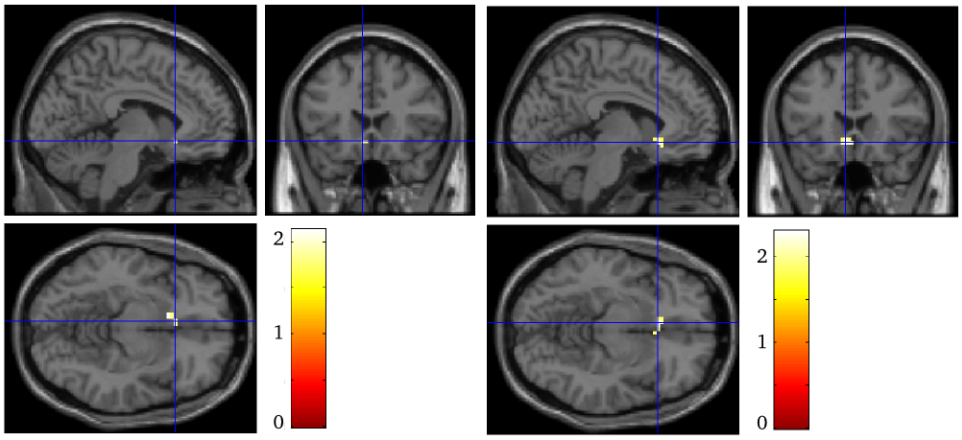

Figure 3.4: sACCl activation during sadness in the *high-sadness* group

Left panel: A significant interaction between *Sadness/Neutral* and *high-sadness/low-sadness* groups in sACCl, ANOVA T-contrast, 6 voxels cluster, peak activation at -6 21 -9, $p_{(SVC,FWE\text{-}corr)} = 0.038$. *Right panel:* significant sACCl activation during sadness relative to neutral in the *high-sadness* group, 20 voxels cluster, peak activation at -3 21 -9, $p_{(SVC,FWE\text{-}corr)} = 0.014$. Note that the intercession of lines mark the -6 21 -9 coordinates.

Based on this interaction, we split the participants in the high-sadness and low-sadness

groups: sadness provocation evoked an increase in the BOLD signal in the sACCl during *Sadness* compared with *Neutral* in the *high-sadness* group (Fig. 3.4, cluster of 20 voxels (right panel), peak activation at –3 21 –9, SVC and FWE, p = 0.014). In other words, subjects who achieved an intense sadness state activated the left sACC.

dlPFCl - sACCl interaction was modulated by sadness intensity

Activation in the left sACC (sACCl) was related with sadness intensity (Fig. 3.4), so we wondered if this could explain the sadness-dependent decrease in working memory performance (Fig. 3.1). To address this question, we performed an inter-individual analysis on the BOLD activity averaged in each of the task epochs, and averaged within the sACCl ROI and a ROI defined around the focus identified in the left dlPFC (Materials and Methods, Table 2.1). Across participants, we found a significant anticorrelation between the Sadness-Neutral epochs contrast in sACCl and the WM2-WM1 epochs contrast in dlPFCl ($R_{Pearson}$ = –0.5197, p = 0.0132; $R_{Spearman}$ = –0.4715, p = 0.0285) (Fig. 3.5A). This shows that, across subjects, the stronger the BOLD activity in the sACCl during *Sadness* relative to *Neutral*, the weaker the BOLD activity in the dlPFCl in WM2 relative to WM1.
Moreover, by dividing the participants between *high-sadness* and *low-sadness* groups, we found a significantly higher anticorrelation between these two ROIs in the *high-sadness* group ($R_{Pearson}$ = –0.6639, p = 0.0186), that in the *low-sadness* group ($R_{Pearson}$ = –0.1264, p = 0.7278) (Fig. 3.5B). The significant difference between groups was calculated with a permutation test, p = 0.042 (see Materials and Methods). Only the group of participants experiencing more intense sadness, and not those with weaker emotional response, showed a relationship between the strength of sACCl BOLD activity during the *Sadness* epoch and the reductions of dlPFCl BOLD activity in WM2. This suggests that the larger deactivation of dlPFCl during WM2 (relative to WM1) could be related to the decrease in working memory performance in the *high-sadness* group (Fig. 3.1). To address specifically the role of inter-areal interactions in the functional aspects of our task we turned to a network analysis of functional connectivity in our fMRI data, in order to see how connectivity gets modulated by our behavioral parameters.

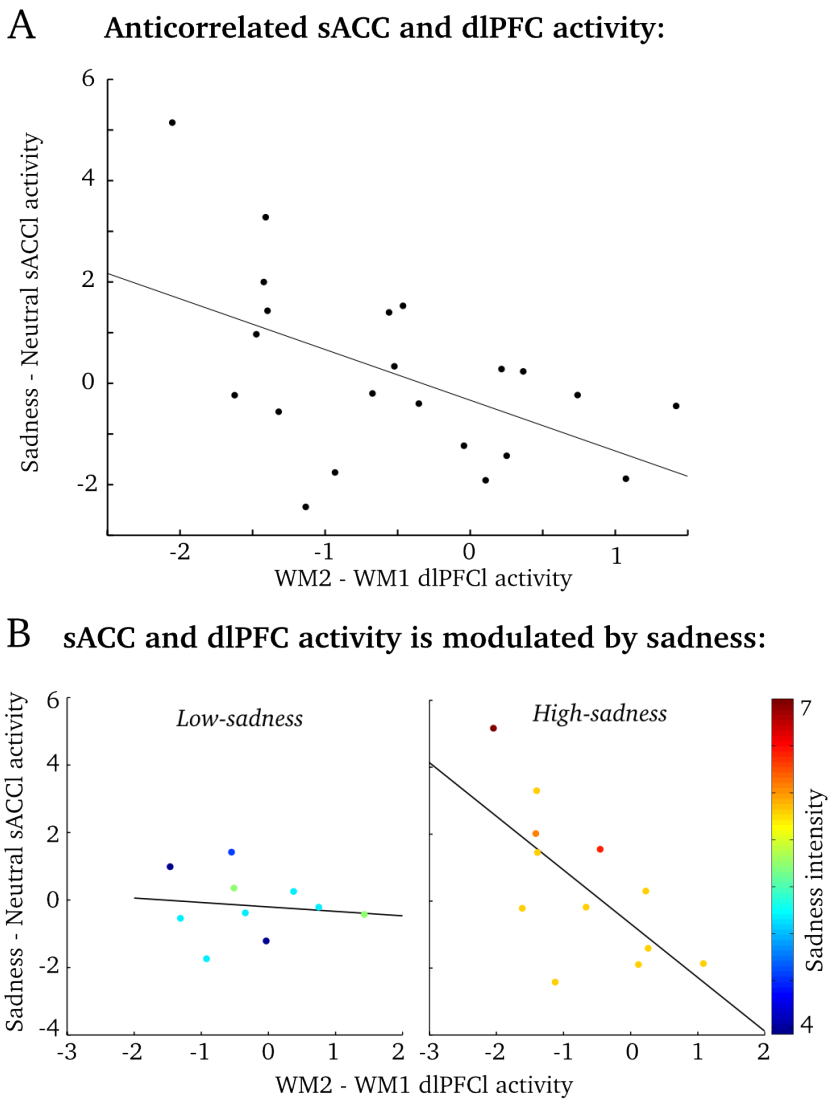

Figure 3.5: Sadness intensity increased the anticorrelation between sACCl-dlPFCl.

A. At the population level, we found a significant anticorrelation between sACCl (Sadness-Neutral) and dlPFCl (WM2- WM1) BOLD activity, as stronger the BOLD activity in sACCl during sadness, the weaker BOLD activity in dlPFCl during WM2. **B.** The *high-sadness* group presents a significant more anticorrelation between sACCl (Sadness-Neutral) and dlPFC (WM2- WM1) BOLD activity relative to *low-sadness* group.

Community structure distinguishes emotional and cognitive networks

Up to here we have described a decay in working memory performance that was associated with intense sadness (Fig. 3.1) and we have explored how the BOLD activity in cortical areas was modulated by cognitive and emotional demands, highlighting the sACCl-dlPFCl

anticorrelation in the *high-sadness* group (Figs. 3.2-3.5). We wondered whether these observations were associated with functional changes in network topology. To address that, we first identified the cortical and subcortical areas that were activated during the sadness and WM epochs in whole brain analyses (Materials and Methods). Based on these activations and on previous literature (Bush et al. 2000; Liotti et al. 2000; Mayberg et al. 2005; Shin LM et al. 2005; Viard et al. 2007; Drevets et al. 2008) we defined a set of ROIs (Table 2.1) that would be presumably implicated in the regulation of cognitive and emotional task demands. For each ROI, participant and paradigm we obtained a time-series signal containing the average activation in the corresponding voxels. We kept only the fluctuations in time scales from 4 s to 1 min and we removed covariations common to all areas (global signal regression) (Materials and Methods).

For each pair of ROIs we estimated their functional connectivity as the linear dependence of the temporal fluctuations in the corresponding signals, as measured by the Pearson correlation coefficient. This led us to define a symmetrical connectivity matrix containing the correlation coefficients between all possible pairs of ROIs. This matrix consists of positive and negative correlations (Materials and Methods). We obtained one such connectivity matrix independently for each subject, and we then averaged together these matrices to obtain a matrix of the averaged connectivities across participants. We applied graph-theoretic analyses by considering ROIs as nodes and the functional connectivity between each pair of ROIs as the corresponding edge.

We first asked if the pattern of connectivities defined subnetworks of areas that had distinct connectivity within and across subnetworks. This can be determined through a community detection algorithm that finds the assignment of nodes (ROIs) in communities (subnetworks) that maximizes the quality Q of the partition (also called *modularity* or *decomposability*, see Materials and Methods). Q is a network-level property that indicates how easily a network can be divided in smaller subnetworks (i.e., communities). Large values of Q reflect more segregation, or equivalently, decreased integration, between different communities. This community detection algorithm applied to our experimental connectivity matrix identified two main communities that coincide with the results of our BOLD contrast analyses above: the cognitive module (areas mSFG, PCG, IPS, dlPFC and iFG) became active during working memory (Fig. 3.2), and the emotional module (areas

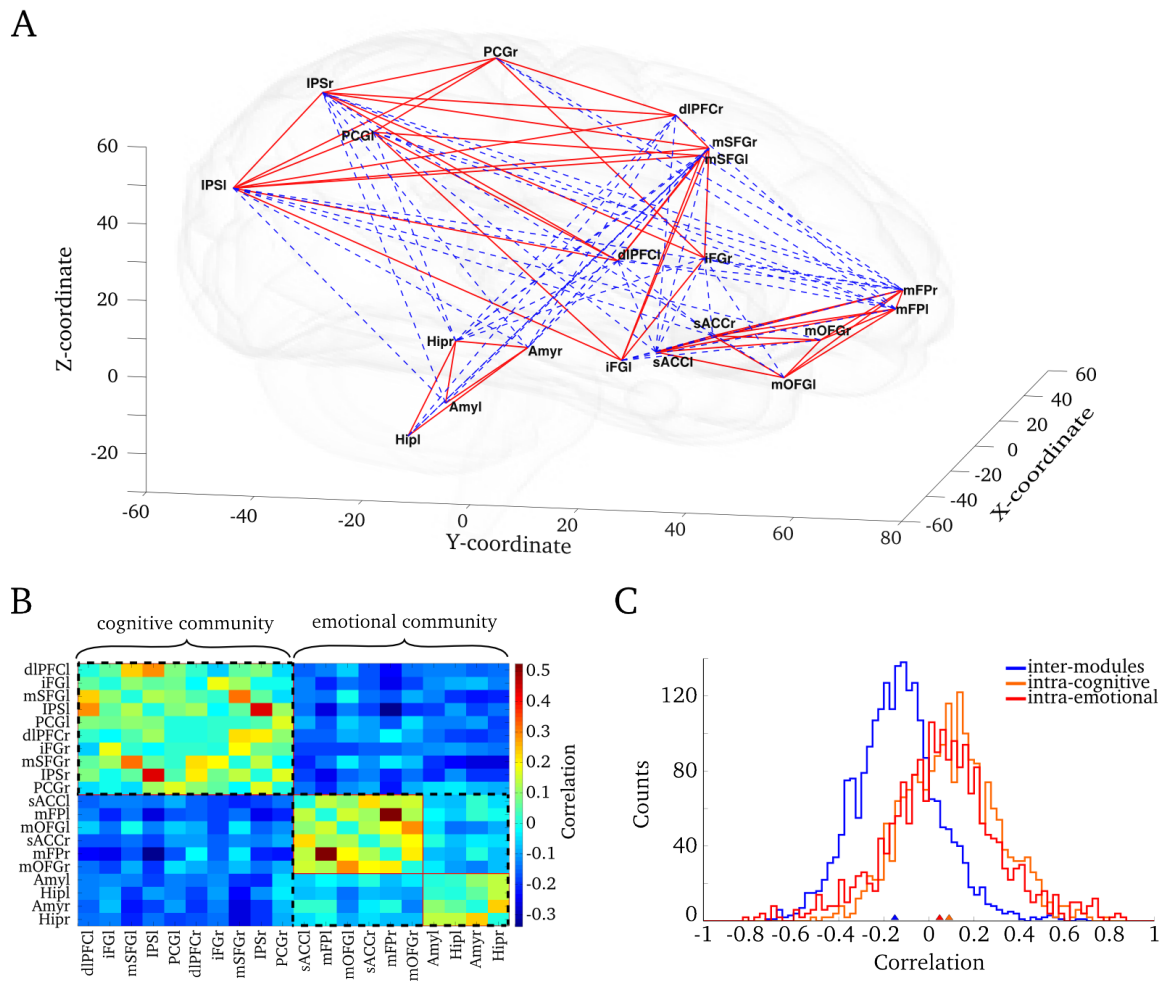

Figure 3.6: Cognitive and emotional communities for Sadness-Working memory.

A. 3D-graphical representation of the networks, the ROIs are located according to real-world coordinates. Mean significant correlations are plotted; the positive correlations in red lines and negative correlations in blue dashed lines, shading brain for schematic purposes. **B.** Matrix of the mean correlations across subjects, the analysis identified two main modules, the cognitive and emotional communities separated by the dashed black line. Into the emotional community, two sub-communities were found (separated by the red line), corresponding to the emotional areas in the cortex and the limbic system (subcortical areas). **C.** Histogram of correlations distribution for all subjects. The correlations between cognitive and emotional modules (inter-modules), plotted in blue are mainly negative (mean ± SEM = –0.15 ± 0.004). The correlations into the cognitive module (intra-cognitive), plotted in orange (mean ± SEM =0.089 ± 0.005) and the correlations into the emotional module (intra-emotional), plotted in red (mean ± SEM = 0.048 ±0.009), both are mainly positive.

sACC, medial Frontal Pole (mFP), medial orbitofrontal gyrus (mOFG), Amygdala (Amy) and Hippocampus (Hip)) that was related to sadness.

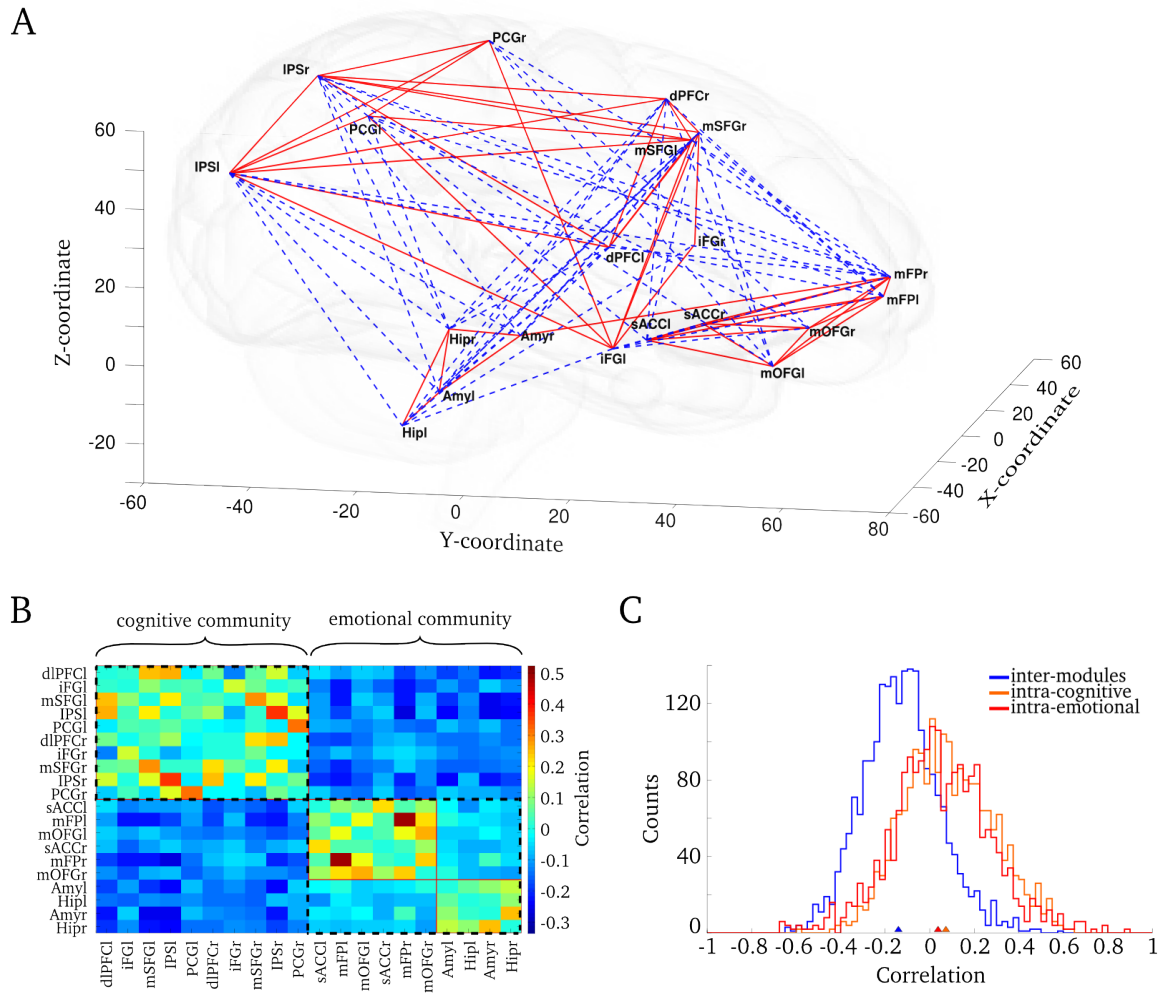

Figure 3.7: Cognitive and emotional communities for Neutral-Working memory.

A. 3D-graphical representation of the networks, the ROIs are located according to real-world coordinates. Mean significant correlations are plotted; the positive correlations in red lines and negative correlations in blue dashed lines, shading brain for schematic purposes. **B.** Matrix of the mean correlations across subjects, the analysis identified two main modules, the cognitive and emotional communities separated by the dashed black line. Into the emotional community, two sub-communities were found (separated by the red line), corresponding to the emotional areas in the cortex and the limbic system (subcortical areas). **C.** Histogram of correlations distribution for all subjects. The correlations between cognitive and emotional modules (inter-modules), plotted in blue are mainly negative (mean ± SEM = –0.14 ± 0.004). The correlations into the cognitive module (intra-cognitive), plotted in orange (mean ± SEM = 0.073 ± 0.005) and the correlations into the emotional module (intra-emotional), plotted in red (mean ± SEM = 0.037 ± 0.008), both are mainly positive.

We can visualize this partition in the average correlations across all subjects during our two paradigms (Fig. 2.1), *Sadness-WM2* (Fig. 3.6A,B) and *Neutral-WM1* (Fig. 3.7A,B). The

pattern of correlations shows two main subnetworks that interact with each other mainly through positive correlations (Fig. 3.6A, 3.7A, red lines) and between them mainly through negative correlations (Fig. 3.6A, 3.7A, blue dashed lines), as seen in the distributions of correlations (Figs. 3.6C and 3.7C).

The modularity Q was higher for *Sadness-WM2* than for *Neutral-WM1* (Q = 0.431 vs. Q = 0.412, permutation test, p = 0.008). In contrast, correlation distributions did not differ significantly between the two paradigms (2-way ANOVAs with factors paradigm and subject, intra-cognitive p = 0.33, intra-emotional p = 0.44, and inter-module p =0.4). This indicates that Q is a measure more sensitive to network modulations than mean correlations, and the corresponding result suggests that the emotional and cognitive communities are more segregated following an episode of intense sadness.

To confirm that sadness intensity had a segregating effect on the community structure we applied the community detection algorithm to the average correlation matrices obtained separately for the *high-sadness* and the *low-sadness* groups in the paradigm *Sadness-WM2*. The community assignment of the different ROIs did not change based on sadness intensity (Fig. 3.8A,B), but the modularity Q was indeed higher for the *high-sadness* group than for the *low-sadness* group (Q = 0.443 vs. Q = 0.405, permutation test, $p < 0.0001$), confirming our hypothesis.

The modularity analysis has some free parameters (resolution parameters, $\boldsymbol{g}+ = \boldsymbol{g}– = 1$ in the above analyses, see equation 1 in Materials and Methods) that allow to weigh differently the positive and negative correlations in the connectivity, and this has an impact in the community structure that the method identifies.

Thus, when we applied more weight to the positive correlations (resolution parameter $\boldsymbol{g}+ = 1$ and $\boldsymbol{g}– = 0.75$), the community detection algorithm identified two sub-communities within the emotional community (Figs. 2.6B and 2.7B, the red line separates the two sub-communities). These sub-communities corresponded to emotional areas in the cortex (sACC, mOFG and mFP) and the limbic system (Amy and Hip), respectively. Consistent with this substructure in the emotional, but not in the cognitive community, the mean correlation within the emotional community was lower than within the cognitive community (Figs. 3.6C and 3.7C; 2-way ANOVA, p = 0.044 and p = 0.0062, respectively). Using these parameters ($\boldsymbol{g}+ = 1$ and $\boldsymbol{g}– = 0.75$), the partition quality Q in *Sadness-WM2* was

higher than in *Neutral-WM1* ($Q = 0.352$ vs. $Q = 0.332$, permutation test, $p < 0.0005$), but it was not significantly different between the *high-sadness* and *low-sadness* groups during *Sadness*-WM2 ($Q = 0.355$ vs. $Q = 0.345$, permutation test, $p = 0.14$).

This reflected the fact that the two emotional sub-communities enhanced their integration in the *high-sadness* group: the community detection algorithm was unable to distinguish the emotional sub-communities in the *high-sadness* group (Fig. 3.8B). Taken together, this suggests that sadness experience causes the segregation of cognitive and emotional

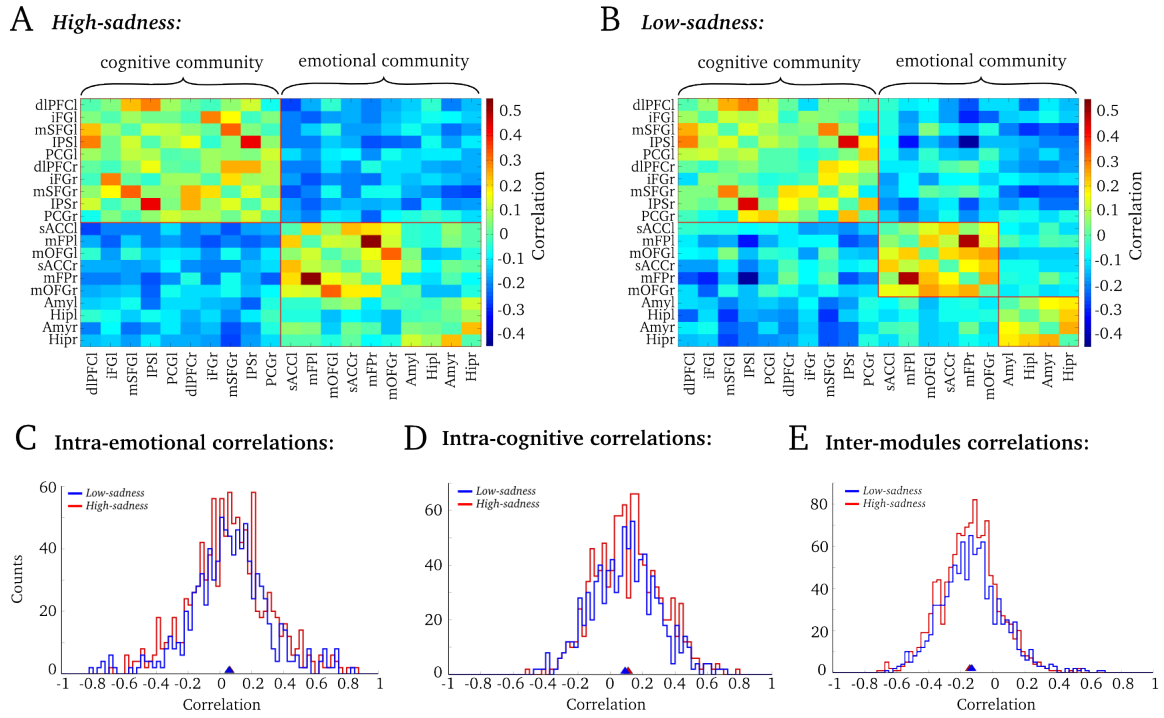

Figure 3.8: Cognitive and emotional communities for *high-sadness* group during Sadness-Working memory.

A. Matrix of the mean correlation across *high-sadness* subjects, the analysis identified two main modules, cognitive and emotional communities separated by the red line. Note that for the high-sadness group the algorithm was unable to detect into the emotional community the two sub-communities reported for all subjects (cortical and subcortical areas). **B.** Matrix of the mean correlation across subjects *low-sadness*, the analysis identified three modules, one cognitive and two emotional communities separated by the red line. Note that for the low-sadness group the algorithm was able to detect into the emotional community the two sub-communities reported for all subjects (cortical and subcortical areas). **C,D,E,** Histograms of correlations distribution for *high-sadness* (red line) and *low-sadness* (blue line) subjects. No significant interaction between *high-sadness* and *low-sadness* groups and paradigms in the correlations distribution into the emotional module (**C**) (3-way ANOVA, $p = 0.85$, mean ± SEM = 0.049 ± 0.008 and 0.046 ± 0.008, respectively), into the cognitive module (**D**) (3-way ANOVA, $p = 0.69$, mean ± SEM = 0.098 ± 0.006 and 0.079 ± 0.007, respectively) and between cognitive and emotional modules (**E**) (3-way ANOVA, $p = 0.8$, mean ± SEM = –0.16 ± 0.005 and –0.14 ± 0.006, respectively).

networks, while at the same time promoting more integration between cortical emotional areas (sACC, OFC and mFP) and the limbic system (Amy and Hip).

We then turned to studying whether subnetworks changed their internal connectivity in the task. Global efficiency (GE) provides a measure of integration of one community in the network. A community with higher GE will have "shorter paths" between the nodes. Path distance between two nodes can be defined as the inverse of the functional connectivity between them (the higher the correlation, the shorter the distance). We ignored negative correlations for this measure, as they represented a small number of intra-community weights. Global efficiency computes an estimate of the average inter-node distance within the community (Materials and Methods). We calculated GE separately for each cognitive and emotional network, and separately for *Sadness-WM2* and *Neutral-WM1*.

We found a significantly higher global efficiency for the emotional network during the *Sadness-WM2* compared to the *Neutral-WM1* paradigms (*GE* = 0.091 and 0.082, respectively, permutation test, $p = 0.016$). The global efficiency for the cognitive network was not significantly different between *Sadness-WM2* and *Neutral-WM1* (permutation test, $p = 0.27$).

When we compared the *high-sadness* and *low-sadness* groups, we did not find a significant difference in the global efficiency of either the emotional or the cognitive networks (permutation tests, $p = 0.72$, $p = 0.56$, respectively).

We summarize the graph-network measures in table 3.3.

Table 3.3: Network- and community-level measures

Network measure	*Sadness-WM2* / *Neutral-WM1*	*high-sadness* / *low-sadness*
Modularity Q ($\boldsymbol{g}+ = \boldsymbol{g}– = 1$)	↑ **($p = 0.008$)**	↑ **($p < 0.0001$)**
Modularity Q ($\boldsymbol{g}+ = 1$, $\boldsymbol{g}– = 0.75$)	↑ **($p < 0.0005$)**	NS ($p = 0.14$)
Global efficiency (emotional)	↑ **($p = 0.016$)**	NS ($p = 0.72$)
Global efficiency (cognitive)	NS ($p = 0.27$)	NS ($p = 0.56$)

Arrow denotes the direction of change, and items in bold are statistically significant. NS = non significant.

Summing up, the modularity Q analysis shows a stronger segregation between emotional and cognitive networks following a strongly emotional experience (Table 3.3), and the emotional module was not susceptible of being decomposed in the *high-sadness* group (Fig. 3.8A). On the other hand, the global efficiency analysis shows an increase in intra-community integration for the emotional module in the sadness paradigm, but not when comparing high-sadness and low-sadness groups (Table 3.3). These results suggest that strong emotional experiences mostly affect the interaction between emotional and cognitive subnetworks, may increase the internal integration of the emotional module, and have little effect on interactions within the cognitive subnetwork.

We then went deeper into studying the mechanisms whereby the emotional and cognitive networks interact. We turned our analysis towards identifying the areas that mediate the interactions between subnetworks (which we will call *hubs*), hypothesizing that these hubs are critical for the emotional modulation of the interaction between subnetworks.

Hub identification and their modulation by strong emotional demands

The network-level properties studied above suggest a modulation in the interaction between the networks according to the emotional or cognitive demands. We wondered if specific areas (*hubs*) mediate these interactions. Thus, we identified the hubs in the subnetworks during both task paradigms. We did this by measuring two network parameters for each node: the degree, and the participation coefficient (Materials and Methods). The degree of a node in the network is the number of connections it has to other nodes, and the participation coefficient compares this number of connections to the number of connections within the node's own subnetwork. To compute these measures, we applied a threshold to the correlation matrix for each participant (we tried a range of thresholds from 30% to 45% of the absolute maximal correlation), in order to take into account only the strongest correlations. Both strong positive and negative correlations are counted by considering only the absolute value of the adjacency matrix for each subject. Connector hub nodes were identified as those ROIs with degree one standard deviation above the network's mean degree, and with participation coefficient above the network's mean participation coefficient, following the criteria of previous studies (Sporns et al. 2007). Such nodes are

highly interconnected (high degree), and primarily with nodes from other subnetworks (high participation coefficient), consistent with our intuition of a hub area.

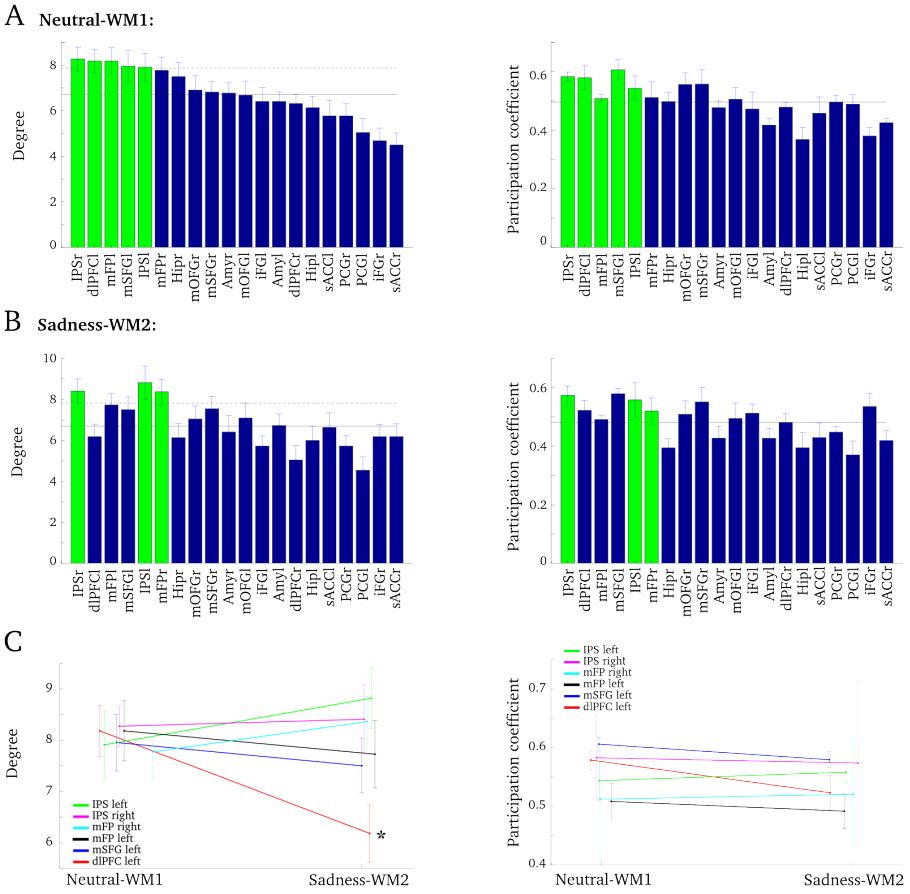

Figure 3.9: Hubs identification, dlPFCl decreases their degree after sadness.

Degree *(left panels)* and participation coefficient *(right panels)* analysis applying a threshold of 35%

A. During Neutral-WM1 paradigm five regions were identifies as hubs (plotted in green): IPSr, IPSl, dlPFCl, mFPl and mSFGl, the participation coefficient for the hubs were above the mean, therefore are classified as connector hubs.

B. During Sadness-WM2 paradigm three regions were identified as hubs (plotted in green): IPSr, IPSl, mFPr that also were classified as connector hubs.

C. The dlPFCl was the only hub that presents a significant decrease in the degree from Neutral-WM1 to Sadness-WM2 paradigm. The participation coefficient showed a marginally-significant decrease. Error bars mark standard error of the mean.

During the *Neutral-WM1* paradigm we identified 5 hub ROIs: IPSr, IPSl, dlPFCl, mFPl and mSFGl (Fig. 3.9A). On the other hand, during the *Sadness-WM2* paradigm we identified 3

hubs: IPSr, IPSl and mFPr (Fig. 3.9B). The identified hubs were consistent with previous literature (Cole and Schneider 2007; Fox and Raichle 2007; Cole et al. 2012, 2013). We noticed that the IPS and mFP were present in both task paradigms, while dlPFCl and mSFGl appeared only in the Neutral-WM1 paradigm.

To quantify the statistical significance of such difference in degree and participation coefficient between Neutral-WM1 and Sadness-WM2, we performed a 3-way ANOVA (factors: task paradigm, high-sadness/low-sadness, and subject) for all the hubs identified. The dlPFCl was the only hub whose degree decreased significantly (Fig. 3.9C, main effect of paradigm p = 0.014, all other effects and interactions not significant). In addition, the dlPFCl participation coefficient also showed a marginally-significant decrease (Fig. 3.9C, main effect of paradigm p = 0.08).

Figure 3.10: The dlPFCl was modulated by sadness state and mFPl was modulated by sadness intensity.

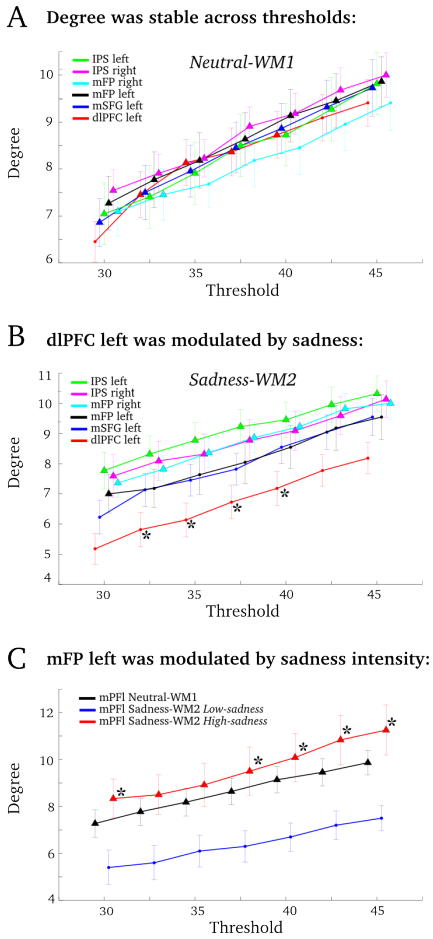

The classification of the hubs identified was stable across thresholds (from 30% to 45%) during Neutral-WM1 (**A**) and Sadness-WM2 (**B**). Regions classified as hubs are plotted as triangles. Error bars mark standard error of the mean. The decrease in the degree for the dlPFCl during Sadness-WM2 was stable across de thresholds. The black asterisks mark the significant differences: 3-way ANOVA, main effect of paradigm p <0.05 (**B**).

C. The mFPl was the only hub that was modulated by the sadness intensity, for the *high-sadness* group increases the degree and for the *low-sadness* group decreases de degree. The black asterisks mark the significant differences: 3-way ANOVA, interaction between task paradigm and sadness intensity p <0.05

The hubs described above were stable across different thresholds for *Neutral-WM1* (Fig. 3.10A) and *Sadness-WM2* (Fig. 3.10B) and the decrease in degree of the dlPFCl after sadness induction was robust across thresholds (Fig. 3.10B). Note, however, that the degree

of the dlPFCl was not significantly modulated by the intensity of sadness (3-way ANOVA, threshold 35%, interaction between task paradigm and sadness intensity $p = 0.55$).

Remarkably, the degree of the mFPl was modulated by sadness intensity (3-way ANOVA, interaction between task paradigm and sadness intensity for 30% threshold, $p = 0.031$): it increased for the *high-sadness* group and it decreased for the *low-sadness* group relative to *Neutral-WM1* (Fig 3.10C). These results identified dlPFCl as a hub in the cognitive subnetwork that reduced its coupling with the emotional subnetwork following sadness induction, and mFPl as a hub in the emotional subnetwork that increased its coupling with the cognitive subnetwork specifically in those participants that experienced a stronger emotional state after sadness induction. Motivated by these findings we then turned to study changes in functional connectivity between these two hubs and all other areas as a possible substrate for behavioral parameters.

Changes in functional connectivity underlie behavioral differences and hub modulations

Looking for the mechanism underlying the hub modulations described above we first tested if a change in the functional connectivity between the 2 hub nodes, dlPFCl and mFPl, could explain the modulation of their degree. We analyzed the change in the correlation between this 2 hub nodes for each participant, task paradigm and sadness-intensity groups. The functional connectivity between dlPFCl and mFPl did not present a main effect between *Neutral-WM1 and Sadness-WM2*, (3-way ANOVA, $p = 0.48$) neither an interaction between *high-sadness/low-sadness* and *Neutral-WM1/Sadness-WM2*, (3-way ANOVA, $p = 0.12$).

Then, we looked for other nodes, which could mediate the modulation of the hubs. We analyzed the change in correlations between the 2 hub nodes identified above (mFPl and dlPFCl) and all other network areas (as a measure of functional connectivity) for each participant, task paradigm and sadness-intensity groups. We thus tested a total of 19 pairwise correlations for each hub node, and we corrected our tests for the multiple comparisons problem by controlling the false discovery rate (FDR) at a level $\alpha=0.05$.

The functional connectivity between dlPFCl and sACCl presented a significant interaction between *high-sadness/low-sadness* and *Neutral-WM1/Sadness-WM2*, (3-way ANOVA, p = 0.0006, $p_{(\text{FDR-corr})}$ = 0.036). The correlations between dlPFCl and sACCl became more negative after sadness provocation only in the *high-sadness* group (Fig. 3.11A, paired sample t-test p=0.0001 for *high-sadness* group and p=0.49 for *low-sadness* group). In other words, only the group reporting more intense sadness presented a stronger anticorrelation between sACCl and dlPFCl after sadness induction. This suggests that the interactions of dlPFCl with sACCl could be associated with the reduction in network degree following sadness induction in dlPFCl (Fig. 3.9C).

In addition, the hub area mFPl presented one uncorrected significant interaction (*high-sadness/low-sadness* groups and *Neutral-WM1 Sadness-WM2*) in its correlation with sACCl (Fig. 3.11B, 3-way ANOVA, p = 0.0434, $p_{(\text{FDR-corr})}$ = 0.4). All other correlations with mFPl were non-significant. The correlation between sACCl and mFPl showed a marginally significant increase after sadness provocation only in the *high-sadness* group (Fig. 3.11B, paired sample t-test p = 0.083 for *high-sadness* group and p = 0.26 for *low-sadness* group). The correlation between mFPl and sACCl is thus the one connection of this

Figure 3.11: Sadness intensity increases the sACCl-dlPFCl anticorrelation and sACCl-mFP correlation.

Correlations subject by subject for sACCl-dlPFCl and sACCl-mFP BOLD fluctuations during Neutral-WM1 and Sadness-WM2, *high-sadness* subjects are plotted in red lines, *low-sadness* subjects in blue lines and the averages are plotted in thick red and blue lines, respectively.

A. *High-sadness* subjects present significant increased between sACCl and dlPFCl anticorrelations during Sadness-WM2, relative to *low-sadness* subjects.

B. *High-sadness* subjects present a marginally significant increased between sACCl and mFPl correlations during Sadness-WM2 in comparison with *low-sadness* subjects.

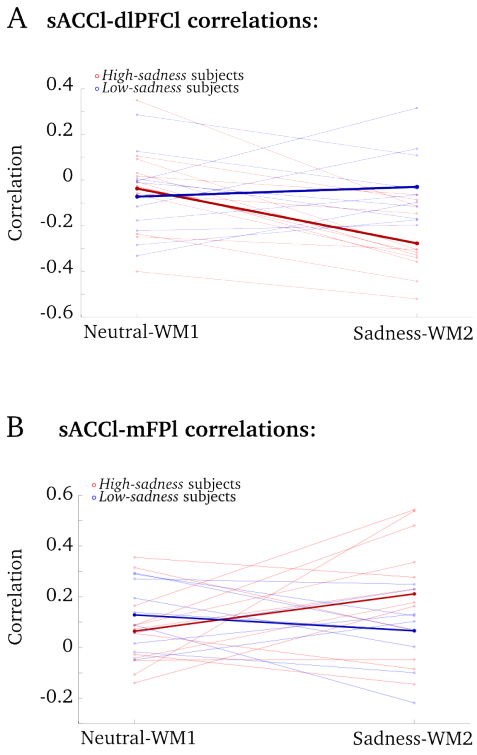

hub area that could be responsible for its sadness-dependent modulation in network degree (see Fig. 3.10C).

Summarizing the findings of this first section, we found sadness-related effects at three different levels: behavioral, in functional activity, and in network structure. Importantly, we typically evaluated sadness-relatedness by testing the interaction between behavioral paradigm and sadness intensity report, which is a strong constraint emphasizing the role of sadness experience in all these modulations. At the behavioral level, the subjects that reported highest emotional scores diminished their performance in the working memory task after sadness provocation (Fig 3.1 and Table 3.2). At the level of functional brain activity, we found an overall decrease in activation in the cognitive areas (Fig. 3.3), an increase in sACCl activity (Fig. 3.4) and an inter-individual anticorrelation between sACCl

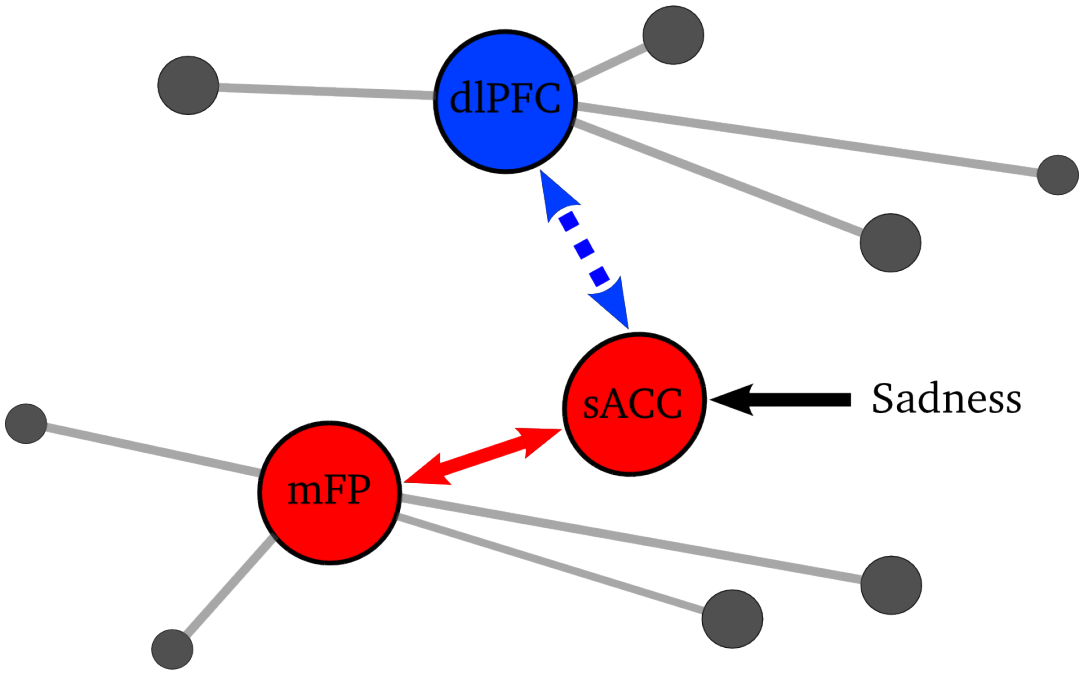

Figure 3.12: Schematic summary: Sadness-related effects in functional activity and in network structure.

The sACC was a key area: it showed a strong increase in the negative functional connectivity with dlPFCl and increase in the positive functional connectivity with mFPl, following sadness provocation and specifically for high-sadness participants. These functional connectivity modulations could underlie the hub modulations. The dlPFCl degree was decreased after sadness provocation and mFPl degree was modulated by the sadness intensity. Red (blue) denotes *degree increases* (*degree decreases*) and dashed (continuous) arrow denote negative (positive) functional connectivity.

and dlPFCl activity (Fig. 3.5). Finally, the graph analysis showed a stronger segregation between emotional and cognitive networks following a strongly emotional experience (Table 3.3), with the connectivity of the cognitive hub dlPFCl being down-regulated after sadness provocation (Fig. 3.9) and that of the emotional hub mFPl up-regulated by sadness intensity (Fig. 3.10C). The sadness intensity also modulated the functional connectivity of these hubs: it increased the correlation between sACCl and mFPl and the anticorrelation between sACCl and dlPFCl (Fig. 3.11). We summarize these findings schematically in Figure 3.12 and we will speculate about the relationship between behavior, BOLD activity, graph-network measures and functional connectivity in Discussion.

Results for cingulo-frontal modeling

The brain image analysis presented above shows that, in conditions of strong conflicting emotional and cognitive demand the dynamics of areas sACC and dlPFC become highly anticorrelated. Associated to this dynamics, we found higher scores in emotional reports and diminished cognitive performance. Based on these findings and previous literature (see Introduction), we complement this work with a computational model of major depressive disorder (MDD), where we will test the possible implication of vACC-dlPFC dynamics in this disease (for the list of hypotheses see Objectives).

Healthy operation based on reciprocal suppression between the cognitive and emotional networks

We simulated situations of strong conflicting emotional and cognitive demand (Fig. 3.13A), with purely emotional (sadness provocation task, SP, (Liotti et al. 2000)) or purely cognitive (working memory task, WM, (Fuster and Alexander 1971; Kubota and Niki 1971)) task epochs. The simulated tasks (SP and WM) were chosen to emphasize the competitive aspect of emotional and cognitive processes. In addition, we modeled also resting epochs before and after these tasks, in which none of the modules received task-dependent inputs.

We tuned our "healthy" cingulo-frontal network model so that each sub-network showed two stable states (Fig. 3.13B, C), one with neurons firing asynchronously at low rates (0.5-1 sp/s) and another one with asynchronous firing at higher rates (25-30 sp/s, Fig. 3.12B, C), synchronized at theta (2-8 Hz) and beta/gamma (12-50 Hz) frequencies (Fig. 3.13D). Normal or "healthy" operation occurred if the dlPFC or vACC circuits stabilized the high-rate state only during epochs of high cognitive or emotional demands, respectively; i.e. only following the activation of their specific afferents.

Thus, in the SP vACC responded persistently to transient stimuli, while brief inputs to dlPFC in the WM triggered its persistent activation (Fig. 3.13). We modeled persistent activity in the vACC and dlPFC circuits based on available electrophysiological data for

relevant behavioral protocols: human ACC neurons show sustained modulations in cognitive and emotional tasks (Davis et al. 2000, 2005) characterized by synchronization in the theta and beta/low-gamma bands (Asada et al. 1999; Tsujimoto et al. 2010; Lipsman,

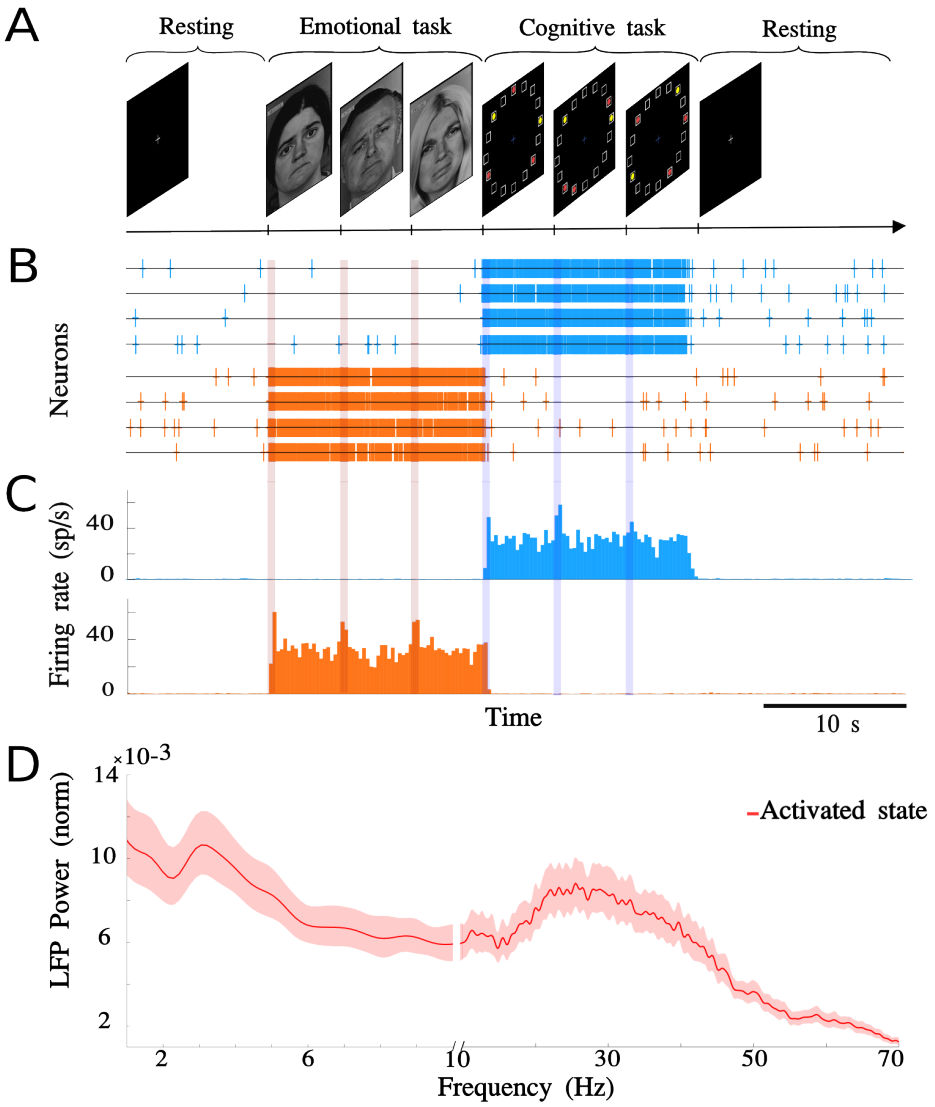

Figure 3.13: "Healthy" operation in the network is the ability to switch from emotional to cognitive processing.

A. We simulated a task composed of i) 10 s resting epoch, ii) 15 s SP epoch (vACC received 3 brief stimulus every 5 s), iii) 15 sec WM epoch (dlPFC received 3 brief stimulus every 5 s), iv) 20 sec resting epoch. Stimulation pulses were 250 ms long Poisson trains at 200 sp/s impinging on AMPARs with conductance 2.4 nS. **B.** Sample activity in four neurons of each network in one simulation. In orange, vACC neurons and in blue, dlPFC neurons. **C.** Histograms of average population activity in each network during one task simulation. Upper panels correspond to dlPFC activity (blue) and lower panels to vACC activity (orange). **D.** LFP normalized power spectrum for the activated state. In both sub-networks (vACC and dlPFC) spectra are characterized by the coexistence of theta (2-8 Hz) and beta/gamma (12-50 Hz) synchronization. Jackknife error bars around the mean mark the 95% CI.

Kaping, et al. 2014), and monkey studies report persistently active neurons in relation to punishment or reward in the vACC (Koyama et al. 2001; Shidara and Richmond 2002; Amemori and Graybiel 2012; Monosov and Hikosaka 2012), and in working memory tasks in the dlPFC (Fuster and Alexander 1971; Kubota and Niki 1971; Funahashi et al. 1989; Goldman-Rakic 1995).

A key factor in the "healthy" operation of this system was the ability of the network to switch from emotional to cognitive processing (Fig. 3.13B, C) when the first cognitive signal arrived to dlPFC. In our network, this occurred through mutual inhibitory mechanisms between the two circuits, so that activation of dlPFC caused the deactivation of neuron firing in vACC.

Progressive nature of MDD

We tested the hypothesis that slower glutamate re-uptake in vACC is a causal mediator of MDD symptoms in our vACC-dlPFC network model (Choudary et al. 2005; Walter et al. 2009; Horn et al. 2010; Portella et al. 2011).

First, for the early stages of MDD (mild MDD network, Fig. 3.14A), a mere 2.5% slow-down in glutamate decay in vACC generated aberrant activity (~40 sp/s) in vACC during the resting epoch. As vACC was already activated when emotional stimuli arrived during the SP epoch, the dynamics of vACC did not change. During the WM epoch, the dlPFC network responded partially to the first inputs, but it was able to respond correctly to subsequent inputs. Although the dlPFC showed a slight alteration in the pattern of activation it was still able to turn off activity in vACC during the WM epoch.

With a 5% slow-down in glutamate decay in vACC, we simulated a network with moderate MDD (Fig. 3.14B): vACC still showed aberrant activity but now dlPFC network barely responded to cognitive inputs in the WM epoch, being unable to turn off the vACC effectively in the WM epoch. A further slow-down of glutamate decay caused more severe disruption of network dynamics, in what we call the severe MDD network (Fig. 3.14C). Here, vACC showed aberrant activity that was not modulated, neither in the SP epoch nor in the WM epoch. The synaptic imbalance induced by slower glutamate decay in vACC

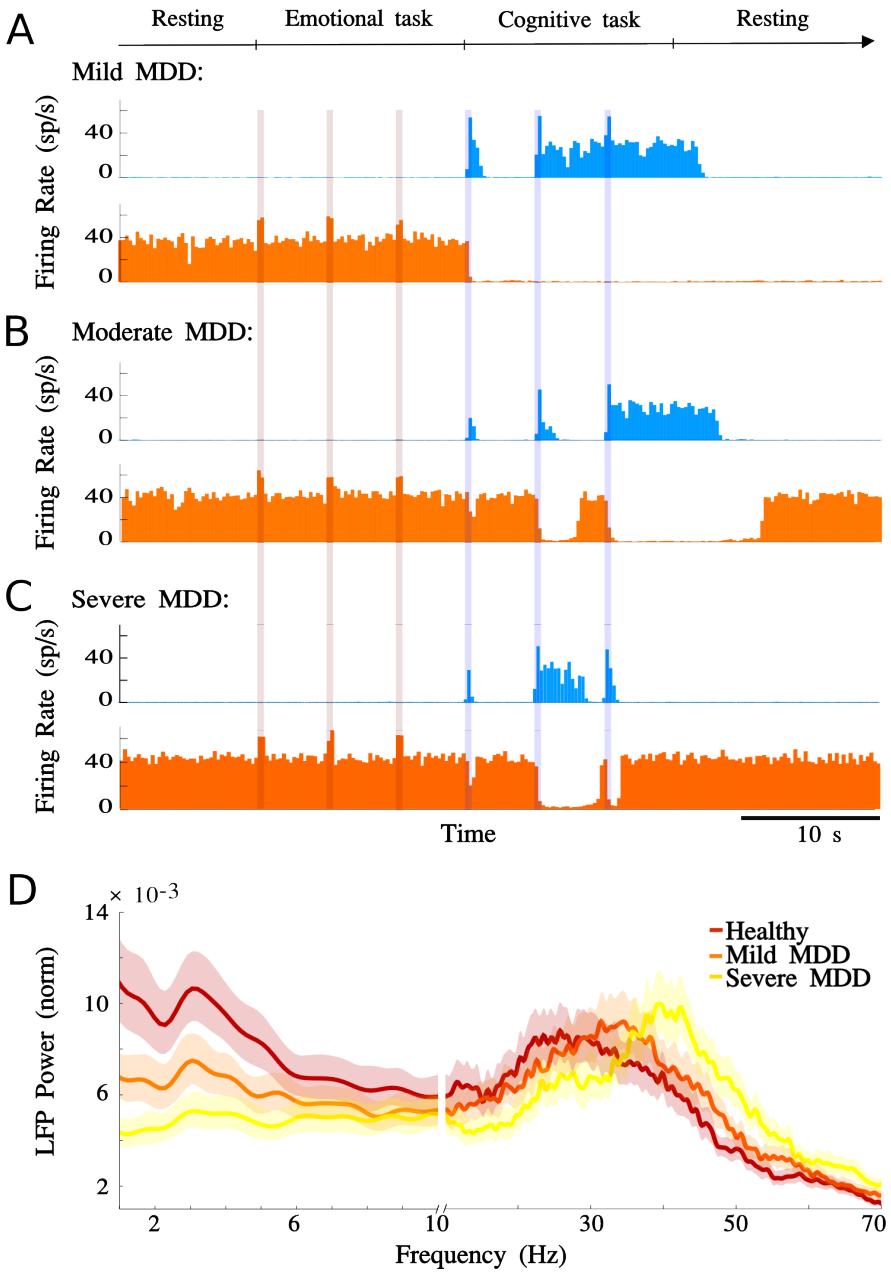

Figure 3.14: Glutamate decay slow-down reproduces the progressive nature of MDD.

A. Mild MDD network (2.5% slow-down in glutamate decay in vACC). Activity histograms for a single simulation show aberrant activity in vACC during the resting epoch. Although dlPFC only responded partially to the first inputs, it was still able to turn off activity in vACC during the WM epoch. **B.** Moderate MDD network (5% slow-down in glutamate decay in vACC). vACC showed aberrant activity in resting epochs and dlPFC showed diminished responsivity to cognitive inputs, now being unable to turn off vACC. **C.** Severe MDD network (7.5% slow-down in glutamate decay in vACC). Aberrant vACC activity was not modulated by any kind of inputs. **D.** LFP normalized power spectrum in vACC. Synchronization in the theta frequency range was progressively reduced, while beta/gamma rhythms were enhanced as glutamate decay was gradually slowed down (healthy, 2.5% and 7.5% slow-down in glutamate decay). Jackknife error bars around the mean mark the 95% CI.

resulted in strong stabilization of the persistent activity state and destabilization of the low-rate state in vACC, while dlPFC became completely inhibited by vACC, and it was unable to respond to cognitive inputs in the WM epoch. The severe MDD model showed a complete inability to switch from emotional to cognitive processing.

In summary, the progressive slow-down of glutamate decay generated aberrant activity in vACC, which was characterized by sustained vACC activation in the absence of emotional signals, and difficulty to switch off when dlPFC received cognitive inputs. We interpreted this pattern as the generation of a spontaneous negative emotional state, which becomes impervious to stimuli with the progression of disease, reminiscent of the clinical progression from *emotional symptoms* (Mild MDD model) to *progressive loss of mood reactivity* (Severe MDD model). In turn, dlPFC also showed alterations as it could not be persistently activated in response to a cognitive signal, due to hyperactivity in vACC. This would be interpreted as a cognitive impairment that progresses with MDD (*cognitive symptoms*) (Fig. 3.14A-C).

Interestingly, the synchronization properties of the vACC active state were also altered by glutamate decay slow-down. Synchronization in the theta frequency range was progressively reduced, while beta/gamma rhythms were enhanced as glutamate decay was slowed down further (Fig. 3.14D). This is consistent with results showing that frontal beta rhythms correlate positively with the severity of depression (Pizzagalli et al. 2002).

Serotonin treatment response decreases with the progression of the disease

Additionally, we simulated the effects of SSRI treatments on the MDD networks by modeling the effect of SSRIs through 5-HT_{1A} receptors as a small hyperpolarization of vACC excitatory neurons (Andrade et al. 1986; Béïque et al. 2004; Santana et al. 2004; Palomero-Gallagher et al. 2009; Castañé et al. 2015). In each MDD network model we increased progressively the dose of SSRI treatment, and we found various behavioral responses that can be grouped into three groups: *non-response*, *optimal response* and *emotional inhibition* (Fig. 3.15).

Non-response to SSRI was found across all MDD network models when the synaptic imbalance was too big to be counteracted by SSRI hyperpolarization (Fig. 3.15A). In this situation, SSRI treatment was insufficient to alter MDD network dynamics and the vACC maintained robust aberrant activity irrespective of the task epoch. The dlPFC network was completely inhibited by the vACC, it could only respond briefly to cognitive inputs during

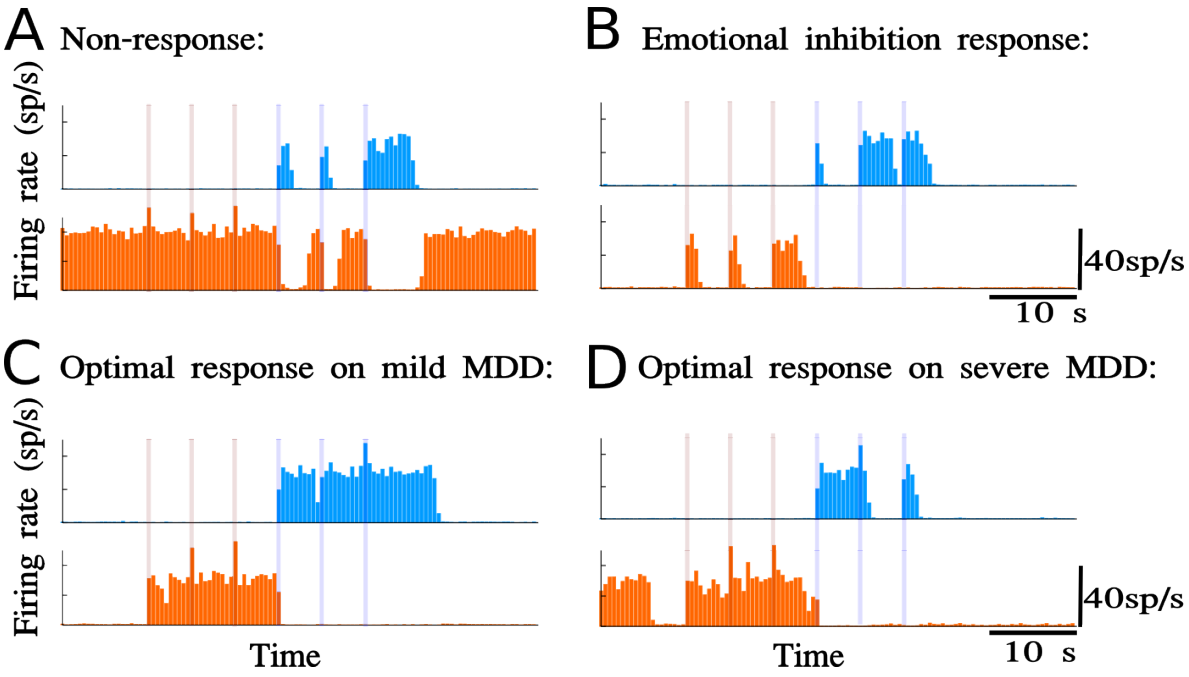

Figure 3.15: Serotonin treatment response on MDD network models decreases with the progression of the disease.

A. Non-response: A moderate MDD model (5% slow-down in glutamate decay) treated with a low dose of SSRI (V_L = –70.05 mV), vACC showed aberrant activity in resting epochs and dlPFC showed diminished responsivity to cognitive inputs. **B.** Emotional inhibition: A moderate MDD model (5% slow-down in glutamate decay) treated with a high dose of SSRI (V_L = –70.5 mV), SSRI treatment could turn off aberrant activity in vACC in the resting epoch, but also inhibited the response of vACC to emotional stimuli during the ET epoch. **C.** Optimal response on mild MDD model: Mild MDD (2.5% glutamate decay slow-down) treated with an optimized dose of SSRI (V_L = –70.18 mV). **D.** Optimal response on severe MDD model: Severe MDD (7.5% glutamate decay slow-down) treated with an optimized dose of SSRI (V_L = –70.6 mV).

the WM epoch, and it was unable to turn off the vACC. Despite SSRI treatment, this MDD network model remained unable to switch from emotional to cognitive processing.

At the other extreme, we found an *emotional inhibition response* when the hyperpolarization induced by SSRIs exceeded the hyperexcitability generated by glutamate

decay slow-down in the vACC network (Fig 3.15B). Here, SSRI treatment could turn off aberrant activity in vACC in the resting epoch. However, SSRI-induced hyperpolarization also inhibited the response of vACC to emotional stimuli during the SP epoch, thus preventing healthy activation in emotional periods. This pattern is reminiscent of *emotional flatness*, a known adverse effect of SSRI treatments (Walsh et al. 2006; Price et al. 2009). Following SSRI-induced inhibition of vACC, the dlPFC network restored its normal response to cognitive inputs.

Adjusting SSRI doses between these two cases we found an *optimal response* scenario, in which treated MDD networks presented a behavior close to normal (Fig. 3.15C, D). Here, the SSRI treatment suppressed aberrant activity in vACC and allowed it to respond to emotional inputs by entering the persistent activation that corresponded to healthy emotional processing. Response to cognitive inputs in dlPFC was similar to normal. In all simulations, activation of the cognitive network turned off the vACC.

In summary, adjusted SSRI treatment doses could improve the function of our networks by deactivating the aberrantly active vACC of our MDD models and thus restoring close-to-normal emotional and cognitive processing (Fig. 3.15C). However, the optimal response to SSRI was worse in networks with slower glutamate decay (simulating more severe MDD conditions), in which the stability of healthy states could not be fully recovered (Fig. 3.15D). We demonstrated the progressive deterioration of the response to optimal treatment in 50 repeated simulations of two network models: a mild MDD model and a severe MDD model, both treated with an *optimal* dose of SSRI (Fig. 3.15C, D). For the mild MDD model, most trial simulations presented healthy-like behavior (Fig. 3.15C) and only a few simulations (18%) had unstable persistent activity during the SP epoch. Instead, the optimally-treated severe MDD model presented a higher incidence of abnormal trials (38%, Fig. 3.15D), with aberrant vACC hyperactivity during the resting epoch or unstable persistent activity during the SP period.

This could be graphically illustrated by repeating simulations for healthy and severe MDD models in a range of membrane potentials for vACC excitatory neurons (representing progressive dose-response to SSRI treatments). Figure 3.16A plots the mean firing rate of excitatory neurons over stable active (upper branches) and inactive (lower branches)

network states. The graph demonstrates the existence of a "bistable range" in which network function is bistable between the two network states. Treatments falling within this bistable range will be effective in recovering proper function. The fact that the severe MDD

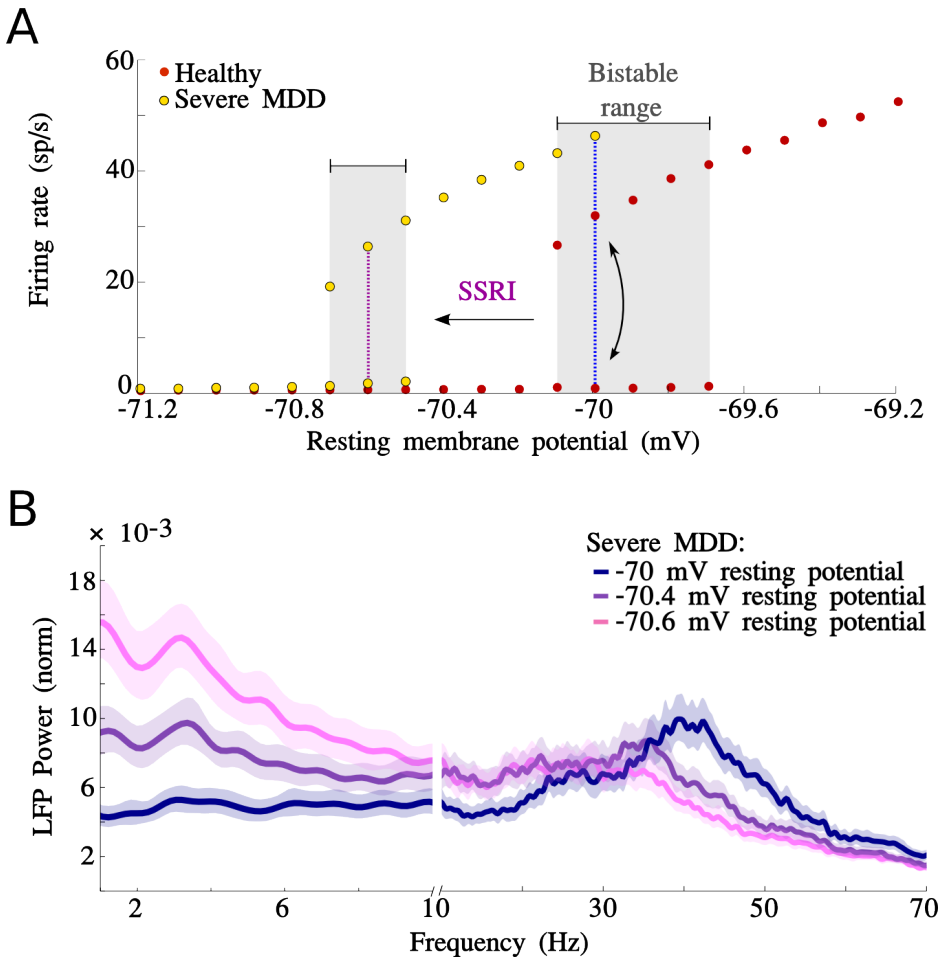

Figure 3.16: The bistable range in vACC network decreases with MDD progression.

A. Bifurcation diagram for healthy and severe MDD models: Mean firing rate of excitatory neurons over stable active (upper branches) and inactive (lower branches) network states. The red (yellow) dots represent stable states for the healthy (severe MDD) model. The plot shows the existence of a bistable range, in which network function is bistable between the two network states. The blue dotted line represents the baseline network's operating regime, which is in the bistable range in the healthy model. For the severe MDD model, the baseline network's operating regime is on the right side of the bistable range, where only the high rate state (activated state) is stable. The magenta dotted line represents the hyperpolarization generated by the SSRI treatment in the optimal response. Note that the reduction in the bistable range in the severe MDD network generates a reduction in the stability of both activated and inactivated states. **B.** LFP normalized power spectrum in vACC of a severe MDD network treated with SSRI. Severe MDD model (7.5% glutamate decay slow-down) treated with progressively increasing doses of SSRI (V_L = –70, –70.4 and –70.6 mV). Synchronization in the theta frequency range was progressively enhanced while beta/gamma rhythm amplitude decreased as the dose of SSRI increased. Jackknife error bars around the mean mark the 95% CI.

network has a narrower bistable range gives a mechanistic explanation to the difficulty of finding optimal treatments for this network (Fig. 3.16A).

In addition, optimal treatment also recovered the oscillatory dynamics characteristic of the healthy activated state: SSRI treatment enhanced theta oscillations and suppressed rhythmic activity in the beta/gamma band (Fig. 3.16B).

Deep brain stimulation restores bistability in the treatment-resistant model

We went further by simulating the acute effects of deep brain stimulation (DBS) in a treatment-resistant model. We tested 2 hypotheses for the mechanism of action of DBS in the vACC of MDD treatment-resistant patients. The first hypothesis considers that the therapeutic action of DBS is mediated by the serotonin system (Hamani et al. 2010, 2012). The second hypothesis postulates that DBS acts by activating interneurons in the vACC (Mayberg et al., 2005). The mechanism of action through the serotonin system was presented in the previous chapter. Essentially, DBS would converge on the same serotonin receptor activation mechanism presented so far by stimulating serotonin release in vACC, as opposed to slowing down serotonin re-uptake as SSRIs did. This would enhance the dynamical range of this serotonergic mechanism to achieve the stabilization of the circuit. Here, we explore the mechanistic hypothesis that DBS action is mediated by interneurons.

First, we generated an MDD *treatment-resistant* model slowing-down by 10% the glutamate decay in vACC and treating it with an insufficient dose of SSRI (–70.5 mV resting potential) (Fig. 3.17A). Then, we simulated DBS treatment in our treatment-resistant network model by stimulating the inhibitory population of vACC with periodic trains of excitatory external inputs at 130 Hz. The parameters for DBS stimulation were the following: duration = 0.01 ms, interpulse interval = 7.69 ms, intensity (g^{syn}_{AMPA}) = 0.62 nS.

The main effect of simulated DBS was a rescue of the switch function between emotional and cognitive processing (Fig. 3.17B). In addition, in most of the simulations DBS treatment also suppressed aberrant activity in vACC (Fig. 3.17B *top*), but in other simulations aberrant activity was present during the resting epoch (Fig. 3.17B *bottom*). In those simulations with no aberrant vACC activity, vACC responded to emotional inputs by

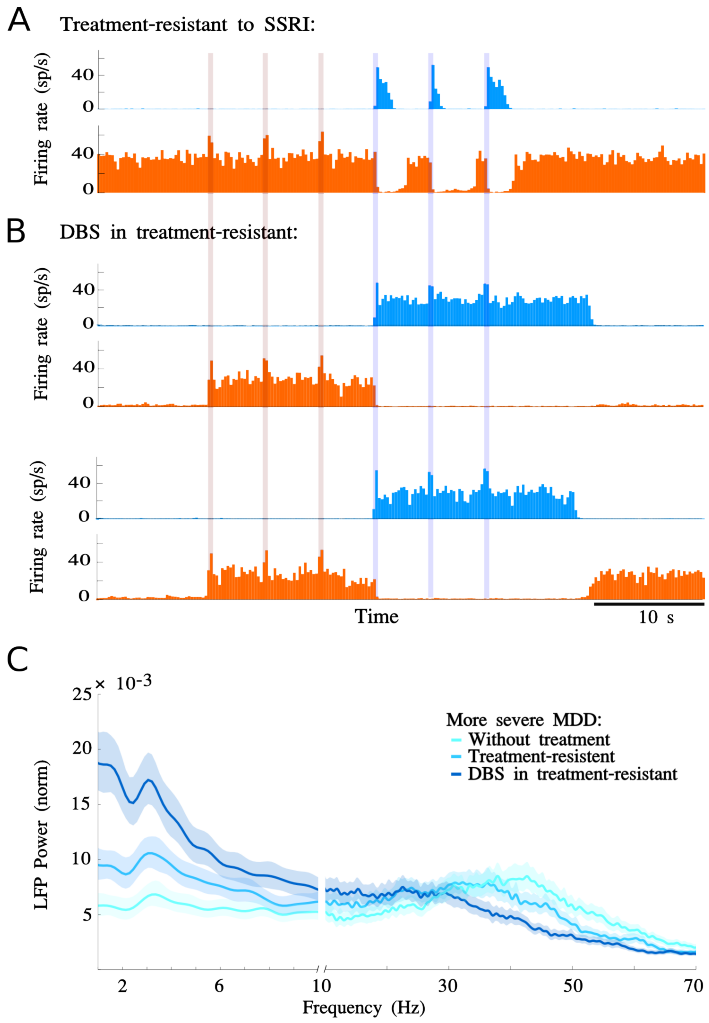

Figure 3.17: DBS restore the switch between emotional and cognitive processes.

A. Treatment-resistant MDD model: A more severe MDD model (10% slow-down in glutamate decay) treated with a insufficient dose of SSRI (V_L = –70.5 mV), vACC showed aberrant activity in resting epochs and dlPFC showed diminished responses to cognitive inputs. The MDD network model was resistant to SSRI treatment. **B.** DBS in treatment-resistant model: Treatment-resistant model (10% glutamate decay slow-down and V_L = –70.5 mV) treated with DBS at 130 Hz. **C.** LFP normalized power spectrum in vACC of a more severe MDD network treated with SSRI and DBS. More severe MDD model (10% glutamate decay slow-down) no-treated (V_L = –70), treated with insufficient dose of SSRI (V_L = –70.5) and treated with SSRI (V_L = –70.5) and DBS. Synchronization in the theta frequency range was progressively enhanced while beta/gamma rhythm amplitude decreased with the dose of SSRI and DBS. Jackknife error bars around the mean mark the 95% CI.

entering the persistent activation that corresponded to healthy emotional processing. Response to cognitive inputs in dlPFC was normal and it could turn off the vACC (Fig. 3.17B). Thus, DBS compensated the synaptic imbalance through the activation of the vACC inhibitory population.

In addition, DBS treatment also recovered the oscillatory dynamics characteristic of the healthy activated state: DBS treatment enhanced theta oscillations and suppressed rhythmic activity in the beta/gamma band (Fig. 3.17C). These oscillations and the incidence of abnormal trials where aberrant activity appeared in the resting epoch suggested that the *treatment-resistant* model treated with DBS also had a narrower bistable range, similar to our results above following the serotonin treatment (Fig. 3.16B). We explore this phenomenon in detail below (see *Deep brain stimulation in the firing-rate model* section)

fMRI prediction from the spiking model

For MDD there is an extensive literature obtained with neuroimaging techniques available (see Introduction). To compare our model with this data we computed an *fMRI* signal from neural activity in our circuits by convolving the total synaptic activity in each module with the standard hemodynamic response function (Glover 1999; Deco et al. 2004) (Materials and Methods).

In Figure 3.18, we plot the simulated *fMRI* signal for "healthy" and MDD network models. In the "healthy" network, the SP epoch generated an increase of *fMRI* signal in vACC (relative to resting epoch) and WM enhanced the *fMRI* signal in dlPFC.

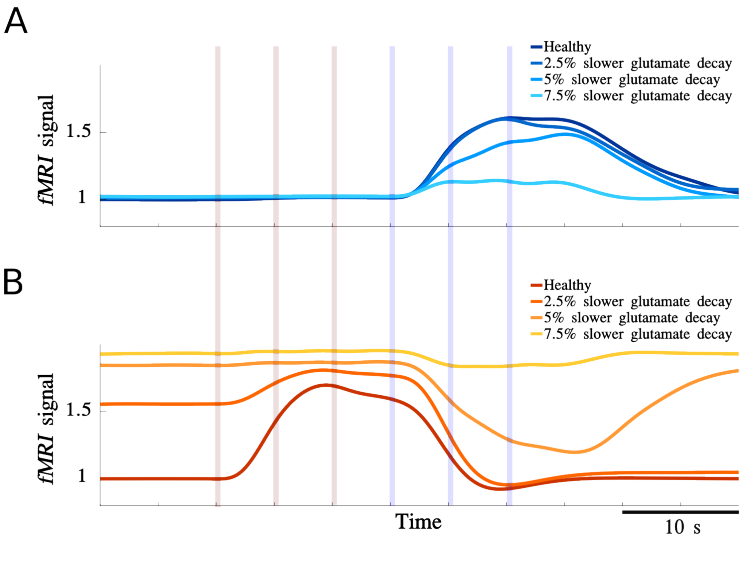

Figure 3.18: Simulated fMRI signal reproduces the evidence from literature.

Percentage of *fMRI* signal change relative to healthy baseline for each population averaged across 50 simulations. **A.** Percentage of *fMRI* signal change relative to healthy resting epoch for the vACC network, averaged across 50 simulations. Progressive hyperactivity in the vACC BOLD signal as glutamate decay is slowed down. **B.** Same for dlPFC network. Progressive hypoactivity in the BOLD signal.

Using simulated *fMRI* data, analogous effects to spike-time histograms presented above (Fig. 3.14) are observable. We calculated the *fMRI* signal change in all MDD networks during all simulated task using as a reference signal the resting epoch of the "healthy" network (Fig. 3.18A, B). The *fMRI* signal showed hyperactivity in the vACC during the resting epoch of MDD networks relative to "healthy" networks (Fig. 3.18B). In neuroimaging experiments this would correspond to a positive contrast in vACC when comparing MDD patients and controls (Mayberg et al. 1999, 2005; Seminowicz et al. 2004; Drevets et al. 2008). The dlPFC network showed a progressive decrease in the *fMRI* signal relative to the healthy network (Fig. 3.18A), consistent with the BOLD hypoactivity reported in dlPFC of depressed patients (Bench et al. 1992; Mayberg 1997; Kennedy 2001;

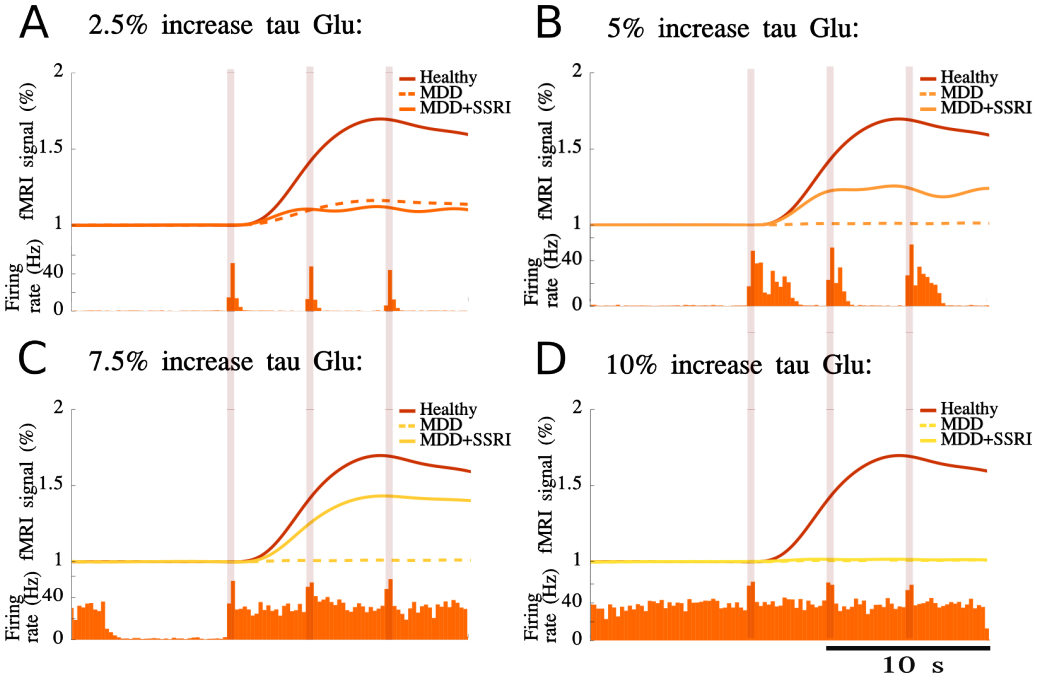

Figure 3.19: The fMRI response in vACC during SP epoch in MDD and MDD treated with SSRI network models.

Percentage of *fMRI* signal change relative to the resting epoch in the MDD models (dashed lines) and MDD models treated with SSRI (V_L = –70.5 mV) (continuous lines) for vACC population averaged across 50 simulations **A, B.** *(top)* MDD (2.5% and 5% slow-down in glutamate decay) and MDD+SSRI networks presented a abolished fMRI-simulated response to SP epoch. *(bottom)* Histogram of average vACC population activity in MDD+SSRI network shows an *emotional inhibition response*. **C.** *(top)* MDD (7.5% slow-down in glutamate decay) network show a abolished response and MDD+SSRI network show a decreased response to SP epoch. *(bottom)* Histogram of average vACC population activity in MDD+SSRI network shows an *optimal response*. **D.** *(top)* MDD (10% slow-down in glutamate decay) and MDD+SSRI networks presented a completely suppressed fMRI-simulated response to SP epoch. *(bottom)* Histogram of average vACC population activity in MDD+SSRI network shows a *non-response*.

Videbech et al. 2002; Oda et al. 2003; Mayberg et al. 2005).

In sadness provocation experiments, however, experiments would typically contrast brain activity before and after sadness induction in the same subjects. In our data, incoming input signals in the SP epoch did not produce much activity change in vACC in MDD networks (Fig. 3.18B). This is in line with previous literature, where acutely depressed patients did not activate vACC during sadness provocation (Liotti et al., 2002), unlike healthy subjects (Liotti et al. 2000). We quantified explicitly these contrasts in our data by calculating the simulated *fMRI* signal change response relative to the resting epoch of each network model (Fig. 3.19). We considered MDD models without treatment and MDD models treated with SSRI ($V_L = -70.5$ mV).

Responses to the SP epoch were abolished in all untreated MDD model (dashed lines Fig. 3.19). The explanation for that is fairly intuitive, vACC was already active when emotional stimuli arrived during the SP epoch (aberrant activity during resting epoch, Fig. 3.14), and the dynamics of vACC did not change (Figs. 3.14 and Fig. 3.18).

Treated MDD models showed a recovery of response to SP inputs, although still diminished relative to the healthy network (Fig. 3.19) . This is due to three different factors. First, the SSRI hyperpolarization may be larger than the hyperexcitability generated by glutamate decay slow-down in the vACC network. In this case (defined above as *emotional inhibition response*), vACC cannot be activated properly and the *fMRI* response is diminished (Fig. 3.19 A, B). Second, the synaptic imbalance may be too big to be counteracted by SSRI hyperpolarization. In this case (named above *non-response*), the dynamics of the vACC is not modulated and the *fMRI* response is also diminished (Fig. 3.19D). Third, the *fMRI* response may be close to normal (*optimal response*) if the SSRI treatment suppressed aberrant activity in vACC and allowed it to respond to emotional inputs by entering the persistent activation (Fig. 3.19C). Nevertheless, even in this case the peak *fMRI* response is decreased compared with the healthy response (Fig. 3.19C) because of the incidence of abnormal trials where aberrant activity appears in the resting epoch, as a result of the narrower bistable range (Fig. 3.16A).

To fully explore how SSRI treatment affected *fMRI* contrasts in all task epochs we calculated the fMRI signal for three different MDD networks across SSRI conditions (i.e.

varying parametrically the resting potential of excitatory vACC neurons) during the resting, SP and WM epochs (Fig. 3.20, see Materials and Methods).

Comparing the resting epoch activation in MDD networks to the healthy network hyperactivity characterized vACC for low doses of SSRI treatment. When the SSRI dose generated an *optimal response* the vACC contrast deactivated, and remained so for increasing SSRI doses, including the *emotional inhibition response* (Fig. 3.20A).

We then compared fMRI resting activity in vACC in the SP epoch relative to the resting epoch for each network (Fig. 3.20B). This contrast increased only when the MDD network was treated with optimal doses of SSRI. Treatments that lead to both *non-response* and

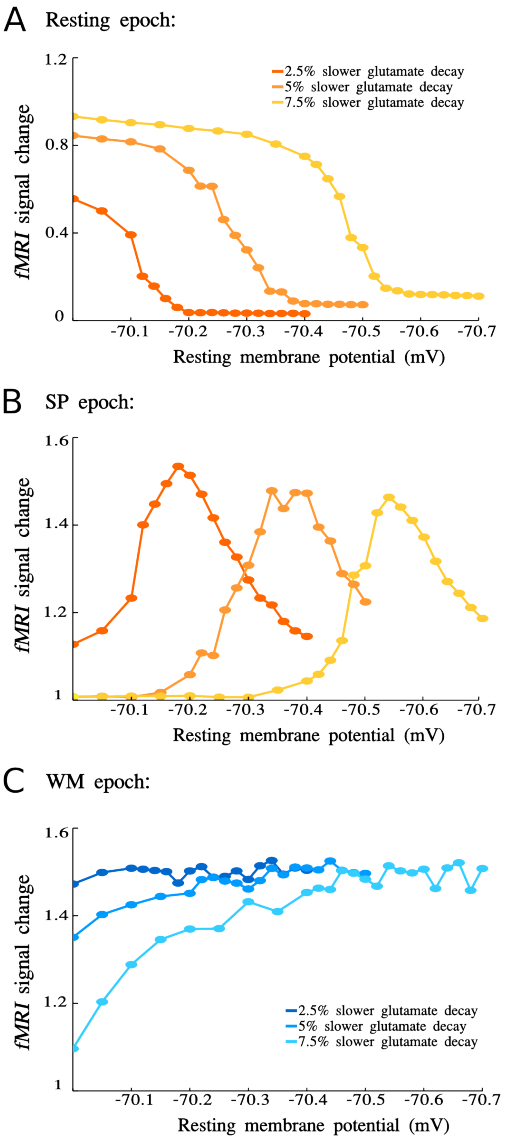

Figure 3.20: The fMRI-simulated response during resting, SP and WM epochs for all MDD and SSRI parameters.

Percentages of *fMRI* signal change for resting, sadness and working memory epochs over 50 simulations for all MDD networks and SSRI conditions.

A. Mean percentage of *fMRI* signal change during resting epoch relative to healthy resting epoch for the vACC network, averaged across 50 simulations. The decrease in the fMRI activity marks the suppression in the aberrant activity.

B. Mean percentage of *fMRI* signal during SP epoch change relative to each resting epoch for the vACC network, averaged across 50 simulations. The increase in the fMRI activity marks the *optimal response*.

C. Mean percentage of *fMRI* signal change for WM epoch relative to healthy resting epoch for the dlPFC network, averaged across 50 simulations. The increase in the fMRI activity marks the recovery of the switch between emotional and cognitive processes.

emotional inhibition network behaviors did not generate an fMRI contrast between the SP and resting epochs (Fig. 3.20B).

When we contrasted fMRI activity in the WM epoch to the resting epoch, the dlPFC network showed hypoactivity for low-dose treatments, which disappeared as the dose increased (Fig. 3.20C).

Dynamics of a rate-model network

The qualitative match between our network model dynamics (both in the time scale of task epochs and in the synaptic scale of fast network oscillations) and the symptoms and physiology in MDD patients, prompted us to investigate the dynamical structure of our networks in a simplified firing-rate model (Materials and Methods) in order to gain insight on the conditions for optimal treatment of our networks.

We built a rate-model network to simulate the dynamics of our spiking network model. Two coupled differential equations described the dynamics of the excitatory and inhibitory firing rates in each of the vACC and dlPFC sub-networks (Materials and Methods), and related them to the relevant network parameters. These include: the synaptic coupling strengths within and between sub-networks, the parameter f_D controlling the degree of vACC excitatory enhancement in MDD conditions (corresponding to glutamate decay slow-down in the spiking network model), the current ΔI_e^v which controls the excitability of vACC excitatory neurons and it is used to simulate SSRI treatments and ΔI_i^v which it is used to simulate DBS treatment.

In the healthy condition (f_D =1), the two sub-networks are equivalent and we tuned the parameters so they had a bistable regime (Figs. 3.21A) consistent with the dynamics of our spiking simulations (Figs. 3.13 and 3.16). For a range of ΔI_e^v (bistable range), each sub-network presented two stable attractors (continuous lines in Fig. 3.21A): the low rate (lower branch) and the high rate (upper branch) attractors. These two stable attractors can be understood as two stable states where the network tends to stay because they have lower "energy cost" (Fig. 3.21B). On the other hand, the unstable attractors (discontinuous lines

in Fig. 3.21A), can be understood as transient states between stable states. The network tends to avoid these states because they have a higher "energy cost" (Fig. 3.21B).

In the baseline operating regime, at a specific level of neuronal excitability in the vACC circuit ΔI_e^v (blue dotted line in Fig. 3.21A), the network has two possible stable states and it resides in the low-rate attractor during the resting epoch of the task. When a brief input arrives to the network that activates it, the network jumps to the upper branch (high rate state), and when the stimulus is removed the network maintains the high rate state stable. A sudden increase in negative external current (for instance when dlPFC causes inhibition in vACC) will cause the network to settle again in the low-rate state.

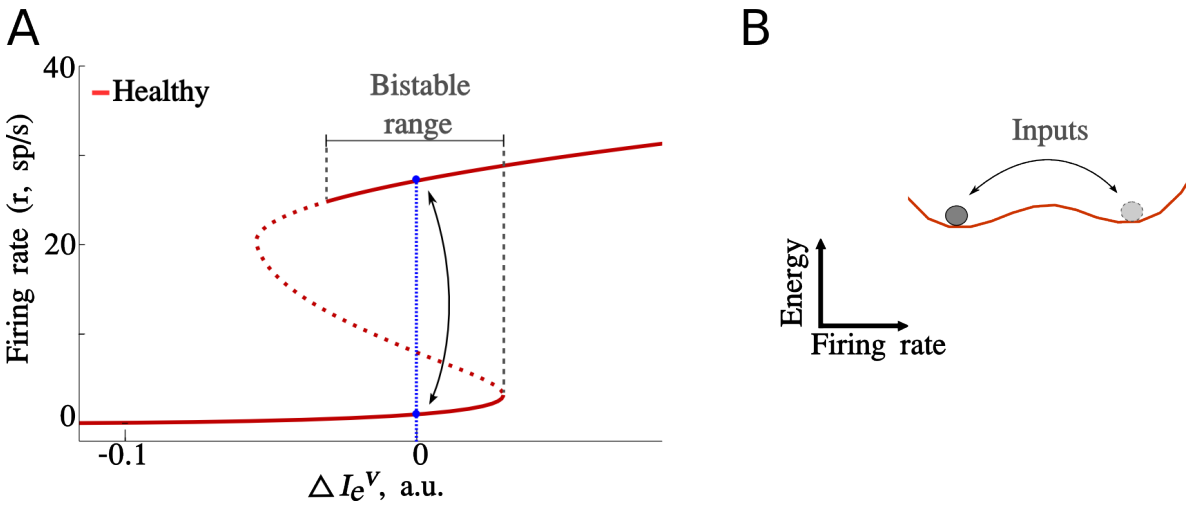

Figure 3.21: Graphical interpretation of vACC dynamics in healthy conditions.

A. The graphical representation of solutions of the rate model upon varying baseline excitability ΔI_e^v presented a bistable dynamics (f_D = 1). Each sub-network presented two stable attractors: the low rate (lower branch) and the high rate (upper branch) attractors, which coexisted for a range of ΔI_e^v (bistable range). The blue dotted line represents the baseline network's operating regime. **B.** Schematic of an "energy landscape" representation that illustrates graphically the network's dynamics in A for a given value of ΔI_e^v (baseline excitability). Population activity (ball) seeks minimum-energy states, but fluctuations can push activity uphill to change attractor.

The "healthy" behavior of the network therefore depends on the existence of a bistable dynamics in the operating regime of the network, and in its tuning so the states are reasonably stable (blue dotted line far enough from bistable range borders) but they can be

destabilized with reasonable inputs (blue dotted line close enough to bistable range borders) in order to effect the switch from one attractor state to the other.

MDD progression in the firing-rate model

The dynamics of our MDD networks could be conceptually understood in the simplified rate model. The slow-down of glutamate decay in the spiking network simulations corresponded in the rate model to an increase in the effective strength of excitation in vACC ($f_D > 1$). This manipulation in the rate model displaced the stability curve to more negative currents progressively (Fig. 3.22A). As a result, MDD networks at the baseline operating regime (blue dotted line) were outside the bistable range for vACC, where the low-rate state destabilized and only the high-rate state was progressively more stable (Fig. 3.22B). This generated permanent persistent activity in the vACC module of MDD networks. In addition, the limit of the bistable range for jumping from the upper to the lower branch moved progressively farther, so that with the progression of the disease the network needed more and more negative current (inhibition) to switch from the high-rate to the low-rate state. This explains conceptually our observation in the spiking network simulations that, with increasing synaptic imbalance, the vACC network became hyperactive and it was progressively more difficult to turn off.

Serotonin treatment in the firing-rate model network

The impact of SSRIs on MDD networks can be also explained conceptually in the rate model. The SSRI-induced hyperpolarization of vACC excitatory neurons in the spiking network simulations corresponded in the rate network model (Eq. (11)) to a negative term added to the external current (ΔI_e^v) in vACC. This manipulation in the rate model (Fig. 3.22C-D) displaced the baseline operating regime to a more negative value (magenta dotted lines). Depending on the severity of MDD (f_D) and the effect of the SSRI (ΔI_e^v), we found three conditions that explain the dynamics observed in the spiking network simulations (*non-response*, *emotional inhibition* and *optimal response*, respectively, Fig. 3.15).

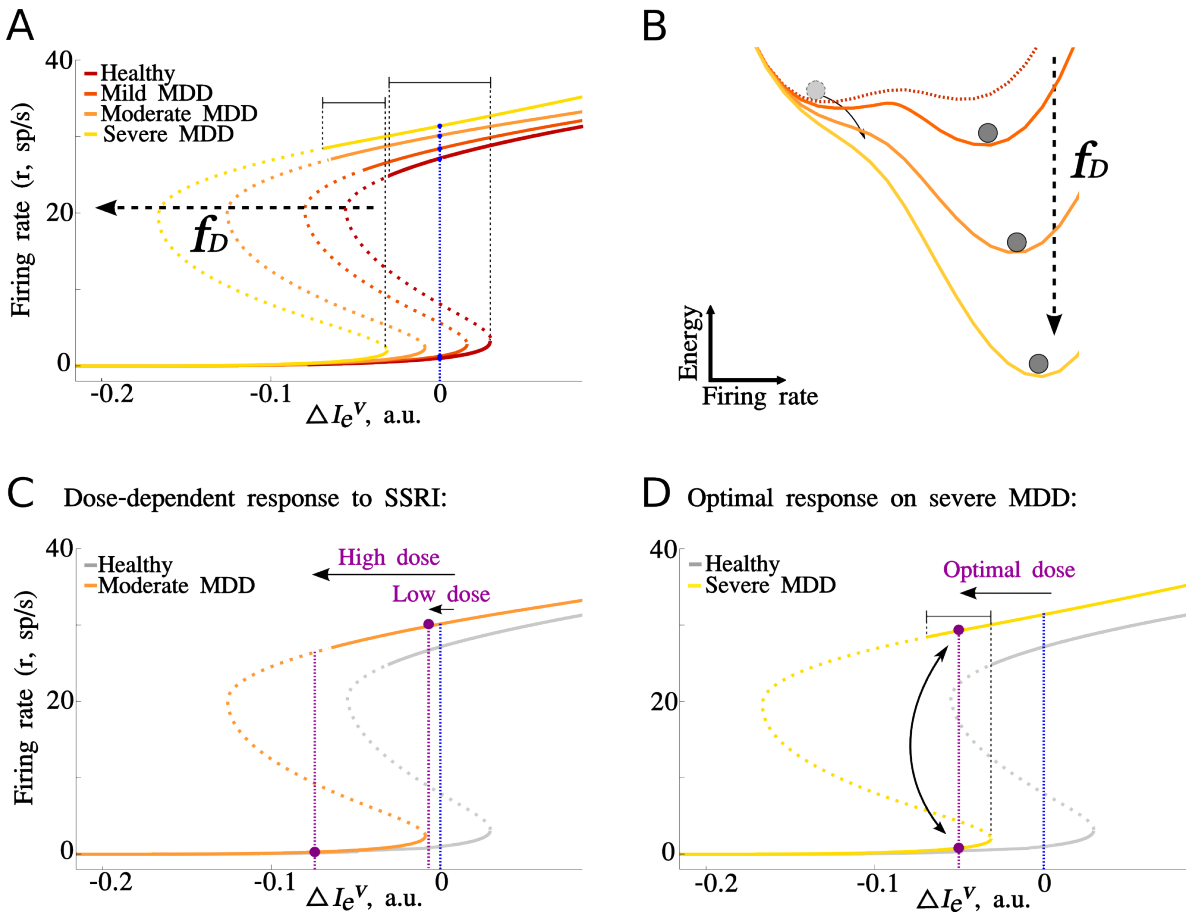

Figure 3.22: Graphical interpretation of vACC dynamics in MDD conditions.

A. Attractor solutions for the MDD rate model after enhancing recurrent excitation in vACC (f_D = 1.05 for mild MDD, f_D = 1.15 for moderate MDD, f_D = 1.25 for severe MDD). The bistable range became narrower and got displaced to more negative currents progressively. MDD networks operated outside the bistable range for vACC, where only the activated state of the upper branch is stable. **B.** Schematic "energy landscape" visualization of C. The energy slope increases with recurrent excitation (f_D) and the population activity (ball) seeks minimum-energy states, which in MDD networks are only activated states. **C.** Non-response and emotional inhibition following SSRI treatment in the moderate MDD model (f_D = 1.15): a low dose SSRI keeps the vACC network out of the bistable range, where only the activated state is stable (*non-response*), and a high dose SSRI moved the vACC network beyond the bistable range, where only the inactivated state is stable (*emotional inhibition*). **D.** Optimal response to SSRI treatment. The severe MDD network model (f_D = 1.25) treated with an *optimal* dose of SSRI (ΔI_e^v = –0.035) operated in the bistable range, but the bistable range was narrower, and thus states were more unstable, than in the healthy network (gray).

For insufficient SSRI hyperpolarization, the network operated on the right side of the bistable range so the low-rate state was unstable and the vACC maintained a high-rate state irrespective of task conditions (*Low dose* case, Fig. 3.22C). For excessive SSRI

hyperpolarization ΔI_e^v, the vACC network operated at the left of the bistable range, where only the low-rate state was stable so that no high-rate attractor could be stabilized (*High dose,* Fig. 3.22C). Finally, ΔI_e^v could be tuned so the vACC network operated within the bistable range and both low-rate and high-rate states were stable, approaching the healthy condition behavior (*optimal response*, Fig. 3.22D).

As with the spiking model (Fig. 3.15D), tuning ΔI_e^v to be in the bistable range (*optimal response* condition, Fig. 3.22D) was more difficult for networks with larger f_D. This is due to the fact that the bistable range becomes narrower as f_D increases (Fig. 3.22A). This is not generally the case in our rate-model network, but a number of conditions are required to obtain this effect (See Materials and Methods and following chapters). As it turns out, under these conditions oscillatory dynamics in and around the bistable range are important markers of network dynamics, and we will argue in the following section (Oscillations as markers of bistable network dynamics) that this may underlie their correlation with MDD and treatment outcome.

Deep brain stimulation in the firing-rate model

The effects of DBS on *treatment-resistant* networks could also be qualitatively explained in the rate model. We explored the 2 hypotheses mentioned above for DBS mechanism action on vACC: one mediated by interneurons in vACC (Mayberg et al., 2005) and another one mediated by the serotonin system (Hamani et al., 2010, 2012).

Electrical stimulation of vACC inhibitory neurons in the spiking network simulations corresponds in the rate model (Eq. (11)) to an increment in the external current (ΔI_i^v) in vACC. This manipulation in the rate model (Fig. 3.23A) displaced the baseline operating regime towards to positive values where the bistable range is recovered (cyan dotted line in Fig. 3.23A), or further, where only the low rate state is stable, depending on stimulation intensity. This result is in line with our observations in the spiking network simulations (Fig. 3.17).

The mechanism of action of the DBS through the serotonin system on vACC excitatory neurons corresponds in the rate model (Eq. (11)) to a further negative increment in the

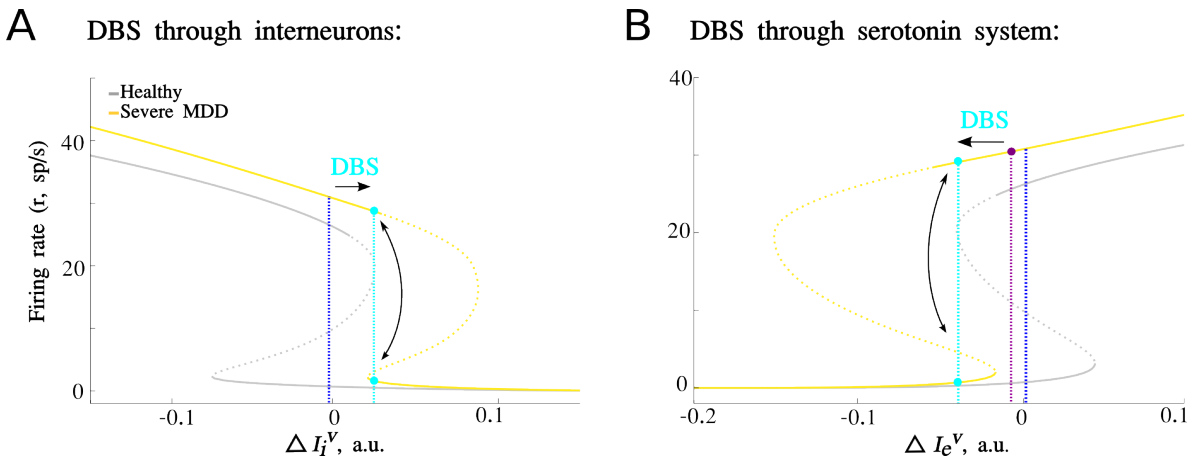

Figure 3.23: Graphical interpretation of DBS mechanism on vACC *treatment-resistant* networks model.

A. DBS treatment through interneurons: Severe MDD model (f_D = 1.25) treated with DBS increases the inhibitory current (ΔI_i^v = 0.026) and operates in the bistable range (cyan dotted line). **B.** DBS treatment through serotonin system: Severe MDD model (f_D = 1.25) SSRI failed to move the vACC network in the bistable range (magenta dotted line), here DBS increases serotonin (ΔI_e^v = –0.033) and reached the bistable range range (cyan dotted line).

external current ($-\Delta I_e^v$), which was studied in the previous section. Nevertheless, conceptually it is slightly different: DBS on the rate model (Fig. 3.23B) displaces the baseline operating regime to more negative values relative to SSRI treatment (*treatment-resistant* model, magenta dotted line in Fig. 3.23B) and recovers the bistable range (cyan dotted line in Fig. 3.23B) or sets the system beyond the bistable range, where only the low rate state is stable, depending on stimulation intensity.

Thus, through both mechanisms, DBS modified *treatment-resistant* networks model so that they could operate in the bistable range, and dlPFC inhibition was able to switch off emotional processing in vACC (Fig 3.23A,B). Similar to serotonin treatment (ΔI_e^v, Fig. 3.22D), tuning ΔI_i^v to be in the bistable range was more difficult for networks with larger f_D due to the narrow bistable range.

Oscillations as markers of bistable network dynamics

The gradual reduction of the bistable range with the progression of MDD (f_D) (Fig. 3.22A) is a robust network phenomenon when slow oscillatory activity is present, as long as

excitatory firing rates remain at moderate levels. This is due to the oscillatory instability, which becomes more prominent as the effective gain in recurrent excitation increases, see Eq.(14) in Materials and Methods. The effective gain increases with f_D, but only if the gain in the neuronal response φ_e' does not decrease, which essentially means avoiding a saturation in firing rates. One way to achieve this is to have the inhibitory neurons convert their inputs to firing-rate outputs through an expansive non-linearity (see in following chapter). When this is the case, the jump in excitatory firing rates from the low-activity to the high-activity state drives an amplified inhibitory response, keeping excitatory firing rates at moderate levels. In these conditions, the network states of the upper branch closer to the knee of the bistable range become unstable quickly as f_D increases, and the remaining stable network states in the bistable range converge with damped oscillatory dynamics (Fig. 3.24A, B) in the theta frequency range. These oscillations have larger amplitude for networks operating near the bistable range limit of the upper branch (Fig. 3.24A, B).

Thus, network oscillations in the 2-8 Hz frequency range characterize active states that sit close to the edge of the bistable range, and are thus easier to be switched off by external events. This analysis suggests that theta rhythms in frontal areas could be markers of bistable dynamics being activated in the course of cognitive function.

Our firing-rate network model did not show oscillatory activity in the beta range of frequencies. This was in contrast with our spiking network simulations (Fig. 3.13D, 3.14D and 3.16B) and led us to think that the underlying cause of such rhythms could be spike-synchronization of periodic neural oscillators, which could be only visible in spiking simulations. We tested this hypothesis by injecting external currents to excitatory neurons of the vACC module in our spiking network in order to change the firing rate of these neurons. We found that this manipulation changed also the frequency of fast oscillations in the network in proportion to firing rate changes (Fig. 3.24C, D), suggesting indeed that these oscillations emerge from spike synchronization mechanisms. While our spiking network generated fast network oscillations through this oscillator-coupling mechanism, other plausible synchronization mechanisms to generate fast oscillations in activated networks have been proposed (Kopell et al. 2000; Tamás et al. 2000; Brunel and Wang 2003).

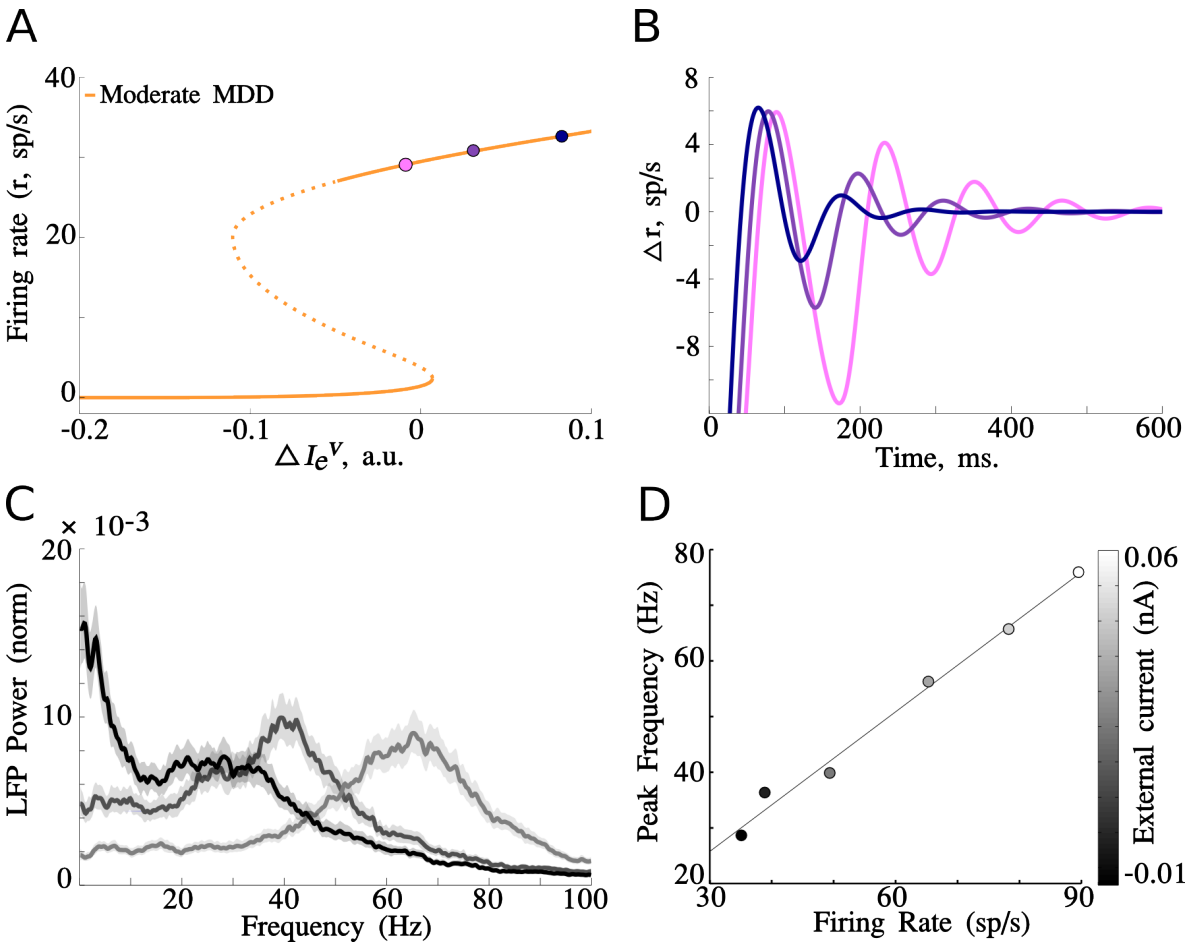

Figure 3.24: Mechanisms of oscillations.

Theta and beta oscillations co-exist in the bistable range, but differ in their mechanism. **A.** Bistable range for the moderate MDD model (f_D = 1.1). We selected three network conditions (ΔI_e^v=0.005, ΔI_e^v=0.02, ΔI_e^v=0.08, respectively) in the upper branch, progressively approaching the edge of the bistable range, to illustrate transient dynamics in panel B. **B.** Damped oscillatory dynamics in the theta frequency range were generated by perturbing the steady state (initial condition, r_e^v = 4 sp/s) of the three conditions indicated in panel A. Damped oscillations had larger amplitude for networks operating near the bistable range limit of the upper branch A. **C.** Spiking simulations can present additional high-frequency oscillations. Normalized power spectra of spiking network activity upon progressive depolarization of the vACC excitatory population (depolarizing currents –0.015, 0 and 0.04 nA) in the severe MDD model (spiking network, 7.5% glutamate decay slow-down), revealed changes in amplitude and frequency of beta/gamma oscillations. **D.** The mechanism of high-frequency oscillations in spiking simulations (panel C) kept a fixed relationship between neuronal firing rate and oscillation frequency, indicating that beta oscillations emerged in the spiking simulations through an oscillator coupling mechanism. Scatter plot shows the frequency of the power spectrum peak in the beta/gamma range versus the network's mean firing rate for a range of vACC depolarizing currents –0.015 to 0.06 nA.

Crucial to our analysis of network oscillations and bistable dynamics is that, whatever the

mechanistic origin of fast oscillations is, these fast rhythms can coexist with slower theta rhythms in and near the bistable range. In this case, they will be modulated inversely in relation to manipulations that modulate network excitability, and they will conjointly mark the proximity of network dynamics to this bistable range of operation. We summarize this view schematically in Figure 3.25: Severity of MDD should correlate negatively with the amplitude of theta rhythms and positively with the amplitude of beta/gamma oscillations because networks more affected by a glutamate dysfunction would operate further away from the bistable range edge (Fig. 3.25A). Also, the treatment (representing a displacement along the axis ΔI_e^v) should induce complementary modulation of these rhythms with larger theta and weaker and slower beta/gamma marking a proximity to the desired operating regime in the bistable range, and thus better prospects for treatment outcome (Fig. 3.25B).

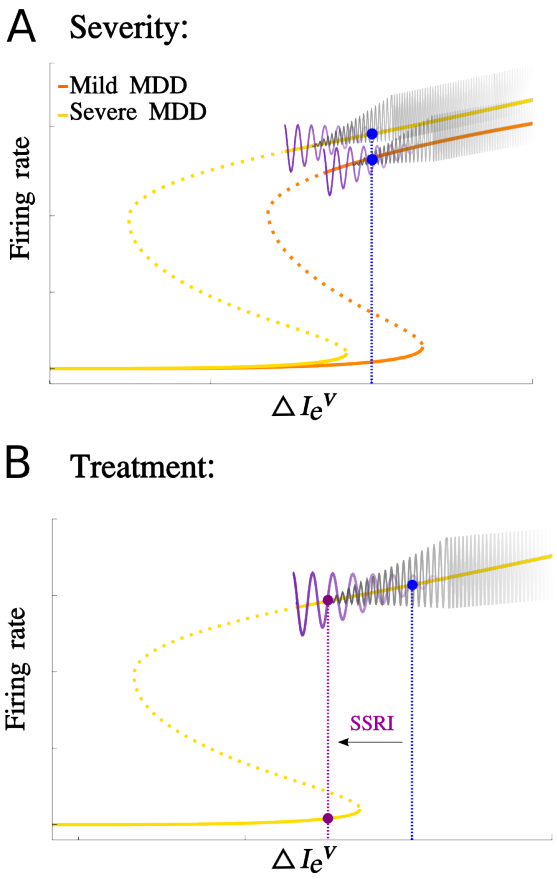

Figure 3.25: Schematic summary: disease and oscillations

Theta and beta oscillations mark the distance to the bistable range. **A.** Bistable range diagrams for Mild and Severe MDD models (f_D = 1.05 and f_D = 1.25, respectively). In the upper branch the magenta oscillation represents schematically the amplitude of theta oscillations generated by the oscillatory instability, the gray oscillation represents schematically the amplitude of beta-gamma generated by synchronization. As the severity of the MDD model increases, the network's state (blue dotted line) lies further away from the bistable range edge and the amplitude of the theta oscillation is reduced and beta-gamma is increased. **B.** Following an SSRI treatment (by reducing network excitability to purple dotted line), the system moves leftward approaching the stability limit of the upper branch. As the system approaches the bistable range the amplitude of theta oscillations (magenta) increases and the frequency and amplitude of beta/gamma oscillations (gray) decrease. A network with more amplitude of theta oscillations is closer to the limits of the bistable range and is more likely to be brought into the optimized operating regime by small network hyperpolarization (i.e. SSRI treatment).

Why the region of bistability became narrower?

In previous chapters we talked about the importance of bistability for the optimal function of the network. The upper panel of Figure 3.26 shows that there is indeed a region of bistability. There is, however an oscillatory instability nearby (dashed orange line). Therefore, the region of bistability is not strictly delineated by the two saddle-node (SN) bifurcations (Fig. 3.26), but rather the rightmost SN and a Hopf bifurcation. When the parameter f_D is increased, the increased excitation broadens the region between the two SNs, but not the region of bistability, because the range of oscillatory instability (dashed orange line) has grown (bottom panel Fig. 3.26).

We would like to be able to draw general conclusions regarding how the region of bistability changes as we increase the parameter f_D, which is meant to model the effects of MDD. In our simulations we found that increasing f_D lead to an increase in the distance

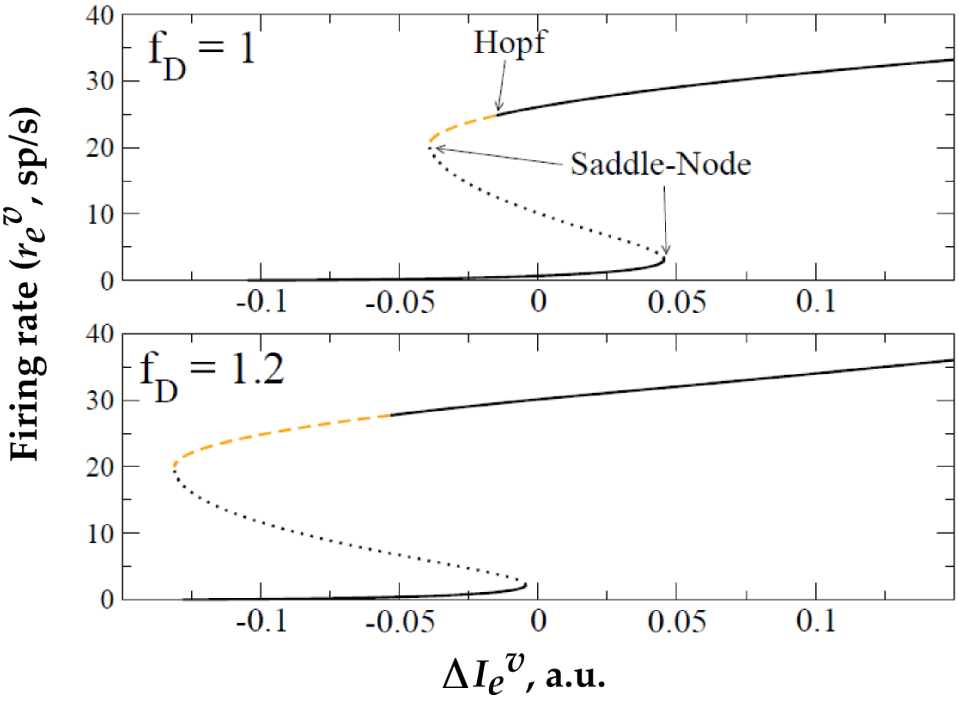

Figure 3.26: The bifurcation diagram for the firing rate of the excitatory population in the ventral area.

Upper: The "healthy" case with $f_D = 1$. Lower: The "depressed" case with $f_D = 1.2$. Solid black line: stable fixed point. Dotted black line: unstable (saddle) point. Dashed orange line: unstable (spiral) point.

between the two SN bifurcations which would usually delineate the region of bistability. However, the presence of an oscillatory instability between the two SNs actually leads to bistability shrinking as we increase f_D.

Due to the simplicity in our choice of the neuronal transfer function φ we are in a position to extract some analytical results. Specifically, for each neuronal population there are two distinct qualitative regimes: 1- The quadratic regime (Q) where the nonlinearity is expansive and hence the curvature is positive, and 2- The square-root regime (S) where the nonlinearity is compressive and hence the curvature is negative. Therefore there are four possible regimes in total: QQ, SQ, QS, SS, where the first letter corresponds to the state of the excitatory population and the second to the state of the inhibitory population. For example, the QQ regime is always the relevant one when firing rates are low in both populations, and conversely when firing rates are high in both then the regime is likely to be SS, etc.

We can see which regimes are relevant for the dynamics we have considered by looking at Figure 3.27, which shows how the SN and Hopf bifurcation lines vary as a function of both the selective external input ΔI_e^v as well as the parameter f_D. The regimes are color-coded: QQ (red), SQ (black) and SS (blue). Clearly the SQ regime is the relevant one for the simulations we have carried out in this thesis. This is so because as f_D increases, the range of bistability shrinks (gray shadowed area).

Why is SQ the relevant regime? Recall that in order for the Hopf bifurcation to persist as f_D is increased we require that excitatory firing rates not increase too much. This is because the instability only occurs if the excitatory gain is sufficiently strong and the gain actually decreases as rates increase (saturation). One way to avoid this is to put the inhibitory population in the Q regime, where the gain is very high; this keeps excitatory rates under control. It can be shown that, in general, if the inhibition is linear or saturating, then the region of bistability would actually increase as f_D increases. Only the SQ regime generically shows the opposite trend.

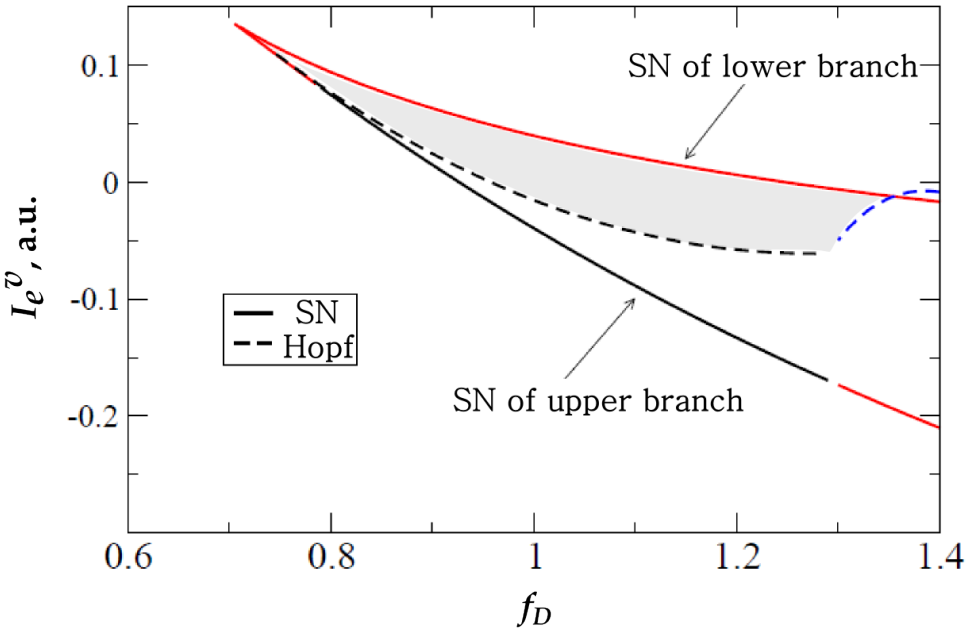

Figure 3.27: Phase diagram.

Saddle-node bifurcations occur along the solid lines and Hopf bifurcations along the dashed lines. The color of the line indicates the fixed-point regime: QQ (red), SQ (black) and SS (blue). The gray shadowed area shown the range if bistability.

In general, an oscillatory instability leads to a stable oscillatory solution, e.g. a limit cycle. In our model this is not the case. Fig. 3.28 shows what happens when the system is simulated with an initial condition very close to the unstable branch (dashed orange line) in Fig. 3.26, for $\Delta I_e^v = -0.07$. There is clearly an oscillatory instability, but instead of approaching a limit cycle solution, the activity eventually reaches the stable node at low rates. In fact, this behavior is generic when a Hopf bifurcation is in the vicinity of a SN bifurcation. The ensuing phenomenology can be completely characterized qualitatively by assuming the Hopf and SN coincide in a so-called Takens-Bogdanov bifurcation. In the stable branch of fixed points leading to the Hopf bifurcation, relaxation to the fixed point occurs through damped oscillations (Fig. 3.24B). In the context of noisy network operation, this is the origin of the theta oscillations observed in the system.

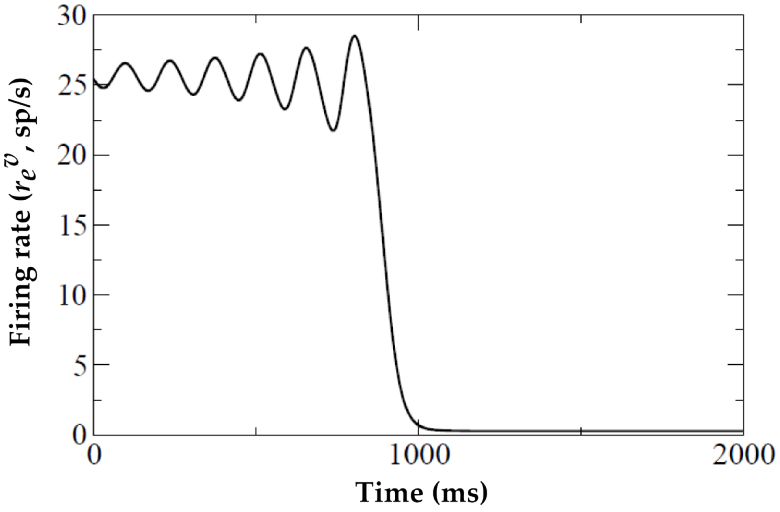

Figure 3.28: Unstable oscillatory activity

Unstable oscillatory activity for $\Delta I_e^v = -0.07$

Other treatment mechanisms in the firing-rate model

The MDD networks explored in previous chapters were characterized by an oscillatory instability in the upper branch which generated a reduction of the bistable range as the disease progressed (i.e. f_D grew, Figs. 3.26, 3.27). This phenomenon was present for bistable ranges computed as a function of both ΔI_e^v (Fig. 3.29B) and ΔI_i^v (Fig. 3.29C). Above, we have associated these two manipulations with MDD treatments, specifically SSRIs (reduction in ΔI_e^v) and DBS (increase in ΔI_i^v).

We were motivated to explore other possible mechanisms for DBS, so we hypothesized that electrical stimulation of vACC could target both excitatory neurons and interneurons. This corresponds in the rate model (Eq. (11)) to an increment in the external current to both populations ($\Delta I_e^v I_i^v$) in vACC. This manipulation in the rate model (Fig. 3.29E) destroyed the oscillatory instability in the upper branch, generating an increase in the bistable range as MDD progressed (f_D grew, Fig. 3.29A, E). This result means that such a mechanism of action for MDD treatment would bring about greater stability in both high and low rate states.

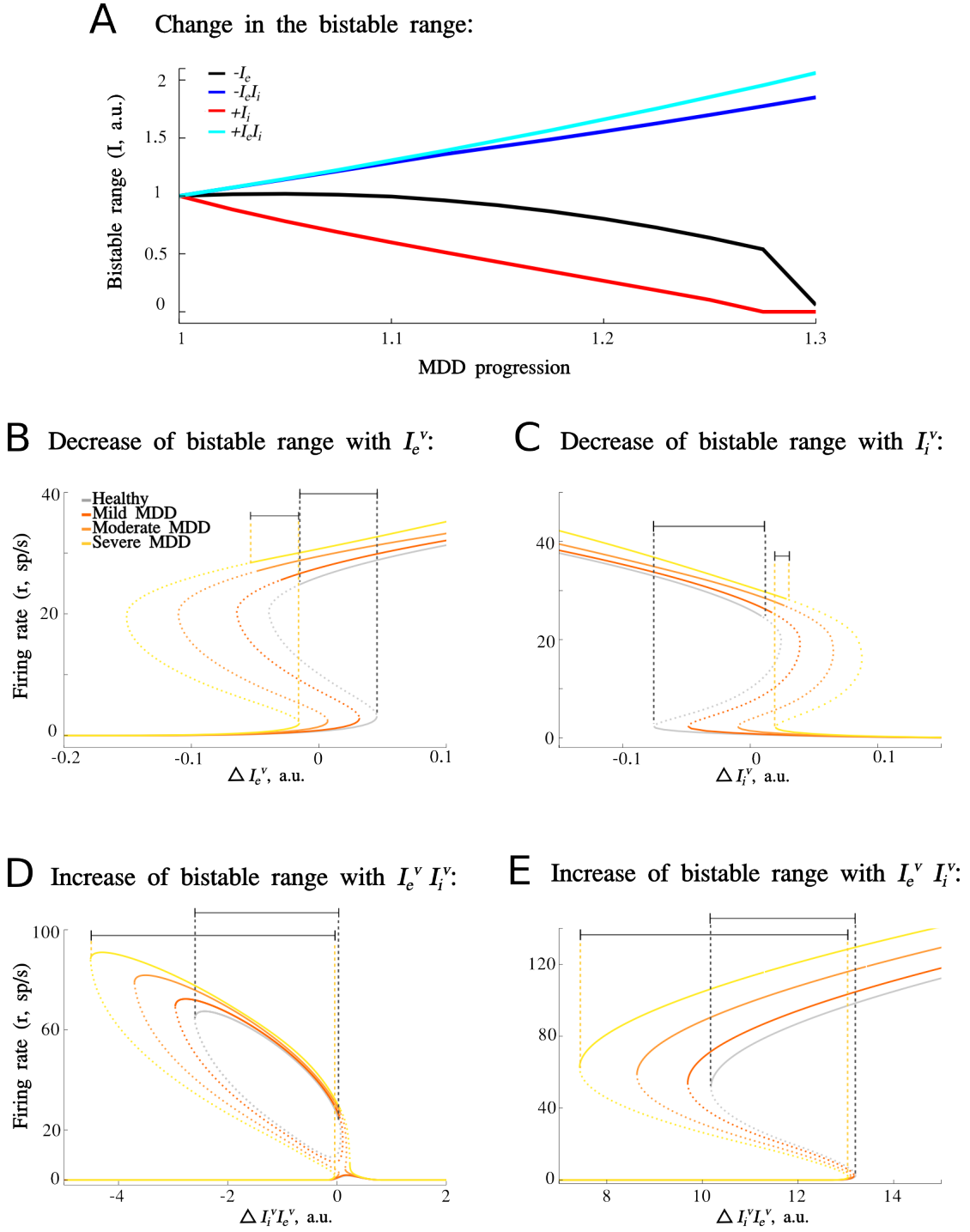

Figure 3.29: Graphical interpretation of vACC dynamics in MDD conditions across different treatments manipulations.

A. Change in the bistable range for different manipulations in the rate model (ΔI_e^v, ΔI_i^v, and $\Delta I_e^v I_i^v$).

B, C, D, E. Attractor solutions for the MDD rate model after enhancing recurrent excitation in vACC (f_D = 1.05 for mild MDD, f_D = 1.15 for moderate MDD, f_D = 1.25 for severe MDD) for ΔI_e^v (**B**), ΔI_i^v (**C**), and $\Delta I_e^v I_i^v$ (**D,E**) manipulations. Note that the bistable range became narrower for ΔI_e^v (**B**) and ΔI_i^v (**C**), and became wider for $\Delta I_e^v I_i^v$ (**D,E**).

The same manipulation but in opposite direction, a reduction in the external current to both populations ($\Delta I_e^{\nu} I_i^{\nu}$) in vACC, also destroyed the oscillatory instability in the upper branch and increased the bistable range as f_D grew (Fig. 3.29A, D). Similar to the previous results, this manipulation generated a greater stability in both high and low rate.

The 2 manipulations presented here ($\Delta I_e^{\nu} I_i^{\nu}$), differed from the manipulations presented in previous chapters (ΔI_e^{ν} and ΔI_i^{ν}), in the greater stability of the upper branch, which resulted in an increase of the bistable range as MDD progressed (Fig 3.29A) and a predicted decrease of theta oscillations following treatment. The specific mechanisms of DBS action are still a matter of debate, and our analyses identify different scenarios with contrasting predictions in terms of treatment outcome stability and pattern of EEG rhythms.

Discussion

In this thesis, we provide a study of the dynamics of emotional and cognitive networks using a set of complementary approaches. We explore the brain dynamics of healthy participants under a competitive emotional and cognitive paradigm using *fMRI* techniques. We describe the structure of cognitive and emotional networks, we identify their hubs and we analyze the dynamics between them. Based on these results and previous literature, we build up a simplified computational model for MDD, testing the glutamate dysfunction hypothesis and their relation with the progression of MDD. In addition, we explore the mechanistic actions of SSRI and DBS treatments.

The results from the brain image analysis provide a graph-theoretic network analysis that characterizes how the emotional and cognitive networks interact in a case of extreme emotional and cognitive contrast. We design a paradigm with a strong conflicting emotional and cognitive demand (Fig. 2.1) by combining sadness provocation (SP) (Liotti et al. 2000) and working memory (WM) (McNab and Klingberg 2008), pure emotional and cognitive tasks, respectively. In these tasks the outcomes do not depend on the integration of emotional and cognitive aspects. We hypothesized that this paradigm would enhance the competition and therefore the modularity of emotional and cognitive networks and would reveal the cortical areas that act as network hubs. A GLM approach was used to define the brain areas activated during each epoch of the paradigm, functional connectivity between regions was calculated subject-by-subject and graph-theoretic network analysis was used to characterize the interaction between emotional and cognitive communities.

To investigate the interaction of emotion and cognition, researchers have studied the modulatory effect of the emotions on diverse cognitive functions, such as attention (Dolan 2002), decision making (Bechara et al. 2000; Bechara 2004), memory (Smith et al. 2004, 2006) and working memory (Erk et al. 2003, 2007). Several studies have found attenuated spatial WM performance during negative task-irrelevant affect (Lavric et al. 2003; Dolcos and McCarthy 2006; Dolcos et al. 2006, 2008; Schaefer et al. 2006; Shackman et al. 2006), although this effect was absent in verbal WM (Lavric et al. 2003; Simon-Thomas and Knight 2005; Simon-Thomas et al. 2005; Shackman et al. 2006). The authors suggest that this effect is due to competition for limited visuospatial attention resources (Lavric et al. 2003; Shackman et al. 2006). On the other hand, there are some early evidences of more marked disruption of verbal WM, as compared to spatial WM, in conditions of anxiety

(Markham and Darke 1991; Ikeda et al. 1996). While the previously reported decrease in spatial working memory performance is in line with our data, the underlying mechanism could be different, because all these studies were performed using task-irrelevant aversive stimuli or inducing anxiety during the WM task. These studies therefore are subject to possible confounds due to attention capture by the noxious stimulus.

Our paradigm addresses this issue. We used a sadness provocation task (Liotti et al. 2000) to induce a sadness state, followed by a spatial WM task (McNab and Klingberg 2008) (*Sadness-WM2* paradigm), and we compared with a control paradigm that concatenates a neutral state and spatial WM task (*Neutral-WM1* paradigm) (Fig. 2.1). In the *Sadness-WM2* paradigm, the cognitive modulations mediated by emotional demands were provoked by an emotional state elicited before the cognitive task. Therefore, unlike previous reports our results do not depend on external distractors or emotional stimuli during the WM task. Only one study before has used a similar strategy (Deckersbach et al. 2008), studying depressed patients (bipolar I disorder) under mood-stabilizing medication. The paradigm concatenated a 2-back WM task and a mood induction through listening to autobiographical scripts. They found behavioral effects in the WM performance after the sadness induction, specifically slower reaction time and lower response accuracy. Remarkably, this effect was present in both controls and depressed patients, but they could not find behavioral differences between them. In our hands, sadness provocation (SP) did not impact WM behavior significantly in our population of healthy participants, but our behavioral analysis reveals that the subjects that reported highest emotional score, *high-sadness* group, presented an increase in the mean number of error trials after the SP (Fig. 3.1, Table 3.2). This result resonates with the findings by Deckersbach et al. (2008) and supports the role of emotional states in conditioning cognitive function, without any confounds of possible acute attentional shifts by intervening cues as in previous studies.

Our behavioral protocol has also some caveats. Because the study was first designed to test changes in brain network structure not only across mood state, but especially between control and depressed patients (which could finally not be included in the study), and this was part of a long experimental protocol that forced us to keep the task short, we did not include controls with neutral autobiographical memory blocks. Also, we did not reverse the order of the paradigms, because previous study found that the sadness block generated

some residual effect in the control blocks (Deckersbach et al. 2008). This could pose interpretation problems, since there are several factors that distinguish our two paradigms: emotional state, practice, tiredness, memory recall (a memory process was elicited before WM2, not WM1). This confound is addressed in our study by testing the relation of our effects with emotion intensity reports.

Intensity and duration are two central characteristics of an emotional response (Frijda 2007). A previous study found that emotion intensity was predicted by appraisals (the emotion-eliciting event was rated on a number of appraisal dimensions) (Brans and Verduyn 2014). Taking account that sadness state has a fixed duration (2 minutes), participants performed a rating of the sadness intensity reached after the scanner session, in order to study the modulatory effect of sadness intensity in the network dynamics. We used this report throughout our analyses to confirm the unambiguous association of sadness with differences between our two behavioral paradigms, and thus overcome the confounds associated with the sequential presentation of our two paradigms (see above). Specifically, we tested the statistical significance of an interaction between the factors *paradigm* and *sadness intensity* in our analyses of variance (ANOVA) tests. Most of the changes in network structure and functional connectivity reported in this study are supported by such a significant ANOVA interaction, thus supporting their unambiguous association with a change in emotional state.

In addition to the behavioral findings, some of the studies discussed above also present functional neuroimaging results suggesting that emotional distractors affected the activity in dlPFC (Perlstein et al. 2002; Dolcos and McCarthy 2006; Dolcos et al. 2006, 2008). Perlstein et al. (2002) studied the dlPFC modulation with task-relevant stimuli, showing that dlPFC activity was influenced by emotional valence of the stimuli, enhanced by pleasant and reduced by unpleasant stimuli. Dolcos and collaborators have studied mainly the effect of distractors, showing that the presence of negative emotional distractors was associated with impairments in cognitive performance and a marked decrease in dlPFC activity (Dolcos and McCarthy 2006; Dolcos et al. 2006, 2008). In our functional imaging analysis we found an overall decrease of the BOLD activity in the cognitive network after sadness, including dlPFC (Fig. 3.3), which was in agreement with previous literature. However, unlike previous literature, in our paradigm the participants performed the WM

task without any distractor or emotional stimulus. As discussed above for the behavioral results, the modulation of the functional imaging during the WM task was made through a mood induction before the cognitive task. Therefore, our approach allows us to postulate that the decrease in the neural modulation was due to an emotional state, sadness. Remarkably, we found an inter-individual negative correlation between sACCl and dlPFCl BOLD activity, which was higher in the *high-sadness* group (Fig. 3.5). Such result is similar to the inter-individual negative correlation found between the amygdala and inferior frontal gyrus during a working memory task with a negative task-irrelevant stimuli presented during the delay (Erk et al. 2007).

Graph-theoretic network analysis was used to identify structural changes of emotional and cognitive networks in our paradigms. The community detection applied to the two paradigms revealed two modules, one comprising cognitive regions (dlPFC, IPS, iFG, mSFG, PCG) and another one comprising emotional regions (mFP, sACC, mOFG, Amy, Hip). Within the emotional community two small sub-communities were detected: one comprising cortical regions and another comprising subcortical regions (Fig. 3.6 and 3.7). Note that the community detection algorithm identified in an unsupervised way subnetworks that matched their functional association (emotional and cognitive), and their anatomical membership (cortical and subcortical). The cortical and subcortical partition of the emotional community has been described previously (Kinnison et al. 2012).

Graph theory gives us the tools to quantify how well a network can be decomposed in separate communities (modularity index or quality of the partition Q). We found that the modularity of the brain network increased in Sadness-WM2 relative to Neutral-WM1, and it correlated with sadness intensity (Table 3.3). This result leads us to conclude that the emotional state *per se* increases the modularity *Q* between the emotional and cognitive networks. This result is in line with our hypothesis that a sadness state increases the competition between emotional and cognitive networks. However, in contrast with our result Kinnison et al. (2012) found a *decrease* in the modularity between cortical and subcortical emotional networks during emotional states. This apparent discrepancy can be resolved based on the fact that Kinnison et al. (2012) studied changes in the structure of *emotional* cortical and subcortical networks, and our own findings also indicate that the emotional state increases the integration (i.e. increases global efficiency) within the

emotional community (Fig 3.8, Table 3.3). Global efficiency is a measure of integration and provides one way to estimate the potential for functional integration between brain areas (Achard and Bullmore 2007). A higher integration in the emotional network during the *Sadness-WM2,* relative to *Neutral-WM1*, could be a reflection of the emotional processing ongoing during *Sadness-WM2*. In contrast, global efficiency for the cognitive network was not significantly different between *Sadness-WM2* and *Neutral-WM1*, which could be explained by the fact that during both paradigms subjects performed a working memory task and cognitive processing was equivalent.

Our analyses allowed us to identify areas that act as hubs for connecting the cognitive and emotional brain subnetworks (Fig. 3.9 and 3.10). Two areas emerged from this analysis as critical based on their modulation by the sadness induction protocol. In the cognitive network, the dlPFCl presented a significant decrease in the degree (Fig. 3.9 and 3.10), suggesting that the sadness state reduced the effective coupling of this area and thus its ability to influence brain processing. Recent evidence has shown that the fronto-parietal brain network, which underlies cognitive control capacity (Cole and Schneider 2007; Duncan 2010), has especially high global connectivity (Cole et al. 2010). Indeed, the global connectivity of the left dlPFC was identified as the mechanism by which the fronto-parietal network might control other networks (Cole et al. 2012). Moreover, previous work from our laboratory also attributed a top-down control role to dlPFC in spatial working memory based on neuroimaging data and computational models (Edin et al. 2009). Integrating previous literature and our results, the decreases in the degree of the dlPFCl could be related with the overall decrease of the BOLD activity in the cognitive network after SP (Fig. 3.3) and the decline in the participants' WM performance (Fig. 3.1, Table 3.2) based on the dlPFC diminished capability of exerting cognitive control during the WM task.

The emotional hub was identified in area mFPl based on its modulations by the emotional demand. Sadness intensity modulated the degree of the mFPl: it increased in the *high-sadness* group relative to the *low-sadness* group (Fig 3.10C), suggesting that intense sadness increases the influence of mFPl on other brain areas. The mFP (part of medial prefrontal cortex) has been described as part of the default mode network, which drives the self-reference processes (Raichle et al. 2001; Greicius et al. 2003; Fox and Raichle 2007; Buckner et al. 2008; Sheline et al. 2009). The modulation in the mFPl degree by sadness

intensity could be related with a more intense self-reference process in the *high-sadness* participants.

Modulations of the mFPl and dlPFCl degree in our study are in line with the flexible hub theory recently presented (Cole et al. 2013) and they suggest that these hubs are capable of functional connectivity adaptations in order to balance cognitive and emotional demands. Do these adaptations occur independently or are they coordinated through direct or indirect interareal interactions? We investigated task modulations of specific effective connectivity between areas to identify the mechanism underlying the hubs modulations. We found that the sACCl was a key area: it showed more negative functional connectivity with dlPFCl and more positive functional connectivity with mFPl following sadness provocation, and specifically for high-sadness participants (Fig. 3.11 and Fig 3.12).

Thus, in our analysis the sACC was not identified as a hub area but it did emerge as a key region that coordinates the modulations of cognitive and emotional hub areas, and thereby possibly modulating the network structure. These results are novel, and they provide a new perspective on the previously reported implication of sACC in sadness and depression. Previous studies consistently associate sACC with acute sadness, major depression and antidepressant treatment effects, suggesting a critical role for this region in modulating negative mood states (Mayberg et al., 1999; Liotti et al., 2000; Seminowicz et al., 2004). In addition, sACC connections to the brainstem, hypothalamus, and insula have been implicated in the disturbances of circadian regulation associated with depression and it has been described as a visceral-motor region (Freedman et al. 2000; Öngür and Price 2000; Barbas et al. 2003). Reciprocal pathways linking sACC to orbitofrontal, medial prefrontal and various parts of the anterior and posterior cingulate cortices constitute the neuroanatomical substrates by which primary autonomic and homeostatic processes influence various aspects of learning, memory, motivation and reward (Vogt and Pandya 1987; Carmichael and Price 1996; Barbas et al. 2003; Haber 2003). In depressed patients, the resting-state sACC functional connectivity with the default mode network (DMN) was found stronger than in control participants, and it further correlated with the length of the patients' depressive episodes (Greicius et al. 2007). All these data reinforce the idea that sACC is implicated in sadness regulation and our results indicate that this could be by means of its regulatory role in relation to two hub network areas, rather than a direct

driving mechanism.

There has been substantial debate surrounding the appropriate interpretation of negative correlations observed with resting state functional connectivity (fMRI) in the setting of a preprocessing step termed global signal regression (Fox et al. 2009; Murphy et al. 2009; Van Dijk et al. 2010; Anderson et al. 2011; Chai et al. 2012; Keller et al. 2013). This processing can improve the specificity of resting state correlations and the correspondence with anatomy (Fox et al. 2009) and electrophysiology (Keller et al. 2013). Related with our work, Fox and colleagues found a sACC-dlPFC anticorrelation in MDD patients using the preprocessing step global signal regression. In addition, they tested this anticorrelation by focal brain stimulation (TMS) on dlPFCl sites. Remarkably, the treatment outcome was proportional to the strength of the anticorrelation between dlPFC and sACC (Fox et al. 2012). However, there are mathematical concerns that anticorrelations could emerge as a processing artifact. While the technical issues surrounding processing strategy and anticorrelations are beyond the scope of this thesis (Fox et al. 2009, 2012; Keller et al. 2013), the current results add information to be considered in the ongoing debate. In *high-sadness* group, in addition to the anticorrelation between the sACC and dlPFC, we found an inter-individual anticorrelation of the BOLD activity between sACC and dlPFC where the global signal regression was not applied, a highest emotional scores and a decrease in the working memory performance. This result provides additional evidence that the sACC-dlPFC anticorrelation reflects functionally meaningful relationships. Moreover, in order to discard that the global signal regression generates the pattern of correlations presented above, we performed the same analysis without global signal regression and we checked that the results obtained were independent of this preprocessing step (Fig. 4.1). Notice however that the results from the data preprocessed with global signal regression fit together more consistently and provide easier interpretation. In particular, note that without global signal regression, the correlation between sACC and dlPFC became practically zero after sadness induction (Fig. 4.1A), meaning that sACC and dlPFC became decoupled. This decoupling does not fit with the rest of data presented, in particular with the strong inter-individual correlation between BOLD activity in sACC and dlPFC, especially in the *high-sadness* group (Fig. 3.5). Because the results are qualitatively unchanged by global signal

Figure 4.1: The correlations pattern is independent of the global signal regression.

Correlations subject by subject for sACCl-dlPFCl and sACCl-mFP BOLD fluctuations during Neutral-WM1 and Sadness-WM2 without the global signal regression, high-sadness subjects are plotted in red lines, low-sadness subjects in blue lines and the averages are plotted in thick red and blue lines, respectively.

A. *High-sadness* subjects present a tendency to decrease the sACCl-dlPFCl correlations during Sadness-WM2 as presented in the Fig. 3.11A (3-way anova, p = 0.0685 for interaction between high-sadness/low-sadness groups and Neutral-WM1 Sadness-WM2).

B. *High-sadness* subjects present a tendency to increase sACCl-mFPl correlations during Sadness-WM2, as presented in the Fig. 3.11B.

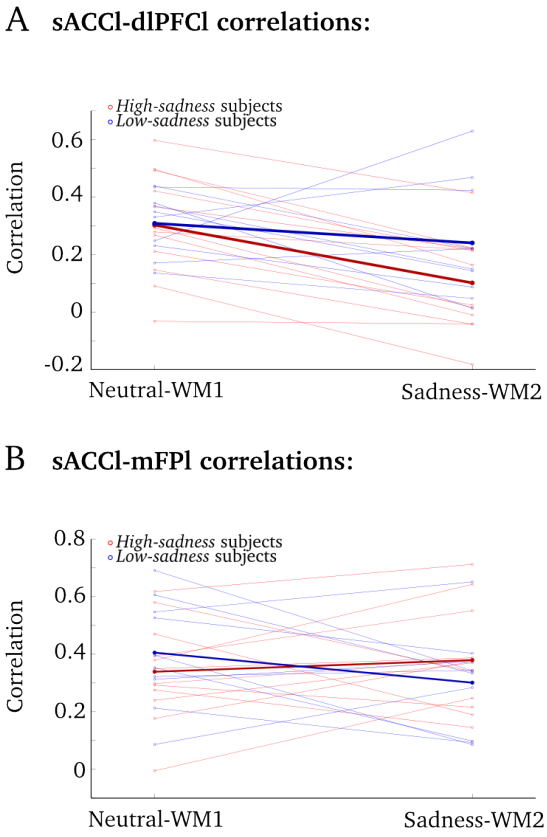

regression, but provide a much more direct interpretation, we favor this preprocessing step in this thesis

The *high-sadness* group presents similar observations to MDD patients: an activation of the sACC (Mayberg et al. 1997, 2005), deactivation of dlPFC (Bench et al. 1992; Kennedy 2001; Mayberg et al. 2005) and remarkably, an increase in the anticorrelation between sACC and dlPFC (Fox et al. 2012). These results suggest the hypothesis that the network dynamics during a high emotional cognitive demand approaches to the depression physiopathology and that it is this highly competitive dynamics that could be exacerbated pathologically in MDD patients. Going further, sACC and dlPFC are common therapeutic targets in mood disorders, SSRIs and TMS, respectively. On the other hand, mFP is not a common therapeutic target, however, a recent evidence suggested that mFP could have an important role in mood regulation. Using diffusion tensor imaging in treatment-resistant depressive patients treated with DBS (subgenual white matter stimulation), Riva-Posse and colleagues found that the non-responder group consistently failed to include medial frontal

pathways, and if present, they generally did not reach the frontal pole (Riva-Posse et al. 2014). The modulation of the mFP degree by the sadness intensity found in this thesis suggests that the therapeutic effect associated with reaching the frontal pole through DBS treatment could be related with modulations of this hub (decreasing their degree) and the network structure.

The second section of this thesis (Results for cingulo-frontal modeling) provides a biophysical computational model for cingulo-frontal cortex dysfunction in MDD. The model articulates mechanistically a role for cingulo-frontal brain areas in alternating between cognitive and emotional processing according to task demands in healthy subjects. The model can explain how the potentiation of excitatory transmission in vACC (as a result of slower glutamate re-uptake in MDD) compromises the ability of the cingulo-frontal network to switch from emotional to cognitive processing, remaining in a permanent negative emotional state that characterizes MDD symptoms. Pharmacological treatments of MDD can also be simulated, converging on a mechanism of vACC deactivation that recovers network function close to the normal, healthy condition. These different network dynamics are characterized by specific rhythms in the theta and beta/gamma bands, which can be used to identify the regime of bistable operation of the network.

The model integrates a wide range of disparate clinical, biochemical, electrophysiological, neuroimaging, and postmortem studies in MDD. The model explains how slower glutamate re-uptake in vACC (Ongür, Drevets, et al. 1998; Cotter et al. 2001; Choudary et al. 2005) disrupts the synaptic balance (Walter et al. 2009; Horn et al. 2010), causes hyperactivity in vACC (Mayberg et al. 1999, 2005; Seminowicz et al. 2004), and generates a persistent negative mood through the inability to disengage from emotional processing during cognitive tasks (Fig. 3.14 and Fig. 3.22) (Watts and Sharrock 1985; Paelecke-Habermann et al. 2005; Rose and Ebmeier 2006; Gohier et al. 2009; Disner et al. 2011). Progressive slow-down of glutamate re-uptake in vACC can be related to the progression of MDD (Fig. 3.14 and Fig. 3.22) (Portella et al. 2011) and weaker response to SSRI treatment as the disease progresses (Fig. 3.15, Fig. 3.16 and Fig. 3.22) (Keller et al. 1992; Kendler 2000; Kendler et al. 2001). In parallel to the emotional subsystem alteration, the model proposes that the reciprocal suppression between emotional and cognitive hubs, vACC and dlPFC is the

substrate for the cognitive impairment and dorsal frontal hypoactivity characteristic of MDD (Bench et al. 1992; Mayberg 1997; Kennedy 2001; Videbech et al. 2002; Oda et al. 2003; Mayberg et al. 2005). Importantly, the model provides a theoretical framework to interpret the observed relationship between theta and beta/gamma frontal rhythms and cognitive processing (Fig. 3.24) (Ray and Cole 1985; Asada et al. 1999; Tsujimoto et al. 2006; Siegel et al. 2012; Hsieh and Ranganath 2014), and how these rhythms are associated with MDD treatment outcome (Fig. 3.25B) (Pizzagalli et al. 2001; Mulert et al. 2007; Iosifescu et al. 2009; Korb et al. 2009; Pizzagalli 2011; Broadway et al. 2012) and severity of disease (Fig. 3.25A) (Pizzagalli et al. 2002).

We studied the mechanisms of two different treatments for MDD: SSRI, the most common treatment used in MDD, and DBS, used for treatment-resistant patients. Both treatments acted in the vACC network by compensating the synaptic imbalance through different strategies. SSRI treatment acted via 5-HT_{1A} receptors to reduce the excitability of pyramidal neurons (Fig. 3.15, Fig. 3.16 and Fig. 3.22). Instead, our DBS treatment (mediated through inhibitory neurons) restored the balance by recruiting inhibitory neurons in vACC through direct external stimulation (Fig. 3.17 and Fig. 3.23). Treatments were effective when they turned off the aberrantly active vACC.

In our SSRI treatment simulations, we found that the decrease in the bistable range for more severe MDD conditions resulted in worse treatment outcome predictions (Fig. 3.15, Fig. 3.16 and Fig. 3.22). These results are consistent with clinical evidence in MDD: As the duration of depressive episodes increases, the probability of recovery substantially decreases (Keller et al. 1992; Kendler 2000).

On the other hand, the fit between the decrease in the bistable range for DBS treatment mediated through inhibitory neurons (worse treatment outcome predictions), and the clinical evidence of MDD patients treated with DBS is less clear. Evidence from MDD patients treated with DBS suggests a progressive improvement in depressive symptoms that tends to be maintained over several years (Kennedy et al. 2011). Interestingly, the mechanisms mediated by external current to both populations ($\Delta I_e^v I_i^v$) in vACC explored in the chapter “Other treatment mechanisms in the firing-rate model” provide more stable clinical outcome predictions (Fig. 3.29). The more stable clinical outcome predictions, is

based on the increase in the bistable range, and therefore, greater stability in both high and low rate states. This speculative interpretation fits better with clinical evidence of MDD patients treated with DBS (Kennedy et al. 2011). A decrease in theta oscillations associated with a clinical recovery in MDD patients treated with DBS could provide a way to test these mechanistic hypotheses ($\Delta I_e^v I_i^v$).

Recent papers have shown single units and LFP recordings in ACC in treatment-resistant patients during electrode implantation (Lipsman, Kaping, et al. 2014; Lipsman, Nakao, et al. 2014). The spontaneous firing rate of subgenual neurons was not modulated by external inputs (Lipsman, Nakao, et al. 2014), in contrast with dorsal ACC neurons in non-depressed patients, which show brisk responses to a variety of stimulation conditions (Davis et al. 2000, 2005). In monkey studies, vACC neurons have also been shown to be highly modulated by external inputs (Koyama et al. 2001; Monosov and Hikosaka 2012). This suggests that non-responsive vACC neurons are characteristic of MDD, consistent with the lack of stimulus responses in vACC in our severe MDD models (Fig. 3.13C, 3.14A). Human studies also show the implication of vACC beta oscillations in depression: 15-20 Hz beta LFP activity was recruited during negative valence information processing in vACC of bipolar patients (Lipsman, Kaping, et al. 2014). All this electrophysiological evidence recorded from patients is still limited and evolving. As more data from these studies becomes available, models will benefit of more stringent experimental constrains and their predictions will be more directly testable.

The study of the dynamics of MDD treatments has clinical relevance. Here we simulate the SSRI effects after the therapeutic delay, which is around 2 weeks of treatment (Anderson et al. 2000; Mitchell 2006). The treatment also has chronic effects which may be qualitatively different (Deshauer et al. 2008). Extensions of our network models could therefore shed light on these issues if plasticity mechanisms are considered, but this is currently out of the scope of this thesis. Also, other treatments have been described as effective for depression: ECT (Nobler et al. 2001), rTMS (Mottaghy et al. 2002; Fox et al. 2012), ketamine (Berman et al. 2000), and cognitive behavioral therapy (CBT) (Gloaguen et al. 1998). We did not attempt to simulate these treatments here, although the model can also accommodate them. For instance, rTMS, unlike SSRI, would act in the dlPFC and through effective inhibitory interactions turn off vACC hyperactivity (Fox et al. 2012) or CBT could also act in the

dlPFC, by increasing its local recurrent connectivity and thus enhancing its ability to modulate vACC hyperactivity (Siegle et al. 2006).

We provide a network model composed of two areas, vACC and dlPFC, which are necessary (according to the data) and sufficient (from our model results) to explain several features of the pathophysiology and behavior in MDD and its treatment. However, these areas are part of a much more complex network, including the thalamus, amygdala, hippocampus, nucleus accumbens, medial prefrontal cortex, orbito-frontal cortex and dorsal ACC, among others (Mayberg et al. 1997; Ongür, An, et al. 1998; Seminowicz et al. 2004; Ghashghaei et al. 2007; Mayberg 2009; Lehman et al. 2011; Zikopoulos and Barbas 2012). We chose to simulate two areas that represented the hubs of emotional and cognitive brain networks and we labeled them according to available evidence implicating vACC and dlPFC in these roles, also supported by evidence of direct connections between these regions (Barbas et al. 1999; Medalla and Barbas 2010). However, our conclusions are not dependent on the specific identity of these hubs and they would apply as well to distributed networks that effectively resulted in two mutually inhibiting, compact subnetworks combining several brain areas. Also, our model does not even require direct disynaptic inhibition between the two hub networks of emotional and cognitive processing. Instead, effective inhibitory interactions through additional sets of interposed areas would yield similar results.

The model is not attempting to simulate all the complexity of MDD. MDD is a complex psychiatric illness, with several biopsychosocial factors, sensitive to various treatments, and dependent on multiple molecular processes (such as glucocorticoids, inflammatory cytokines, brain-derived growth factors, neurotransmitters and neuropeptides), genetic factors, plasticity processes, etc. (Maletic et al. 2007; Krishnan and Nestler 2008). Our network model could not possibly integrate all these elements at this point so we opted to simplify the model and include those biological, anatomical, and electrophysiological details that appeared to have a more direct impact in testing our initial hypothesis. This choice of mechanisms could need revision depending on what questions we want our model to address. For instance, if we were interested in exploring chronic vs. acute treatment effects plasticity mechanisms should be incorporated.

An additional limitation of our study is the stereotyped response patterns in the two areas. vACC and dlPFC have a rich repertoire of neuronal responses depending on the behavioral task. Thus, dlPFC activates during emotional tasks with a cognitive component (Sanfey et al. 2003) and vACC activates in cognitive tasks with emotional component (Rogers et al. 2004). Neurons in both areas can be coactivated by emotion and cognition, depending on the task (Kennerley et al. 2011; Monosov and Hikosaka 2012). In our model, we chose to simulate purely emotional and cognitive tasks (SP and WM), in order to emphasize the competitive aspect of emotional and cognitive processes and thus simplify our modeling to two areas with clearly delimited responses to either cognitive or emotional task components. Extensions of the model to address more integrated task designs should take into account the diverse set of stimulus and task selectivities observed in vACC.

One important result from our study is the detailed analysis of underlying mechanisms for the emergence of oscillatory dynamics within the bistable range of a recurrent circuit (Fig. 3.23 and 3.24). While the precise conditions for the co-existence of bistability and oscillations in such networks have been identified in previous studies, e.g. (Borisyuk and Kirillov 1992), ours is the first to discuss how the nature of the resulting oscillatory dynamics impacts the functionality of the circuit as a bistable switch. Specifically, our analysis has implications for the interpretation of theta and beta band rhythms in cognitive function and MDD. For one, the association between frontal midline theta and cognitive function (Hsieh and Ranganath 2014) would be interpreted within our model as marking the activation of bistable memory circuits during such tasks. Also, our model predicts a complementary modulation of theta and beta/gamma bands as a system moves in and out of bistable function, as it is often observed during cognitive processes (Lara and Wallis 2014). Viewing MDD as a systemic imbalance that perturbs bistable dynamics in vACC, theta band activity would be a marker of proximity to the desired bistable operating regime (Fig. 3.24B) and this would support its utility as biomarker of treatment outcome in MDD (Pizzagalli 2011). One final prediction emanating from our model's dynamics is the complementary relationship between theta and beta/gamma activity in MDD patients before and after treatment. Assuming that MDD treatments represent excitability changes, i.e. displacements along the axis of the bistable range in Figure 3.24, the process of calibrating treatments would scan the region of network dynamics where these two rhythms have

complementary patterns (Fig. 3.24B) and thus lead to a negative correlation that could be observed electrophysiologically.

Few psychiatric diseases have been studied with computational models (Hoffman and Dobscha 1989; Cohen and Servan-Schreiber 1992; Cohen et al. 1996; Hoffman 1997; Ownby 1998; Braver et al. 1999; Salum et al. 2000; Hoffman and McGlashan 2001; Loh et al. 2007; Rolls, Loh, and Deco 2008; Rolls, Loh, Deco, et al. 2008; Cano-Colino and Compte 2012). In depression, a very interesting study was published in 1990 by Sashin and Callahan (Sashin and Callahan 1990), where they studied mood disorders by combining concepts of psychoanalysis and system dynamics. The authors proposed in their model that a hysteretic loop underlies abnormal affective response, which bears some similarity to the biologically grounded mechanism that we propose in our network model (Fig. 3.20 and 3.21). Another recent model studied the role of hippocampal neurogenesis in depression (Becker et al. 2009). However, our model is the first to integrate a broad range of evidence of cingulo-frontal network dynamics alterations in MDD and its treatments in a unified theory. These results underscore the potential of quantitative modeling approaches to psychiatric diseases as a means of articulating coherent mechanistic frameworks that integrate disperse results and generate new model-derived hypotheses to test experimentally (Stephan and Mathys 2014; Wang and Krystal 2014).

Conclusions

1) The graph analysis of brain activity in working memory before and after sadness induction identified two main communities: the cognitive and the emotional subnetworks. The quality of modularity of such communities increased with high emotional-cognitive demands.

2) The degree analysis revealed that the dlPFC was modulated by the sadness state and mFP was modulated by the sadness intensity.

3) The sACCl was a key area: it showed a strong increase in the anticorrelation with dlPFCl and increase in the correlation with mFPl following sadness provocation, and specifically for high-sadness participants, which could underlie the hub modulations of the mFP and dlPFC.

4) We integrated experimental evidence in a biophysical computational model for cingulo-frontal network healthy function and its dysfunction in MDD.

5) The model explains mechanistically how the potentiation of excitatory transmission in vACC compromises the ability of the cingulo-frontal network to switch from emotional to cognitive processing, remaining in permanent negative mood, and results in selective cognitive impairment in MDD.

6) Serotonin treatment (via hyperpolarization through 5-HT1A) can be simulated, converging on a mechanism of vACC deactivation that recovers network function close to the normal, healthy condition.

7) The model relates the gradual slow-down of Glutamate reuptake in vACC to the progression of MDD and to weaker response to SSRI treatment as the disease progresses.

8) A reduction in the bistable range may underlie the treatment response difficulty in MDD.

9) DBS (via periodic stimulation of target vACC interneurons) can be simulated, converging on a mechanism of vACC deactivation that recovers network function, the switch between emotional and cognitive processes.

10) Theta band activity is a marker of proximity to the desired bistable operating regime and this would support its utility as a biomarker of treatment outcome in MDD.

11) Conversely, beta-gamma rhythms increase as the system moves further away from the bistable range. This could explain previous results relating beta-gamma rhythms with MDD severity.

12) Current theta and beta oscillatory patterns in MDD suggest an underlying bistable structure for frontal network dynamics.

References

Achard S, Bullmore E. 2007. Efficiency and cost of economical brain functional networks. PLoS Comput Biol. 3:e17.

Amemori K, Graybiel AM. 2012. Localized microstimulation of primate pregenual cingulate cortex induces negative decision-making. Nat Neurosci. 15:776–785.

Anderson IM, Nutt DJ, Deakin JFW. 2000. Evidence-based guidelines for treating depressive disorders with antidepressants: a revision of the 1993 British Association for Psychopharmacology guidelines. J Psychopharmacol. 14:3–20.

Anderson JS, Druzgal TJ, Lopez-Larson M, Jeong E-K, Desai K, Yurgelun-Todd D. 2011. Network anticorrelations, global regression, and phase-shifted soft tissue correction. Hum Brain Mapp. 32:919–934.

Andrade R, Malenka RC, Nicoll RA. 1986. A G protein couples serotonin and GABAB receptors to the same channels in hippocampus. Science. 234:1261–1265.

Arnold MB. 1960. Emotion and personality. New York, NY, US: Columbia University Press.

Asada H, Fukuda Y, Tsunoda S, Yamaguchi M, Tonoike M. 1999. Frontal midline theta rhythms reflect alternative activation of prefrontal cortex and anterior cingulate cortex in humans. Neuroscience Letters. 274:29–32.

Auger C, Attwell D. 2000. Fast Removal of Synaptic Glutamate by Postsynaptic Transporters. Neuron. 28:547–558.

Barbas H, Ghashghaei H, Dombrowski SM, Rempel-Clower NL. 1999. Medial prefrontal cortices are unified by common connections with superior temporal cortices and distinguished by input from memory-related areas in the rhesus monkey. J Comp Neurol. 410:343–367.

Barbas H, Pandya DN. 1989. Architecture and intrinsic connections of the prefrontal cortex in the rhesus monkey. Journal of comparative neurology. 286:353–375.

Barbas H, Saha S, Rempel-Clower N, Ghashghaei T. 2003. Serial pathways from primate prefrontal cortex to autonomic areas may influence emotional expression. BMC Neuroscience. 4:25.

Barker FG. 1995. Phineas among the phrenologists: the American crowbar case and nineteenth-century theories of cerebral localization. J Neurosurg. 82:672–682.

Bassett DS, Bullmore ET. 2009. Human brain networks in health and disease. Curr Opin Neurol. 22:340–347.

Bassett DS, Wymbs NF, Porter MA, Mucha PJ, Carlson JM, Grafton ST. 2011. Dynamic reconfiguration of human brain networks during learning. Proc Natl Acad Sci U S A. 108:7641–7646.

Bechara A. 2004. The role of emotion in decision-making: Evidence from neurological patients with orbitofrontal damage. Brain and Cognition, Development of

Orbitofrontal Function. 55:30–40.

Bechara A, Damasio H, Damasio AR. 2000. Emotion, Decision Making and the Orbitofrontal Cortex. Cereb Cortex. 10:295–307.

Becker S, Macqueen G, Wojtowicz JM. 2009. Computational modeling and empirical studies of hippocampal neurogenesis-dependent memory: Effects of interference, stress and depression. Brain Res. 1299:45–54.

Béïque J-C, Campbell B, Perring P, Hamblin MW, Walker P, Mladenovic L, Andrade R. 2004. Serotonergic regulation of membrane potential in developing rat prefrontal cortex: coordinated expression of 5-hydroxytryptamine (5-HT)1A, 5-HT2A, and 5-HT7 receptors. J Neurosci. 24:4807–4817.

Bench CJ, Friston KJ, Brown RG, Scott LC, Frackowiak RSJ, Dolan RJ. 1992. The anatomy of melancholia – focal abnormalities of cerebral blood flow in major depression. Psychological Medicine. 22:607–615.

Berman RM, Cappiello A, Anand A, Oren DA, Heninger GR, Charney DS, Krystal JH. 2000. Antidepressant effects of ketamine in depressed patients. Biol Psychiatry. 47:351–354.

Blondel VD, Guillaume J-L, Lambiotte R, Lefebvre E. 2008. Fast unfolding of communities in large networks. J Stat Mech. 2008:P10008.

Bokil H, Andrews P, Kulkarni JE, Mehta S, Mitra P. 2010. Chronux: A Platform for Analyzing Neural Signals. J Neurosci Methods. 192:146–151.

Borisyuk RM, Kirillov AB. 1992. Bifurcation analysis of a neural network model. Biol Cybern. 66:319–325.

Botteron KN, Raichle ME, Drevets WC, Heath AC, Todd RD. 2002. Volumetric reduction in left subgenual prefrontal cortex in early onset depression. Biological Psychiatry. 51:342–344.

Brans K, Verduyn P. 2014. Intensity and Duration of Negative Emotions: Comparing the Role of Appraisals and Regulation Strategies. PLoS ONE. 9:e92410.

Braver TS, Barch DM, Cohen JD. 1999. Cognition and control in schizophrenia: a computational model of dopamine and prefrontal function. Biol Psychiatry. 46:312–328.

Bressler SL. 1995. Large-scale cortical networks and cognition. Brain Res Brain Res Rev. 20:288–304.

Broadway JM, Holtzheimer PE, Hilimire MR, Parks NA, DeVylder JE, Mayberg HS, Corballis PM. 2012. Frontal Theta Cordance Predicts 6-Month Antidepressant Response to Subcallosal Cingulate Deep Brain Stimulation for Treatment-Resistant Depression: A Pilot Study. Neuropsychopharmacology. 37:1764–1772.

Brooks JOI, Vizueta N, Penfold C, Townsend JD, Bookheimer SY, Altshuler LL. 2015. Prefrontal hypoactivation during working memory in bipolar II depression. Psychological Medicine. FirstView:1–10.

Brunel N, Wang X-J. 2003. What determines the frequency of fast network oscillations with irregular neural discharges? I. Synaptic dynamics and excitation-inhibition balance. J Neurophysiol. 90:415–430.

Buckner RL, Andrews-Hanna JR, Schacter DL. 2008. The Brain's Default Network. Annals of the New York Academy of Sciences. 1124:1–38.

Bullmore E, Sporns O. 2009. Complex brain networks: graph theoretical analysis of structural and functional systems. Nat Rev Neurosci. 10:186–198.

Bush G, Luu P, Posner MI. 2000. Cognitive and emotional influences in anterior cingulate cortex. Trends in Cognitive Sciences. 4:215–222.

Cajal S. 1902. Estudios sobre la corteza cerebral humana.

Cajal S. 1909. Histologic du Systkme Nerveux de I'homme et des Vertkbris, Vol. 1. A Maloine, Paris.

Cajal S. 1928. Degeneration & regeneration of the nervous system. Oxford University Press, Humphrey Milford.

Cano-Colino M, Compte A. 2012. A computational model for spatial working memory deficits in schizophrenia. Pharmacopsychiatry. 45 Suppl 1:S49–S56.

Carmichael S t., Price J l. 1996. Connectional networks within the orbital and medial prefrontal cortex of macaque monkeys. J Comp Neurol. 371:179–207.

Castañé A, Kargieman L, Celada P, Bortolozzi A, Artigas F. 2015. 5-HT2A receptors are involved in cognitive but not antidepressant effects of fluoxetine. European Neuropsychopharmacology.

Chai XJ, Castañón AN, Ongür D, Whitfield-Gabrieli S. 2012. Anticorrelations in resting state networks without global signal regression. Neuroimage. 59:1420–1428.

Charlson ME, Pompei P, Ales KL, MacKenzie CR. 1987. A new method of classifying prognostic comorbidity in longitudinal studies: Development and validation. Journal of Chronic Diseases. 40:373–383.

Choudary PV, Molnar M, Evans SJ, Tomita H, Li J z., Vawter MP, Myers RM, Bunney WE, Akil H, Watson SJ, Jones EG. 2005. Altered cortical glutamatergic and GABAergic signal transmission with glial involvement in depression. Proceedings of the National Academy of Sciences of the United States of America. 102:15653–15658.

Cohen JD, Braver TS, O'Reilly RC. 1996. A computational approach to prefrontal cortex, cognitive control and schizophrenia: recent developments and current challenges. Philos Trans R Soc Lond, B, Biol Sci. 351:1515–1527.

Cohen JD, Forman SD, Braver TS, Casey BJ, Servan-Schreiber D, Noll DC. 1993. Activation of the prefrontal cortex in a nonspatial working memory task with functional MRI. Human Brain Mapping. 1:293–304.

Cohen JD, Servan-Schreiber D. 1992. Context, cortex, and dopamine: a connectionist approach to behavior and biology in schizophrenia. Psychol Rev. 99:45–77.

Cole MW, Pathak S, Schneider W. 2010. Identifying the brain's most globally connected regions. NeuroImage. 49:3132–3148.

Cole MW, Reynolds JR, Power JD, Repovs G, Anticevic A, Braver TS. 2013. Multi-task connectivity reveals flexible hubs for adaptive task control. Nat Neurosci. 16:1348–1355.

Cole MW, Schneider W. 2007. The cognitive control network: Integrated cortical regions with dissociable functions. Neuroimage. 37:343–360.

Cole MW, Yarkoni T, Repovs G, Anticevic A, Braver TS. 2012. Global connectivity of prefrontal cortex predicts cognitive control and intelligence. J Neurosci. 32:8988–8999.

Corbetta M, Shulman GL. 2002. Control of goal-directed and stimulus-driven attention in the brain. Nat Rev Neurosci. 3:201–215.

Cotter D, Mackay D, Landau S, Kerwin R, Everall I. 2001. Reduced glial cell density and neuronal size in the anterior cingulate cortex in major depressive disorder. Arch Gen Psychiatry. 58:545–553.

Covington HE, Lobo MK, Maze I, Vialou V, Hyman JM, Zaman S, LaPlant Q, Mouzon E, Ghose S, Tamminga CA, Neve RL, Deisseroth K, Nestler EJ. 2010. Antidepressant effect of optogenetic stimulation of the medial prefrontal cortex. J Neurosci. 30:16082–16090.

Damasio A. 1994. Descartes' Error: Emotion, Reason and the Human Brain. Putnam, G. P. New York.

Davis KD, Hutchison WD, Lozano AM, Tasker RR, Dostrovsky JO. 2000. Human Anterior Cingulate Cortex Neurons Modulated by Attention-Demanding Tasks. Journal of Neurophysiology. 83:3575–3577.

Davis KD, Taylor KS, Hutchison WD, Dostrovsky JO, McAndrews MP, Richter EO, Lozano AM. 2005. Human Anterior Cingulate Cortex Neurons Encode Cognitive and Emotional Demands. The Journal of Neuroscience. 25:8402–8406.

Deckersbach T, Rauch SL, Buhlmann U, Ostacher MJ, Beucke J-C, Nierenberg AA, Sachs G, Dougherty DD. 2008. An fMRI investigation of working memory and sadness in females with bipolar disorder: a brief report. Bipolar Disorders. 10:928–942.

Deco G, Rolls ET, Horwitz B. 2004. "What" and "Where" in Visual Working Memory: A Computational Neurodynamical Perspective for Integrating fMRI and Single-Neuron Data. Journal of Cognitive Neuroscience. 16:683–701.

Deshauer D, Moher D, Fergusson D, Moher E, Sampson M, Grimshaw J. 2008. Selective serotonin reuptake inhibitors for unipolar depression: a systematic review of classic long-term randomized controlled trials. CMAJ. 178:1293–1301.

Devinsky O, Morrell MJ, Vogt BA. 1995. Contributions of anterior cingulate cortex to behaviour. Brain. 118 (Pt 1):279–306.

Disner SG, Beevers CG, Haigh EAP, Beck AT. 2011. Neural mechanisms of the cognitive model of depression. Nature Reviews Neuroscience. 12:467–477.

Dolan RJ. 2002. Emotion, cognition, and behavior. Science. 298:1191–1194.

Dolcos F, Diaz-Granados P, Wang L, McCarthy G. 2008. Opposing influences of emotional and non-emotional distracters upon sustained prefrontal cortex activity during a delayed-response working memory task. Neuropsychologia. 46:326–335.

Dolcos F, Kragel P, Wang L, McCarthy G. 2006. Role of the inferior frontal cortex in coping with distracting emotions: NeuroReport. 17:1591–1594.

Dolcos F, McCarthy G. 2006. Brain systems mediating cognitive interference by emotional distraction. J Neurosci. 26:2072–2079.

Dougherty DD, Weiss AP, Cosgrove GR, Alpert NM, Cassem EH, Nierenberg AA, Price BH, Mayberg HS, Fischman AJ, Rauch SL. 2003. Cerebral metabolic correlates as potential predictors of response to anterior cingulotomy for treatment of major depression. J Neurosurg. 99:1010–1017.

Drevets WC, Bogers W, Raichle ME. 2002. Functional anatomical correlates of antidepressant drug treatment assessed using PET measures of regional glucose metabolism. European Neuropsychopharmacology. 12:527–544.

Drevets WC, Price JL, Simpson JR, Todd RD, Reich T, Vannier M, Raichle ME. 1997. Subgenual prefrontal cortex abnormalities in mood disorders. Nature. 386:824–827.

Drevets WC, Raichle ME. 1998. Suppression of Regional Cerebral Blood during Emotional versus Higher Cognitive Implications for Interactions between Emotion and Cognition. Cognition & Emotion. 12:353–385.

Drevets WC, Savitz J, Trimble M. 2008. The Subgenual Anterior Cingulate Cortex in Mood Disorders. CNS Spectr. 13:663–681.

Duncan J. 2010. The multiple-demand (MD) system of the primate brain: mental programs for intelligent behaviour. Trends in Cognitive Sciences. 14:172–179.

Edin F, Klingberg T, Johansson P, McNab F, Tegnér J, Compte A. 2009. Mechanism for top-down control of working memory capacity. Proc Natl Acad Sci USA. 106:6802–6807.

Ekman P. 1992. An argument for basic emotions. Cognition and Emotion. 6:169–200.

Erk S, Kiefer M, Grothe J o, Wunderlich AP, Spitzer M, Walter H. 2003. Emotional context modulates subsequent memory effect. NeuroImage. 18:439–447.

Erk S, Kleczar A, Walter H. 2007. Valence-specific regulation effects in a working memory task with emotional context. NeuroImage. 37:623–632.

Fava M. 2003. Diagnosis and definition of treatment-resistant depression. Biol Psychiatry. 53:649–659.

Fava M, Davidson KG. 1996. Definition and epidemiology of treatment-resistant depression. Psychiatric Clinics of North America. 19:179–200.

Fornito A, Zalesky A, Bassett DS, Meunier D, Ellison-Wright I, Yücel M, Wood SJ, Shaw K, O'Connor J, Nertney D, Mowry BJ, Pantelis C, Bullmore ET. 2011. Genetic Influences on Cost-Efficient Organization of Human Cortical Functional Networks. J Neurosci. 31:3261–3270.

Fox MD, Buckner RL, White MP, Greicius MD, Pascual-Leone A. 2012. Efficacy of Transcranial Magnetic Stimulation Targets for Depression Is Related to Intrinsic Functional Connectivity with the Subgenual Cingulate. Biological psychiatry.

Fox MD, Raichle ME. 2007. Spontaneous fluctuations in brain activity observed with functional magnetic resonance imaging. Nat Rev Neurosci. 8:700–711.

Fox MD, Zhang D, Snyder AZ, Raichle ME. 2009. The Global Signal and Observed Anticorrelated Resting State Brain Networks. Journal of Neurophysiology. 101:3270–3283.

Freedman LJ, Insel TR, Smith Y. 2000. Subcortical projections of area 25 (subgenual cortex) of the macaque monkey. J Comp Neurol. 421:172–188.

Fries P. 2005. A mechanism for cognitive dynamics: neuronal communication through neuronal coherence. Trends Cogn Sci (Regul Ed). 9:474–480.

Frijda NH. 2007. The laws of emotion. Mahwah, NJ, US: Lawrence Erlbaum Associates Publishers.

Funahashi S, Bruce CJ, Goldman-Rakic PS. 1989. Mnemonic coding of visual space in the monkey's dorsolateral prefrontal cortex. J Neurophysiol. 61:331–349.

Furukawa TA, Yoshimura R, Harai H, Imaizumi T, Takeuchi H, Kitamura T, Takahashi K. 2009. How many well vs. unwell days can you expect over 10 years, once you become depressed? Acta Psychiatr Scand. 119:290–297.

Fuster JM. 2003. Cortex and mind: Unifying cognition. New York, NY, US: Oxford University Press.

Fuster JM, Alexander GE. 1971. Neuron Activity Related to Short-Term Memory. Science. 173:652–654.

Ghashghaei HT, Hilgetag CC, Barbas H. 2007. Sequence of information processing for emotions based on the anatomic dialogue between prefrontal cortex and amygdala. Neuroimage. 34:905–923.

Ginestet CE, Simmons A. 2011. Statistical parametric network analysis of functional connectivity dynamics during a working memory task. NeuroImage. 55:688–704.

Gloaguen V, Cottraux J, Cucherat M, Blackburn IM. 1998. A meta-analysis of the effects of cognitive therapy in depressed patients. J Affect Disord. 49:59–72.

Glover GH. 1999. Deconvolution of Impulse Response in Event-Related BOLD fMRI1. NeuroImage. 9:416–429.

Gohier B, Ferracci L, Surguladze SA, Lawrence E, El Hage W, Kefi MZ, Allain P, Garre J-B, Le Gall D. 2009. Cognitive inhibition and working memory in unipolar depression. Journal of Affective Disorders. 116:100–105.

Goldapple K, Segal Z, Garson C, Lau M, Bieling P, Kennedy S, Mayberg H. 2004. Modulation of cortical-limbic pathways in major depression: treatment-specific effects of cognitive behavior therapy. Arch Gen Psychiatry. 61:34–41.

Goldman-Rakic P. 1995. Cellular basis of working memory. Neuron. 14:477–485.

Greicius MD, Flores BH, Menon V, Glover GH, Solvason HB, Kenna H, Reiss AL, Schatzberg AF. 2007. Resting-state functional connectivity in major depression: abnormally increased contributions from subgenual cingulate cortex and thalamus. Biol Psychiatry. 62:429–437.

Greicius MD, Krasnow B, Reiss AL, Menon V. 2003. Functional connectivity in the resting brain: a network analysis of the default mode hypothesis. Proc Natl Acad Sci USA. 100:253–258.

Haber SN. 2003. The primate basal ganglia: parallel and integrative networks. Journal of Chemical Neuroanatomy, Special Issue on the Human Brain - The Structural Basis for understanding Human Brain function and dysfunction. 26:317–330.

Hamani C, Diwan M, Macedo CE, Brandão ML, Shumake J, Gonzalez-Lima F, Raymond R, Lozano AM, Fletcher PJ, Nobrega JN. 2010. Antidepressant-Like Effects of Medial Prefrontal Cortex Deep Brain Stimulation in Rats. Biological Psychiatry. 67:117–124.

Hamani C, Machado DC, Hipólide DC, Dubiela FP, Suchecki D, Macedo CE, Tescarollo F, Martins U, Covolan L, Nobrega JN. 2012. Deep Brain Stimulation Reverses Anhedonic-Like Behavior in a Chronic Model of Depression: Role of Serotonin and Brain Derived Neurotrophic Factor. Biological Psychiatry. 71:30–35.

Harlow, John Martyn. 1848. Passage of an Iron Rod Through the Head. Boston Medical and Surgical Journal 39: 389-393 (Republished in *Journal of Neuropsychiatry and Clinical Neuroscience*11, 281-283; and in Macmillan 2000).

Harlow J. M. 1868. Recovery from the Passage of an Iron Bar through the Head. Pub. Mass. Med. Soc. 2, 237. *Publications of the Massachusetts Medical Society* 2: 327-347 (Republished in in Macmillan 2000).

Hastings RS, Parsey RV, Oquendo MA, Arango V, Mann JJ. 2004. Volumetric Analysis of the Prefrontal Cortex, Amygdala, and Hippocampus in Major Depression. Neuropsychopharmacology. 29:952–959.

Heitger MH, Ronsse R, Dhollander T, Dupont P, Caeyenberghs K, Swinnen SP. 2012. Motor learning-induced changes in functional brain connectivity as revealed by means of graph-theoretical network analysis. Neuroimage. 61:633–650.

Heuvel MP van den, Stam CJ, Kahn RS, Pol HEH. 2009. Efficiency of Functional Brain Networks and Intellectual Performance. J Neurosci. 29:7619–7624.

Hoffman RE. 1997. Neural network simulations, cortical connectivity, and schizophrenic psychosis. MD Comput. 14:200–208.

Hoffman RE, Dobscha SK. 1989. Cortical pruning and the development of schizophrenia: a computer model. Schizophr Bull. 15:477–490.

Hoffman RE, McGlashan TH. 2001. Neural network models of schizophrenia. Neuroscientist. 7:441–454.

Horn DI, Yu C, Steiner J, Buchmann J, Kaufmann J, Osoba A, Eckert U, Zierhut KC, Schiltz K, He H, Biswal B, Bogerts B, Walter M. 2010. Glutamatergic and Resting-State Functional Connectivity Correlates of Severity in Major Depression – The Role of Pregenual Anterior Cingulate Cortex and Anterior Insula. Front Syst Neurosci. 4.

Horwitz B, Tagamets MA. 1999. Predicting human functional maps with neural net modeling. Hum Brain Mapp. 8:137–142.

Hsieh L-T, Ranganath C. 2014. Frontal midline theta oscillations during working memory maintenance and episodic encoding and retrieval. NeuroImage. 85:721–729.

Hwang K, Hallquist MN, Luna B. 2013. The Development of Hub Architecture in the Human Functional Brain Network. Cereb Cortex. 23:2380–2393.

Ikeda M, Iwanaga M, Seiwa H. 1996. Test anxiety and working memory system. Perceptual and Motor Skills. 82:1223–1231.

Iosifescu DV, Greenwald S, Devlin P, Mischoulon D, Denninger JW, Alpert JE, Fava M. 2009. Frontal EEG predictors of treatment outcome in major depressive disorder. European Neuropsychopharmacology. 19:772–777.

Ishikawa A, Nakamura S. 2003. Convergence and Interaction of Hippocampal and Amygdalar Projections within the Prefrontal Cortex in the Rat. The Journal of Neuroscience. 23:9987–9995.

Johansen-Berg H, Gutman DA, Behrens TEJ, Matthews PM, Rushworth MFS, Katz E, Lozano AM, Mayberg HS. 2008. Anatomical Connectivity of the Subgenual

Cingulate Region Targeted with Deep Brain Stimulation for Treatment-Resistant Depression. Cerebral Cortex. 18:1374–1383.

Jonides J, Smith EE, Koeppe RA, Awh E, Minoshima S, Mintun MA. 1993. Spatial working memory in humans as revealed by PET. Nature. 363:623–625.

Kean S. 2014. The True Story of Phineas Gage Is Much More Fascinating Than the Mythical Textbook Accounts. Slate Magazine.

Keller CJ, Bickel S, Honey CJ, Groppe DM, Entz L, Craddock RC, Lado FA, Kelly C, Milham M, Mehta AD. 2013. Neurophysiological Investigation of Spontaneous Correlated and Anticorrelated Fluctuations of the BOLD Signal. J Neurosci. 33:6333–6342.

Keller MB, Lavori PW, Mueller TI, Endicott J, Coryell W, Hirschfeld RMA, Shea T. 1992. Time to Recovery, Chronicity, and Levels of Psychopathology in Major Depression: A 5-Year Prospective Follow-up of 431 Subjects. Arch Gen Psychiatry. 49:809–816.

Kendler KS. 2000. Stressful Life Events and Previous Episodes in the Etiology of Major Depression in Women: An Evaluation of the "Kindling" Hypothesis. American Journal of Psychiatry. 157:1243–1251.

Kendler KS, Thornton LM, Gardner CO. 2001. Genetic risk, number of previous depressive episodes, and stressful life events in predicting onset of major depression. Am J Psychiatry. 158:582–586.

Kennedy N, Abbott R, Paykel ES. 2003. Remission and recurrence of depression in the maintenance era: long-term outcome in a Cambridge cohort. Psychol Med. 33:827–838.

Kennedy SH. 2001. Changes in Regional Brain Glucose Metabolism Measured With Positron Emission Tomography After Paroxetine Treatment of Major Depression. American Journal of Psychiatry. 158:899–905.

Kennedy SH, Giacobbe P, Rizvi SJ, Placenza FM, Nishikawa Y, Mayberg HS, Lozano AM. 2011. Deep Brain Stimulation for Treatment-Resistant Depression: Follow-Up After 3 to 6 Years. AJP. 168:502–510.

Kennerley SW, Behrens TEJ, Wallis JD. 2011. Double dissociation of value computations in orbitofrontal and anterior cingulate neurons. Nat Neurosci. 14:1581–1589.

Kessler RC, Berglund P, Demler O, Jin R, Koretz D, Merikangas KR, Rush AJ, Walters EE, Wang PS. 2003. The Epidemiology of Major Depressive Disorder. JAMA: The Journal of the American Medical Association. 289:3095–3105.

Kinnison J, Padmala S, Choi J-M, Pessoa L. 2012. Network analysis reveals increased integration during emotional and motivational processing. J Neurosci. 32:8361–8372.

Kopell N, Ermentrout GB, Whittington MA, Traub RD. 2000. Gamma rhythms and beta rhythms have different synchronization properties. PNAS. 97:1867–1872.

Korb AS, Hunter AM, Cook IA, Leuchter AF. 2009. Rostral anterior cingulate cortex theta current density and response to antidepressants and placebo in major depression. Clin Neurophysiol. 120:1313–1319.

Koyama T, Kato K, Tanaka YZ, Mikami A. 2001. Anterior cingulate activity during pain-avoidance and reward tasks in monkeys. Neuroscience Research. 39:421–430.

Krishnan V, Nestler EJ. 2008. The molecular neurobiology of depression. Nature. 455:894–902.

Kubota K, Niki H. 1971. Prefrontal cortical unit activity and delayed alternation performance in monkeys. Journal of Neurophysiology. 34:337–347.

Kumar S, Black SJ, Hultman R, Szabo ST, DeMaio KD, Du J, Katz BM, Feng G, Covington HE, Dzirasa K. 2013. Cortical Control of Affective Networks. J Neurosci. 33:1116–1129.

Lang PJ, Bradley MM. 2010. Emotion and the motivational brain. Biological Psychology. 84:437–450.

Lara AH, Wallis JD. 2014. Executive control processes underlying multi-item working memory. Nat Neurosci. 17:876–883.

Lavric A, Rippon G, Gray JR. 2003. Threat-Evoked Anxiety Disrupts Spatial Working Memory Performance: An Attentional Account. Cognitive Therapy and Research. 27:489–504.

Lehman JF, Greenberg BD, McIntyre CC, Rasmussen SA, Haber SN. 2011. Rules ventral prefrontal cortical axons use to reach their targets: implications for diffusion tensor imaging tractography and deep brain stimulation for psychiatric illness. J Neurosci. 31:10392–10402.

Liotti M. 2002. Unmasking Disease-Specific Cerebral Blood Flow Abnormalities: Mood Challenge in Patients With Remitted Unipolar Depression. American Journal of Psychiatry. 159:1830–1840.

Liotti M, Mayberg HS, Brannan SK, McGinnis S, Jerabek P, Fox PT. 2000. Differential limbic--cortical correlates of sadness and anxiety in healthy subjects: implications for affective disorders. Biol Psychiatry. 48:30–42.

Lipsman N, Kaping D, Westendorff S, Sankar T, Lozano AM, Womelsdorf T. 2014. Beta coherence within human ventromedial prefrontal cortex precedes affective value choices. Neuroimage. 85 Pt 2:769–778.

Lipsman N, Nakao T, Kanayama N, Krauss JK, Anderson A, Giacobbe P, Hamani C, Hutchison WD, Dostrovsky JO, Womelsdorf T, Lozano AM, Northoff G. 2014. Neural overlap between resting state and self-relevant activity in human subcallosal cingulate cortex--single unit recording in an intracranial study. Cortex. 60:139–144.

Liu Y, Liang M, Zhou Y, He Y, Hao Y, Song M, Yu C, Liu H, Liu Z, Jiang T. 2008. Disrupted small-world networks in schizophrenia. Brain. 131:945–961.

Loh M, Rolls ET, Deco G. 2007. A dynamical systems hypothesis of schizophrenia. PLoS Comput Biol. 3:e228.

Lozano AM, Mayberg HS, Giacobbe P, Hamani C, Craddock RC, Kennedy SH. 2008. Subcallosal Cingulate Gyrus Deep Brain Stimulation for Treatment-Resistant Depression. Biological Psychiatry. 64:461–467.

Lynall M-E, Bassett DS, Kerwin R, McKenna PJ, Kitzbichler M, Muller U, Bullmore E. 2010. Functional Connectivity and Brain Networks in Schizophrenia. J Neurosci. 30:9477–9487.

MacDonald AW, Cohen JD, Stenger VA, Carter CS. 2000. Dissociating the Role of the Dorsolateral Prefrontal and Anterior Cingulate Cortex in Cognitive Control. Science. 288:1835–1838.

Macmillan M. 2000. Restoring Phineas Gage: a 150th retrospective. J Hist Neurosci. 9:46–66.

Markham R, Darke S. 1991. The effects of anxiety on verbal and spatial task performance. Australian Journal of Psychology. 43:107–111.

Maletic V, Robinson M, Oakes T, Iyengar S, Ball SG, Russell J. 2007. Neurobiology of depression: an integrated view of key findings. International Journal of Clinical Practice. 61:2030–2040.

Malizia AL. 1997. The frontal lobes and neurosurgery for psychiatric disorders. J Psychopharmacol (Oxford). 11:179–187.

Manji HK, Drevets WC, Charney DS. 2001. The cellular neurobiology of depression. Nat Med. 7:541–547.

Ma S, Calhoun VD, Eichele T, Du W, Adali T. 2012. Modulations of functional connectivity in the healthy and schizophrenia groups during task and rest. Neuroimage. 62:1694–1704.

Mayberg HS. 1997. Limbic-cortical dysregulation: a proposed model of depression. J Neuropsychiatry Clin Neurosci. 9:471–481.

Mayberg HS. 2009. Targeted electrode-based modulation of neural circuits for depression. Journal of Clinical Investigation. 119:717–725.

Mayberg HS, Brannan SK, Mahurin RK, Jerabek PA, Brickman JS, Tekell JL, Silva JA, McGinnis S, Glass TG, Martin CC, Fox PT. 1997. Cingulate function in depression: a potential predictor of treatment response. Neuroreport. 8:1057–1061.

Mayberg HS, Brannan SK, Tekell JL, Silva JA, Mahurin RK, McGinnis S, Jerabek PA. 2000. Regional metabolic effects of fluoxetine in major depression: serial changes and relationship to clinical response. Biol Psychiatry. 48:830–843.

Mayberg HS, Liotti M, Brannan SK, McGinnis S, Mahurin RK, Jerabek PA, Silva JA, Tekell JL, Martin CC, Lancaster JL, Fox PT. 1999. Reciprocal limbic-cortical function and negative mood: converging PET findings in depression and normal sadness. Am J Psychiatry. 156:675–682.

Mayberg HS, Lozano AM, Voon V, McNeely HE, Seminowicz D, Hamani C, Schwalb JM, Kennedy SH. 2005. Deep Brain Stimulation for Treatment-Resistant Depression. Neuron. 45:651–660.

McCarthy G, Blamire AM, Puce A, Nobre AC, Bloch G, Hyder F, Goldman-Rakic P, Shulman RG. 1994. Functional magnetic resonance imaging of human prefrontal cortex activation during a spatial working memory task. PNAS. 91:8690–8694.

McCormick DA, Connors BW, Lighthall JW, Prince DA. 1985. Comparative electrophysiology of pyramidal and sparsely spiny stellate neurons of the neocortex. J Neurophysiol. 54:782–806.

McNab F, Klingberg T. 2008. Prefrontal cortex and basal ganglia control access to working memory. Nat Neurosci. 11:103–107.

Medalla M, Barbas H. 2010. Anterior cingulate synapses in prefrontal areas 10 and 46 suggest differential influence in cognitive control. J Neurosci. 30:16068–16081.

Meunier D, Achard S, Morcom A, Bullmore E. 2009. Age-related changes in modular organization of human brain functional networks. Neuroimage. 44:715–723.

Mitchell AJ. 2006. Two-week delay in onset of action of antidepressants: new evidence. BJP. 188:105–106.

Moll J, Zahn R, de Oliveira-Souza R, Krueger F, Grafman J. 2005. The neural basis of human moral cognition. Nat Rev Neurosci. 6:799–809.

Monosov IE, Hikosaka O. 2012. Regionally Distinct Processing of Rewards and Punishments by the Primate Ventromedial Prefrontal Cortex. J Neurosci. 32:10318–10330.

Mottaghy FM, Keller CE, Gangitano M, Ly J, Thall M, Parker JA, Pascual-Leone A. 2002. Correlation of cerebral blood flow and treatment effects of repetitive transcranial magnetic stimulation in depressed patients. Psychiatry Res. 115:1–14.

Moussa MN, Vechlekar CD, Burdette JH, Steen MR, Hugenschmidt CE, Laurienti PJ. 2011. Changes in Cognitive State Alter Human Functional Brain Networks. Front Hum Neurosci. 5.

Mulert C, Juckel G, Brunnmeier M, Karch S, Leicht G, Mergl R, Möller H-J, Hegerl U, Pogarell O. 2007. Rostral anterior cingulate cortex activity in the theta band predicts response to antidepressive medication. Clin EEG Neurosci. 38:78–81.

Murphy K, Birn RM, Handwerker DA, Jones TB, Bandettini PA. 2009. The impact of global signal regression on resting state correlations: Are anti-correlated networks introduced? Neuroimage. 44:893–905.

Nemeroff CB. 2002. Recent advances in the neurobiology of depression. Psychopharmacol Bull. 36 Suppl 2:6–23.

Nestler EJ, Barrot M, DiLeone RJ, Eisch AJ, Gold SJ, Monteggia LM. 2002. Neurobiology of depression. Neuron. 34:13–25.

Nobler MS, Oquendo MA, Kegeles LS, Malone KM, Campbell CC, Sackeim HA, Mann JJ. 2001. Decreased regional brain metabolism after ect. Am J Psychiatry. 158:305–308.

Oda K, Okubo Y, Ishida R, Murata Y, Ohta K, Matsuda T, Matsushima E, Ichimiya T, Suhara T, Shibuya H, Nishikawa T. 2003. Regional cerebral blood flow in

depressed patients with white matter magnetic resonance hyperintensity. Biological Psychiatry. 53:150–156.

Ongür D, An X, Price JL. 1998. Prefrontal cortical projections to the hypothalamus in macaque monkeys. J Comp Neurol. 401:480–505.

Ongür D, Drevets WC, Price JL. 1998. Glial reduction in the subgenual prefrontal cortex in mood disorders. Proc Natl Acad Sci USA. 95:13290–13295.

Öngür D, Price JL. 2000. The Organization of Networks within the Orbital and Medial Prefrontal Cortex of Rats, Monkeys and Humans. Cereb Cortex. 10:206–219.

Ownby RL. 1998. Computational model of obsessive-compulsive disorder: Examination of etiologic hypothesis and treatment strategies. Depression and Anxiety. 8:91–103.

Paelecke-Habermann Y, Pohl J, Leplow B. 2005. Attention and executive functions in remitted major depression patients. Journal of Affective Disorders. 89:125–135.

Palomero-Gallagher N, Vogt BA, Schleicher A, Mayberg HS, Zilles K. 2009. Receptor architecture of human cingulate cortex: Evaluation of the four-region neurobiological model. Human Brain Mapping. 30:2336–2355.

Pardo JV, Sheikh SA, Schwindt GC, Lee JT, Kuskowski MA, Surerus C, Lewis SM, Abuzzahab FS, Adson DE, Rittberg BR. 2008. Chronic vagus nerve stimulation for treatment-resistant depression decreases resting ventromedial prefrontal glucose metabolism. NeuroImage. 42:879–889.

Perlstein WM, Elbert T, Stenger VA. 2002. Dissociation in human prefrontal cortex of affective influences on working memory-related activity. PNAS. 99:1736–1741.

Pessoa L. 2008. On the relationship between emotion and cognition. Nat Rev Neurosci. 9:148–158.

Phelps EA. 2006. Emotion and Cognition: Insights from Studies of the Human Amygdala. Annual Review of Psychology. 57:27–53.

Pizzagalli DA. 2011. Frontocingulate dysfunction in depression: toward biomarkers of treatment response. Neuropsychopharmacology. 36:183–206.

Pizzagalli DA, Nitschke JB, Oakes TR, Hendrick AM, Horras KA, Larson CL, Abercrombie HC, Schaefer SM, Koger JV, Benca RM, Pascual-Marqui RD, Davidson RJ. 2002. Brain electrical tomography in depression: the importance of symptom severity, anxiety, and melancholic features. Biological Psychiatry. 52:73–85.

Pizzagalli D, Pascual-Marqui RD, Nitschke JB, Oakes TR, Larson CL, Abercrombie HC, Schaefer SM, Koger JV, Benca RM, Davidson RJ. 2001. Anterior cingulate activity as a predictor of degree of treatment response in major depression: evidence from brain electrical tomography analysis. Am J Psychiatry. 158:405–415.

Portella MJ, de Diego-Adeliño J, Gómez-Ansón B, Morgan-Ferrando R, Vives Y, Puigdemont D, Pérez-Egea R, Ruscalleda J, Enric Álvarez, Pérez V. 2011. Ventromedial prefrontal spectroscopic abnormalities over the course of depression: a comparison among first episode, remitted recurrent and chronic patients. J Psychiatr Res. 45:427–434.

Price J, Cole V, Goodwin GM. 2009. Emotional side-effects of selective serotonin reuptake inhibitors: qualitative study. Br J Psychiatry. 195:211–217.

Raichle ME, MacLeod AM, Snyder AZ, Powers WJ, Gusnard DA, Shulman GL. 2001. A default mode of brain function. PNAS. 98:676–682.

Rajkowska G, Miguel-Hidalgo JJ, Wei J, Dilley G, Pittman SD, Meltzer HY, Overholser JC, Roth BL, Stockmeier CA. 1999. Morphometric evidence for neuronal and glial prefrontal cell pathology in major depression. Biol Psychiatry. 45:1085–1098.

Ray WJ, Cole HW. 1985. EEG alpha activity reflects attentional demands, and beta activity reflects emotional and cognitive processes. Science. 228:750–752.

Riva-Posse P, Choi KS, Holtzheimer PE, McIntyre CC, Gross RE, Chaturvedi A, Crowell AL, Garlow SJ, Rajendra JK, Mayberg HS. 2014. Defining Critical White Matter Pathways Mediating Successful Subcallosal Cingulate Deep Brain Stimulation for Treatment-Resistant Depression. Biological Psychiatry, N-Methyl-D-Aspartate Receptors, Synaptic Plasticity, Psychopathology, and Treatment. 76:963–969.

Rodriguez E, George N, Lachaux J-P, Martinerie J, Renault B, Varela FJ. 1999. Perception's shadow: long-distance synchronization of human brain activity. Nature. 397:430–433.

Rogers RD, Ramnani N, Mackay C, Wilson JL, Jezzard P, Carter CS, Smith SM. 2004. Distinct portions of anterior cingulate cortex and medial prefrontal cortex are activated by reward processing in separable phases of decision-making cognition. Biol Psychiatry. 55:594–602.

Rolls ET. 2007. Emotion Explained. Oup Oxford.

Rolls ET, Loh M, Deco G. 2008. An attractor hypothesis of obsessive-compulsive disorder. Eur J Neurosci. 28:782–793.

Rolls ET, Loh M, Deco G, Winterer G. 2008. Computational models of schizophrenia and dopamine modulation in the prefrontal cortex. Nat Rev Neurosci. 9:696–709.

Rose EJ, Ebmeier KP. 2006. Pattern of impaired working memory during major depression. Journal of Affective Disorders. 90:149–161.

Rubinov M, Sporns O. 2010. Complex network measures of brain connectivity: uses and interpretations. Neuroimage. 52:1059–1069.

Rubinov M, Sporns O. 2011. Weight-conserving characterization of complex functional brain networks. NeuroImage. 56:2068–2079.

Salum C, Morato S, Roque-da-Silva AC. 2000. Anxiety-like behavior in rats: a computational model. Neural Netw. 13:21–29.

Sanacora G, Treccani G, Popoli M. 2012. Towards a glutamate hypothesis of depression: An emerging frontier of neuropsychopharmacology for mood disorders. Neuropharmacology, Anxiety and Depression. 62:63–77.

Sanfey AG, Rilling JK, Aronson JA, Nystrom LE, Cohen JD. 2003. The neural basis of economic decision-making in the Ultimatum Game. Science. 300:1755–1758.

Santana N, Bortolozzi A, Serrats J, Mengod G, Artigas F. 2004. Expression of Serotonin1A and Serotonin2A Receptors in Pyramidal and GABAergic Neurons of the Rat Prefrontal Cortex. Cereb Cortex. 14:1100–1109.

Sanz-Arigita EJ, Schoonheim MM, Damoiseaux JS, Rombouts SARB, Maris E, Barkhof F, Scheltens P, Stam CJ. 2010. Loss of "Small-World" Networks in Alzheimer's Disease: Graph Analysis of fMRI Resting-State Functional Connectivity. PLoS ONE. 5:e13788.

Sashin JI, Callahan J. 1990. A Model of Affect Using Dynamical Systems. Ann Psychoanal. 18:213–231.

Schaefer A, Braver TS, Reynolds JR, Burgess GC, Yarkoni T, Gray JR. 2006. Individual Differences in Amygdala Activity Predict Response Speed during Working Memory. J Neurosci. 26:10120–10128.

Seminowicz D., Mayberg H., McIntosh A., Goldapple K, Kennedy S, Segal Z, Rafi-Tari S. 2004. Limbic–frontal circuitry in major depression: a path modeling metanalysis. NeuroImage. 22:409–418.

Shackman AJ, Sarinopoulos I, Maxwell JS, Pizzagalli DA, Lavric A, Davidson RJ. 2006. Anxiety selectively disrupts visuospatial working memory. Emotion. 6:40–61.

Sheehan DV, Lecrubier Y, Sheehan KH, Amorim P, Janavs J, Weiller E, Hergueta T, Baker R, Dunbar GC. 1998. The Mini-International Neuropsychiatric Interview (M.I.N.I.): the development and validation of a structured diagnostic psychiatric interview for DSM-IV and ICD-10. J Clin Psychiatry. 59 Suppl 20:22–33;quiz 34–57.

Sheline YI, Barch DM, Price JL, Rundle MM, Vaishnavi SN, Snyder AZ, Mintun MA, Wang S, Coalson RS, Raichle ME. 2009. The default mode network and self-referential processes in depression. PNAS. 106:1942–1947.

Shidara M, Richmond BJ. 2002. Anterior Cingulate: Single Neuronal Signals Related to Degree of Reward Expectancy. Science. 296:1709–1711.

Shin LM, Wright CI, Cannistraro PA, et al. 2005. A functional magnetic resonance imaging study of amygdala and medial prefrontal cortex responses to overtly presented fearful faces in posttraumatic stress disorder. Archives of General Psychiatry. 62:273–281.

Siegel M, Donner TH, Engel AK. 2012. Spectral fingerprints of large-scale neuronal interactions. Nat Rev Neurosci. 13:121–134.

Siegle GJ, Carter CS, Thase ME. 2006. Use of fMRI to Predict Recovery From Unipolar Depression With Cognitive Behavior Therapy. AJP. 163:735–738.

Sierra-Mercado D, Padilla-Coreano N, Quirk GJ. 2011. Dissociable Roles of Prelimbic and Infralimbic Cortices, Ventral Hippocampus, and Basolateral Amygdala in the Expression and Extinction of Conditioned Fear. Neuropsychopharmacology. 36:529–538.

Simon GE, VonKorff M, Heiligenstein JH, Revicki DA, Grothaus L, Katon W, Wagner EH. 1996. Initial antidepressant choice in primary care. Effectiveness and cost of fluoxetine vs tricyclic antidepressants. JAMA. 275:1897–1902.

Simon-Thomas ER, Knight RT. 2005. Affective and cognitive modulation of performance monitoring: Behavioral and ERP evidence. Cognitive, Affective, & Behavioral Neuroscience. 5:362–372.

Simon-Thomas ER, Role KO, Knight RT. 2005. Behavioral and Electrophysiological Evidence of a Right Hemisphere Bias for the Influence of Negative Emotion on Higher Cognition. Journal of Cognitive Neuroscience. 17:518–529.

Simpson JR, Snyder AZ, Gusnard DA, Raichle ME. 2001. Emotion-induced changes in human medial prefrontal cortex: I. During cognitive task performance. PNAS. 98:683–687.

Singer W. 1999. Neuronal Synchrony: A Versatile Code for the Definition of Relations? Neuron. 24:49–65.

Smith APR, Henson RNA, Dolan RJ, Rugg MD. 2004. fMRI correlates of the episodic retrieval of emotional contexts. NeuroImage. 22:868–878.

Smith APR, Stephan KE, Rugg MD, Dolan RJ. 2006. Task and Content Modulate Amygdala-Hippocampal Connectivity in Emotional Retrieval. Neuron. 49:631–638.

Smith R, Fadok RA, Purcell M, Liu S, Stonnington C, Spetzler RF, Baxter LC. 2011. Localizing sadness activation within the subgenual cingulate in individuals: a novel functional MRI paradigm for detecting individual differences in the neural circuitry underlying depression. Brain Imaging Behav. 5:229–239.

Sporns O. 2014. Contributions and challenges for network models in cognitive neuroscience. Nat Neurosci. 17:652–660.

Sporns O, Chialvo DR, Kaiser M, Hilgetag CC. 2004. Organization, development and function of complex brain networks. Trends in Cognitive Sciences. 8:418–425.

Sporns O, Honey CJ, Kötter R. 2007. Identification and Classification of Hubs in Brain Networks. PLoS ONE. 2:e1049.

Steffens DC, Krishnan KR, Helms MJ. 1997. Are SSRIs better than TCAs? Comparison of SSRIs and TCAs: a meta-analysis. Depress Anxiety. 6:10–18.

Stephan KE, Mathys C. 2014. Computational approaches to psychiatry. Current Opinion in Neurobiology, Theoretical and computational neuroscience. 25:85–92.

Tamás G, Buhl EH, Lörincz A, Somogyi P. 2000. Proximally targeted GABAergic synapses and gap junctions synchronize cortical interneurons. Nat Neurosci. 3:366–371.

Tian L, Wang J, Yan C, He Y. 2011. Hemisphere- and gender-related differences in small-world brain networks: a resting-state functional MRI study. Neuroimage. 54:191–202.

Tsujimoto T, Shimazu H, Isomura Y. 2006. Direct Recording of Theta Oscillations in Primate Prefrontal and Anterior Cingulate Cortices. Journal of Neurophysiology. 95:2987–3000.

Tsujimoto T, Shimazu H, Isomura Y, Sasaki K. 2010. Theta oscillations in primate prefrontal and anterior cingulate cortices in forewarned reaction time tasks. J Neurophysiol. 103:827–843.

Tuckwell HC. 1988. Introduction to Theoretical Neurobiology: Volume 1, Linear Cable Theory and Dendritic Structure. Cambridge University Press.

Vaidya VA, Duman RS. 2001. Depresssion--emerging insights from neurobiology. Br Med Bull. 57:61–79.

Van Dijk KRA, Hedden T, Venkataraman A, Evans KC, Lazar SW, Buckner RL. 2010. Intrinsic Functional Connectivity As a Tool For Human Connectomics: Theory, Properties, and Optimization. J Neurophysiol. 103:297–321.

Varela F, Lachaux J-P, Rodriguez E, Martinerie J. 2001. The brainweb: Phase synchronization and large-scale integration. Nat Rev Neurosci. 2:229–239.

Viard A, Piolino P, Desgranges B, Chételat G, Lebreton K, Landeau B, Young A, Sayette VDL, Eustache F. 2007. Hippocampal Activation for Autobiographical Memories over the Entire Lifetime in Healthy Aged Subjects: An fMRI Study. Cereb Cortex. 17:2453–2467.

Vidal-Gonzalez I, Vidal-Gonzalez B, Rauch SL, Quirk GJ. 2006. Microstimulation reveals opposing influences of prelimbic and infralimbic cortex on the expression of conditioned fear. Learn Mem. 13:728–733.

Videbech P, Ravnkilde B, Pedersen TH, Hartvig H, Egander A, Clemmensen K, Rasmussen NA, Andersen F, Gjedde A, Rosenberg R. 2002. The Danish PET/depression project: clinical symptoms and cerebral blood flow. A regions-of-interest analysis. Acta Psychiatrica Scandinavica. 106:35–44.

Vlassenko A, Sheline YI, Fischer K, Mintun MA. 2004. Cerebral perfusion response to successful treatment of depression with different serotoninergic agents. J Neuropsychiatry Clin Neurosci. 16:360–363.

Vogt B. 2009. Cingulate Neurobiology and Disease. Oxford University Press.

Vogt BA, Pandya DN. 1987. Cingulate cortex of the rhesus monkey. II: cortical afferents. Journal of comparative neurology. 262:271–289.

Walsh R, Victor B, Bitner R. 2006. Emotional effects of sertraline: novel findings revealed by meditation. Am J Orthopsychiatry. 76:134–137.

Walter M, Henning A, Grimm S, Schulte RF, Beck J, Dydak U, Schnepf B, Boeker H, Boesiger P, Northoff G. 2009. The Relationship Between Aberrant Neuronal Activation in the Pregenual Anterior Cingulate, Altered Glutamatergic Metabolism, and Anhedonia in Major Depression. Arch Gen Psychiatry. 66:478–486.

Wang J, Zuo X, He Y. 2010. Graph-based network analysis of resting-state functional MRI. Front Syst Neurosci. 4:16.

Wang L, Li Y, Metzak P, He Y, Woodward TS. 2010. Age-related changes in topological patterns of large-scale brain functional networks during memory encoding and recognition. NeuroImage. 50:862–872.

Wang X-J, Krystal JH. 2014. Computational Psychiatry. Neuron. 84:638–654.

Warden MR, Selimbeyoglu A, Mirzabekov JJ, Lo M, Thompson KR, Kim S-Y, Adhikari A, Tye KM, Frank LM, Deisseroth K. 2012. A prefrontal cortex-brainstem neuronal projection that controls response to behavioural challenge. Nature. 492:428–432.

Watts FN, Sharrock R. 1985. Description and measurement of concentration problems in depressed patients. Psychol Med. 15:317–326.

Young MP, Scannell JW, Burns GA, Blakemore C. 1994. Analysis of connectivity: neural systems in the cerebral cortex. Rev Neurosci. 5:227–250.

Yucel K, McKinnon MC, Chahal R, Taylor VH, Macdonald K, Joffe R, MacQueen GM. 2008. Anterior Cingulate Volumes in Never-Treated Patients with Major Depressive Disorder. Neuropsychopharmacology. 33:3157–3163.

Zikopoulos B, Barbas H. 2012. Pathways for emotions and attention converge on the thalamic reticular nucleus in primates. J Neurosci. 32:5338–5350.